Genetics and Genomics

Single-cell profiling of trabecular meshwork identifies mitochondrial dysfunction in a glaucoma model that is protected by vitamin B3 treatment

Reviewed Preprint
v2 • October 13, 2025
Revised by authors

Reviewed Preprint
v1 • July 15, 2025

Nicholas Tolman, Taibo Li, Revathi Balasubramanian, Guorong Li, Rebecca Pfeiffer, Violet Bupp-Chickering, Ruth A Kelly, Marina Simón, John Peregrin, Christa Montgomery, Bryan Jones, W Daniel Stamer, Jiang Qian, Simon WM John

Department of Ophthalmology, Columbia University Irving Medical Center, New York, United States • Department of Biomedical Engineering, Johns Hopkins University, Baltimore, United States • Department of Ophthalmology, Duke University, Durham, United States • Department of Ophthalmology, University of Pittsburgh, Pittsburgh, United States • Department of Ophthalmology, Johns Hopkins School of Medicine, Baltimore, United States • Zuckerman Mind Brain Behavior Institute, Columbia University, New York, United States

eLife Assessment

This study provides a **fundamental** advancement in our understanding of trabecular meshwork cell diversity and its role in eye pressure regulation and glaucoma using multimodal single-cell analysis, spatial validation, and functional testing that go beyond the current state-of-the-art. The study demonstrates that mitochondrial dysfunction, specifically in one of three distinct cell subtypes (TM3), contributes to elevated IOP in a genetic mouse model of glaucoma carrying a mutation in the transcription factor Lmx1b. While the identification of TM3 cells as metabolically specialized is **compelling**, there is somewhat limited evidence linking mitochondrial dysfunction to the Lmx1b mutation in TM3 cells.

https://doi.org/10.7554/eLife.107161.2.sa3

Abstract

Since the trabecular meshwork (TM) is central to intraocular pressure (IOP) regulation and glaucoma, a deeper understanding of its genomic landscape is needed. We present a multimodal, single-cell resolution analysis of mouse limbal cells (includes TM). In total, we sequenced 9,394 wild-type TM cell transcriptomes. We discovered three TM cell subtypes with characteristic signature genes validated by immunofluorescence on tissue sections and whole-mounts. The subtypes are robust, being detected in datasets for two diverse mouse strains and in independent data from two institutions. Results show compartmentalized enrichment of critical pathways in specific TM cell subtypes. Distinctive signatures include increased expression of genes responsible for 1) extracellular matrix structure and metabolism (TM1 subtype), 2) secreted ligand signaling to support Schlemm's canal cells (TM2), and 3) contractile and mitochondrial/metabolic activity (TM3). ATAC-sequencing data

identified active transcription factors in TM cells, including LMX1B. Mutations in *LMX1B* cause high IOP and glaucoma. LMX1B is emerging as a key transcription factor for normal mitochondrial function and its expression is much higher in TM3 cells than other limbal cells. To understand the role of LMX1B in TM function and glaucoma, we single-cell sequenced limbal cells from *Lmx1b*$^{V265D/+}$mutant mice (2,491 TM cells). In *V265D/+* mice, TM3 cells were uniquely affected by pronounced mitochondrial pathway changes. Mitochondria in TM cells of *V265D/+* mice are swollen with a reduced cristae area, further supporting a role for mitochondrial dysfunction in the initiation of IOP elevation in these mice. Importantly, treatment with vitamin B_3 (nicotinamide), to enhance mitochondrial function and metabolic resilience, significantly protected *Lmx1b* mutant mice from IOP elevation.

Introduction

Aqueous humor (AH) dynamics and pressure homeostasis are important for proper ocular inflation and vision. Elevated intraocular pressure (IOP) is a key risk factor for glaucoma, a serious blinding disorder that affects 80 million people worldwide [1]. IOP is controlled by continually adjusting resistance to drainage (outflow) of AH through the trabecular meshwork (TM) and Schlemm's canal (SC), the primary route of AH outflow from the eye. AH percolates through the TM before exiting the eye through SC and then entering the venous circulation. As the most abundant constituent of the conventional outflow pathway, TM cells are central in regulating AH drainage and IOP. Despite significant advances over the past few decades, a much deeper understanding of the molecular mechanisms governing TM cell health and function, as well as the pathological alterations responsible for increased outflow resistance, elevated IOP, and increased glaucoma risk are still needed.

The TM is located at the inner aspect of the wall of the eye at the iridocorneal angle just anterior to where the iris and cornea meet (i.e. the limbus). In humans, the TM is morphologically separated into distinct zones, including the uveal, corneoscleral, and juxtacanalicular trabecular meshwork (JCT), which lies adjacent to the SC. AH first drains through the uveal and corneoscleral meshwork whose TM cells have endothelial-like properties [2–4]. In these regions, the TM consists of beams and plates made of various extracellular matrix (ECM) components including fibrillar collagens [5–9]. The beams and plates are covered with monolayers of TM cells. AH drains through a tortuous series of intertrabecular spaces, which run between the beams, ensuring interaction with TM cells. Next, AH flows into the less structured JCT region before entering the SC. The JCT consists of TM cells that are fibroblast-like extending their processes onto neighboring JCT and SC cells. JCT TM cells are embedded within a diffuse ECM ground substance (including glycosaminoglycans) [2, 10–12], and have contractile smooth muscle-like properties [2, 13]. Importantly, cells in the JCT region impose critical resistance to AH outflow with a major site of resistance to outflow being located in the tissue where the JCT and SC meet [5, 12, 14, 15].

Regulation of AH outflow resistance and IOP homeostasis by TM cells is complicated. AH outflow is modulated by: 1) The physical properties (shape/volume and contractility) of the TM cells. For example, some TM cells have smooth muscle-like properties that adjust outflow resistance and thus IOP by controlling cellular contractility [16–23]. 2) The effects of different TM cell types on both the composition and abundance of ECM in the JCT due to ECM synthesis/ metabolism and phagocytic activity. 3) The paracrine or physical effects of TM cells on SC and possibly the vasculature just distal to SC [24–27].

Due to their importance, a more detailed molecular characterization of TM cells is still required. The degree to which specific pathways and modulatory roles are compartmentalized or shared by specific TM cell subtypes and how specific subtypes influence each other and the SC are not known. In fact, the number of molecularly distinct subtypes is currently unknown as is the role of

the > 120 genes associated with elevated IOP within these subtypes [28]. Although the TM has fewer beams and a narrower drainage path in mice, developmental, functional and anatomical similarities between human and mouse TM make mice a valuable model for studying the molecular characteristics, heterogeneity, subtypes and distribution of TM cells [29, 30].

Single-cell resolution transcriptomic profiling is revolutionizing the molecular characterization of cell types and cellular heterogeneity (single-cell RNA sequencing, scRNA-seq; and single-nucleus, snRNA-seq). Initial single-cell-level studies have characterized cell types of the ocular anterior segment, including TM cells [24, 26, 31–33], but further depth, validation, and more uniform molecular consensus/ naming of cell types are needed. This is especially true for TM cells. Currently, reports differ in the naming and definition of TM cell subtypes and offer limited validation by immunohistochemistry (IHC) or immunofluorescence (IF) on tissue sections or flat mounts.

Here we more deeply characterized the mouse TM and validated findings by immunostaining tissue sections and flat mounts and by in situ hybridization (ISH). We independently isolated and sequenced limbal cells of mice at 2 institutions and characterized the same 3 TM cell subtypes at both. Additionally, single-nucleus assay for transposase-accessible chromatin with sequencing (snATAC-seq) identified LIM homeobox transcription factor 1 beta (LMX1B) as one of the most active transcription factors in TM cells. Variants in *LMX1B* cause IOP elevation and glaucoma [28, 34–38]. By analyzing $Lmx1b^{V265D/+}$ mutant mice (develop elevated IOP and glaucoma) [39, 40], we show that mitochondrial pathways are primarily disturbed in the TM3 cell subtype, which most strongly expresses *Lmx1b*. Treatment with nicotinamide lessened IOP elevation in $Lmx1b^{V265D/+}$ mutants supporting testing of therapeutics that boost mitochondrial health and function in human patients.

Results

Three molecularly distinct TM cell subtypes

Using scRNA-seq, we sequenced 17,914 cells from dissected limbal tissue (contains drainage structures) of 2-month-old mice. The dataset included 13,251 cells from strain C57BL/6J (B6) and 4,663 cells from strain 129/Sj (129). The data for both strains were integrated (S1 Fig).

Computational analysis revealed six distinct clusters of cells that were TM-containing, epithelia, pigmented epithelia (iris and ciliary body), endothelial, immune and neuron (**Fig 1A**). The identity of each of these cell clusters was based on various well-characterized marker genes (S2A-B Fig) [24, 26, 31]. There were no major differences in the distributions of strain B6 and strain 129 cells within the relevant cell-type clusters (**S3A-C Fig**). Therefore, to improve statistical power, downstream analyses used the integrated dual-strain dataset.

Cells of cluster 1 expressed various TM genes, including *Acta2* (α-SMA), *Pitx2*, *Tfap2b*, and *Myoc* (S2A-B Fig) [26, 31, 41–43]. Unbiased sub-clustering of Cluster 1 revealed 10 distinct sub-clusters (**Fig 1B**), which included three TM cell clusters based on signature gene expression (**Fig 1D-E**). We named these clusters TM1, TM2, and TM3. Hierarchical clustering of these cell types indicated that TM1 and TM2 are more molecularly similar to each other than to TM3 (**Fig 1C**). The remaining seven clusters were identified as cells from other ocular tissue including the iris stroma, sclera, corneal keratocytes, corneal endothelium, ciliary muscle, pericytes, and Schwann cells (S2C Fig) [32, 44–50].

Next, we integrated an additional limbal tissue scRNA-seq dataset (14,912 cells, Duke University) from 3 months old C57BL/6J mice with our initial 2 months old C57BL/6J dataset. Due to batch effects most likely based on differences in cell isolation techniques and environment (Columbia

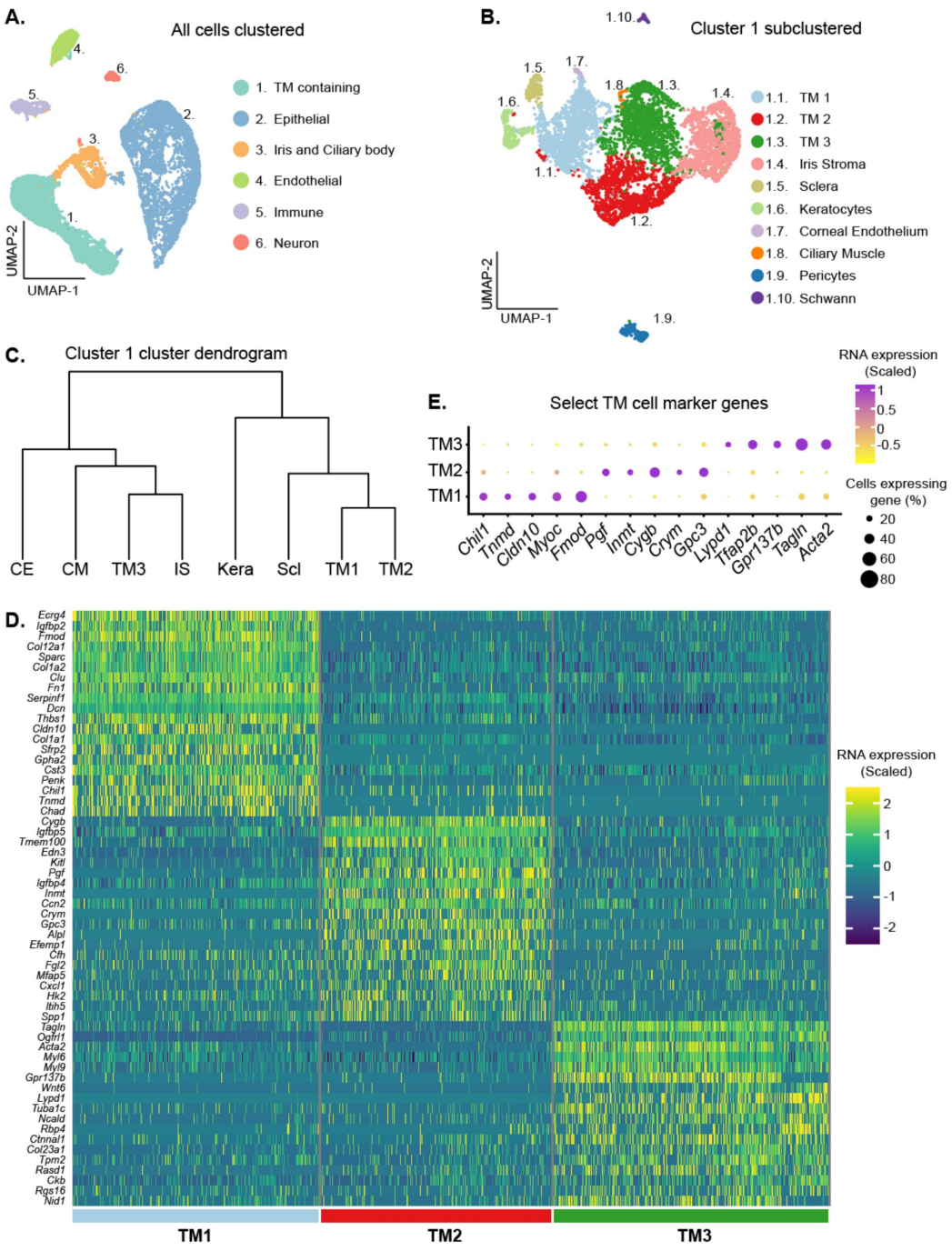

Fig 1.

scRNA-seq data identifies three TM cell clusters.

(A) Cells from limbal tissue dissected and sequenced at Columbia University (integrated B6 and 129/Sj datasets) are depicted in clusters on a UMAP space. **(B)** A separate UMAP representation of the trabecular meshwork (TM) containing cluster following subclustering. Three distinct TM cell clusters are identified (TM1, TM2, and TM3). **(C)** Dendrogram illustrating the relationships among these subclusters. TM1 and TM2 are more similar to each other than to TM3. **(D)** Heatmap showing the signature genes for TM1, TM2, and TM3 cells. The scaled RNA expression indicates how many standard deviations a given gene's expression is from the average expression across all examined cells (positive value is greater than the expression average and negative values are lower than expression average). **(E)** The scaled expression of select marker genes that robustly differentiate TM cell subsets from each other are shown with a dot plot. CE: corneal endothelium, CM: ciliary muscle, IS: iris stroma, Kera: corneal keratocytes, Scl: scleral.

University vs. Duke University, see Methods), TM cells from these datasets occupied adjacent, partially overlapping, but not identical UMAP space (**S4A Fig**). Individual analysis of the Duke dataset also identified 3 TM cell subtypes with the same marker gene expression and enriched molecular pathways compared to the Columbia University data (**S4B-E Fig**, S1 Table). In datasets from previous mouse limbal scRNA-seq studies, there was also a high degree of overlap of marker gene expression with our 3 TM cell clusters (**S5A-B Fig**) [24, 31, 51]. However, some TM subtype clusters reported in previous studies expressed genes that overlapped with both of our TM2 and scleral cell clusters (**S5B-C Fig**) [24, 31]. To resolve this discrepancy, we performed IF for two of the discordantly annotated markers previously reported to be expressed in TM cells but present in our scleral cluster (CD34 and LY6C1). This immunolabeling showed that these markers are expressed in scleral but not TM cells (**S6A-B Fig**). In addition, in previous studies, cells with markers matching TM3 (e.g. Lypd1) were named uveal cells without IF confirmation [24, 31, 51]. IF revealed that our TM3 cells are neither located in the uvea nor abundant in the uveal adjacent TM but primarily reside in the anterior TM closer to the cornea (see below).

TM subtypes differentially occupy TM zones

To further explore the sub-anatomical localization of the TM cell subtypes, we used a combination of IF and ISH to identify subtype markers. Each TM cell subtype had a higher percentage of cells expressing, and an increased average expression of, its respective subtype markers (all $P < 1E\text{-}100$ compared to other TM cells, **S7A Fig**). To analyze the distribution of subtypes, we first divided the TM into zones along its anterior/posterior and inner/outer axes (**S7B-E Fig**). The total area of TM occupied by each individual subtype marker was assessed in each zone on more than 150 tissue sections. This detected biases for the subtypes to be differentially localized in specific TM zones (**Fig 2A-F**). For instance, TM1 cells were significantly more frequent in the posterior and outer TM zones, while TM3 cells were overrepresented in the anterior and inner zones (all $P < 0.01$). The different marker molecules that were assessed for each TM cell subtype gave highly consistent results regarding zonal occupancy (**S8A-B Fig**, **S9 Fig**). In addition, we confirmed the localization biases in 3D whole mounts of the mouse limbus (**Fig 2G-H**, TM1 – MYOC, TM3 – α-SMA) [25]. Collectively, these data indicate clear localization biases that differ for the TM1 and TM3 subtypes.

To better understand the location of TM cell subtypes, we analyzed marker expression patterns in 50-60 exceptionally high-quality sections for each marker of each TM cell subtype (see Methods). For this analysis, the TM was divided into eight regions (**S7F Fig**). Not only did this refine the localization bias of TM1 and TM3 cells, but it discovered that TM2 cells are most concentrated in the mid-posterior two-thirds of the TM (mid regarding inner-outer axis, all $P < 0.01$, **Fig 2I-K**). Despite their biased distributions, some cells of each TM subtype were detected in most TM regions.

Molecular comparison of TM cell subtypes

To determine the molecular functions of TM cells, we first conducted gene ontology (GO) analysis using genes that were differentially expressed genes (DEGs) in all TM cells as a group compared to other sequenced cells (S2 Table). Additionally, we used gene set enrichment analysis (GSEA) to assess whether these GO pathways are relatively enriched or underrepresented in TM cells. Compared to other cells, TM cells were enriched for pathways associated with extracellular matrix (ECM) structure and function, including signaling associated with collagens, proteases, integrins, and glycosaminoglycans (**Fig 3A**, **S10A Fig**, S3 Table). TM cells were also enriched for growth factor signaling. Conversely, underrepresented pathways in TM cells were associated with desmosomes, peroxisomes, and certain cytoskeletal and plasma membrane elements. These pathways help define TM cells relative to other cells in the region.

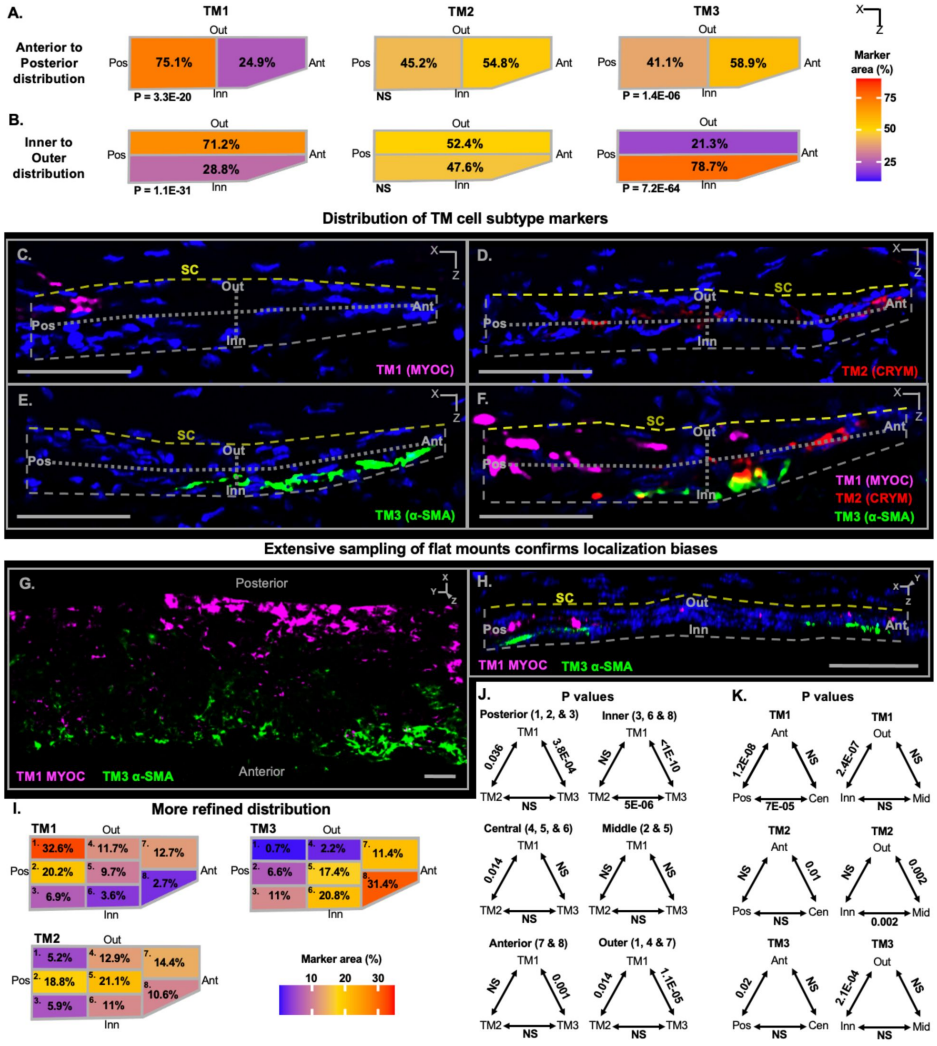

Fig 2.

Biased localization of TM cell subtypes within the TM.

(A-B) Summary diagrams showing the location of expression of TM1, TM2, and TM3 signature markers in the TM. For quantification of marker distributions, the TM was divided in half along both anterior-posterior (A) and inner-outer (B) axes (see **Figure S7** localization of TM and SC). The area of the TM that was positive for each marker within each region was calculated as a percentage of the total area occupied by that marker in the entire TM on each section. The percentage of marker localization to each region was averaged across all analyzed sections. The average localization across all markers used for each TM cell subtype (see S8 and **S9 Figs**) is shown on the diagrammatic representations of the TM using heatmaps. TM1 localization is biased towards the posterior and outer TM, whereas TM3 is biased towards the anterior and inner TM. No clear bias for TM2 was observed. A total of 286 sections were examined using immunofluorescence (IF) and in situ hybridization (ISH). Between 130-160 sections were examined for each TM cell subtype. **(C-F)** Representative sections for a subset of markers for each subtype used for quantification. See **Figure S6** for explanation of indicated tissue orientations. **(G)** En face image of the TM in a 3D reconstruction of a tissue whole mount, clearly demonstrating the anterior vs posterior localization bias for TM1 (posterior bias) and TM3 (anterior bias) cell types. **(H)** Orthogonal 3D image that is cropped and oriented in the same planes as the tissue sections. The inner bias for α-SMA (*Acta2*, TM3) compared to an outer bias for MYOC (TM1) is evident. **(I)** More spatially refined analyses were subsequently conducted using extremely high-quality sections (50-60 per marker) by dividing the TM into 8 smaller zones (**S7 Fig**). In this more refined study, TM2 cells have a biased localization to a posterior and central region of TM (most enriched in zones 2 and 5, see **Figure S7**). **(J-K)** The TM subtype distributions were statistically compared across the combined zones (in parentheses) as indicated. ANOVA followed by Tukey's honestly significant difference test. Ant: anterior TM, Pos: posterior TM, Inn: inner TM, Out: outer TM, SC: Schlemm's canal. Grey dotted lines mark the TM zones, yellow dotted lines mark inner wall of Schlemm's canal. All scale bars: 50 μm.

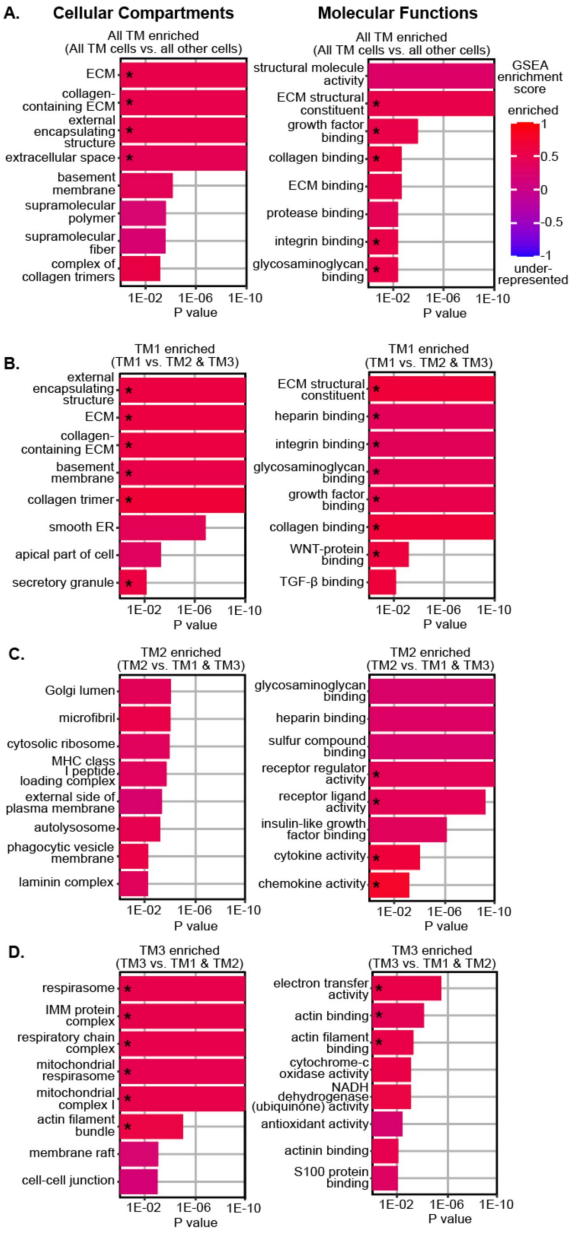

Fig 3.

Pathway analysis suggests differential involvement of TM cell subtypes in extracellular matrix regulation, growth factor signaling, and actin-binding.

(A-B) Molecular comparison of all three TM cell subtypes to all other sequenced cells using gene ontology (GO) of differentially expressed genes (DEGs). The top five most significant pathways as well as three additional pathways of interest are shown for each indicated comparison (adjusted P values, X-axis was cutoff at P < 1E-10). GSEA analysis was also used to assess the enrichment or underrepresentation of these GO pathways with GSEA scores color coded on the GO charts above. Pathways significantly different by GSEA analysis are indicated by asterisks. Overall, TM cells have over-representation of various extracellular matrix (ECM) molecules/ pathways including collagens, glycosaminoglycans, and integrins compared to non-TM cells. Growth factor signaling is also enriched in TM cells compared to other cell types. **(C-D)** When comparing TM cell subtypes, TM1 cells are further enriched for ECM molecules such as collagens, glycosaminoglycans, and integrins as well as TGF-β signaling. **(E-F)** TM2-enriched ECM pathways include glycosaminoglycan binding and the laminin complex. TM2 cells are also enriched for receptor-ligand signaling and insulin growth factor binding. **(G-H)** Actin-binding and mitochondrial metabolism genes are enriched in TM3 cells. ECM = extracellular matrix. ECS = extracellular structure. ER = endoplasmic reticulum. IMM = inner mitochondrial membrane.

Next, we compared TM cell subtypes to each other (**Fig 3B-D**). TM1 cells were most enriched for ECM pathways, particularly structural components such as collagens, integrins, and other ECM elements (**Fig 3B**, **S10B Fig**). The expression of several ECM genes that are reported to impact IOP are heightened in TM1 cells, including Type VIII collagens, fibronectin, and *Ltbp2* [53–55]. Both TM1 and TM2 cells have enriched expression of glycosaminoglycan (GAG) genes (**Fig 3B-C**, **S10B-C Fig**). GAGs in the JCT and intertrabecular spaces form a gel-like consistency and changes in GAG abundance correlate with altered AH outflow resistance [56–58]. TM2 cells are uniquely enriched for the laminin complex, a key component of basement membranes [59]. Pathways related to clearing debris and monitoring the extracellular environment including phagocytic vesicles, antigen presentation, and lysosomal function are also enhanced in TM2 cells. In contrast, TM3 cells are underrepresented for ECM-related pathways compared to other TM cells but are enriched for pathways related to actin binding and mitochondrial metabolism (**Fig 3D**, **S10D Fig**). The actomyosin system plays a crucial role in maintaining TM cell contractility and in regulating outflow facility [16–20]. The enrichment of mitochondrial metabolism pathways in TM3 cells emphasizes their energetic needs and their expected heightened susceptibility to genetic and environmental contexts that compromise metabolic functions. Importantly, genetic variation in mitochondrial/ metabolic pathways contributes risk for IOP elevation and glaucoma [60–62].

We next compared growth factor signaling and ligand-target interactions between TM cells subtypes and other cells. TM1 cells were enriched for transforming growth factor beta (TGF-β) pathway signaling (**Fig 3B**). Receptor ligand activity was enriched in TM2 cells while the membrane raft pathway (a site of signal transduction) was enriched in TM3 cells (**Fig 3C-D**).

Next, we used LRLoop [63], which was developed based on NicheNet [64], to predict significant ligand-target interactions between TM cells and other local endothelial cells that are relevant to AH drainage (**Figure 4A-D**). TGF-β ligands (*Tgfb1*, 2, & 3) were predominantly expressed in TM1 cells. By contrast, TM2 cells expressed molecules critical for vascular function, such as *Angpt1*, *Vegfa*, and *Edn3* (**S11A-D Fig**) [65–67]. These TM-secreted molecules have been directly associated with SC maintenance and IOP [68–71].

Comparison to human TM cells

We next worked to relate our findings to human data. We compared marker genes for each of our TM cell subtypes to sequenced human TM cells from two previous studies [31, 33]. These previous studies differed in the number of human TM cell subtypes that they reported and in the identities of their clusters. Van Zyl et al. identified three TM cell subtypes that they called JCT, beam A, and beam B [31], whereas Patel et al. identified two subtypes that they called fibroblast-like and myofibroblast-like [33]. TM1 marker genes were most enriched in Van Zyl et al's human JCT cells (**S12A Fig**). Similarly, *Dcn* was expressed in mouse TM1 cells and was localized to fibroblast-like TM cells adjacent to SC by Patel et al. TM1 cell nuclei were typically shorter with greater sphericity than the elongated endothelial-like nuclei of TM3 cells (**S13A-D Fig**). This nuclear morphology was more consistent with a JCT than beam cell identity.

Together, these data support a JCT identity for TM1 cells. TM2 cells were more closely related to human beam A and beam B cells than to the JCT cells reported by Van Zyl et al (**S12B Fig**). TM2 cells also shared expression of the *RSPO2* marker gene with the human myofibroblast-like cells reported by Patel et al. Together, this suggests that TM2 cells are myofibroblast-like beam cells. TM3 cells also shared marker genes with Patel et al's myofibroblast-like cells (*TAGLN* and *ACTA2*), suggesting TM3 cells are also beam cells. There was relatively equal TM3 marker gene enrichment across all human TM cell subtypes of Van Zyl et al (**S12C Fig**). Nuclei immediately adjacent to TM2 and TM3 cell marker staining had an elongated, endothelial-like shape (S13A-C Fig). This nuclear morphology was also consistent with the location of TM2 and TM3 cells on beams and analogous to the endothelial-like morphology of human beam cells [2].

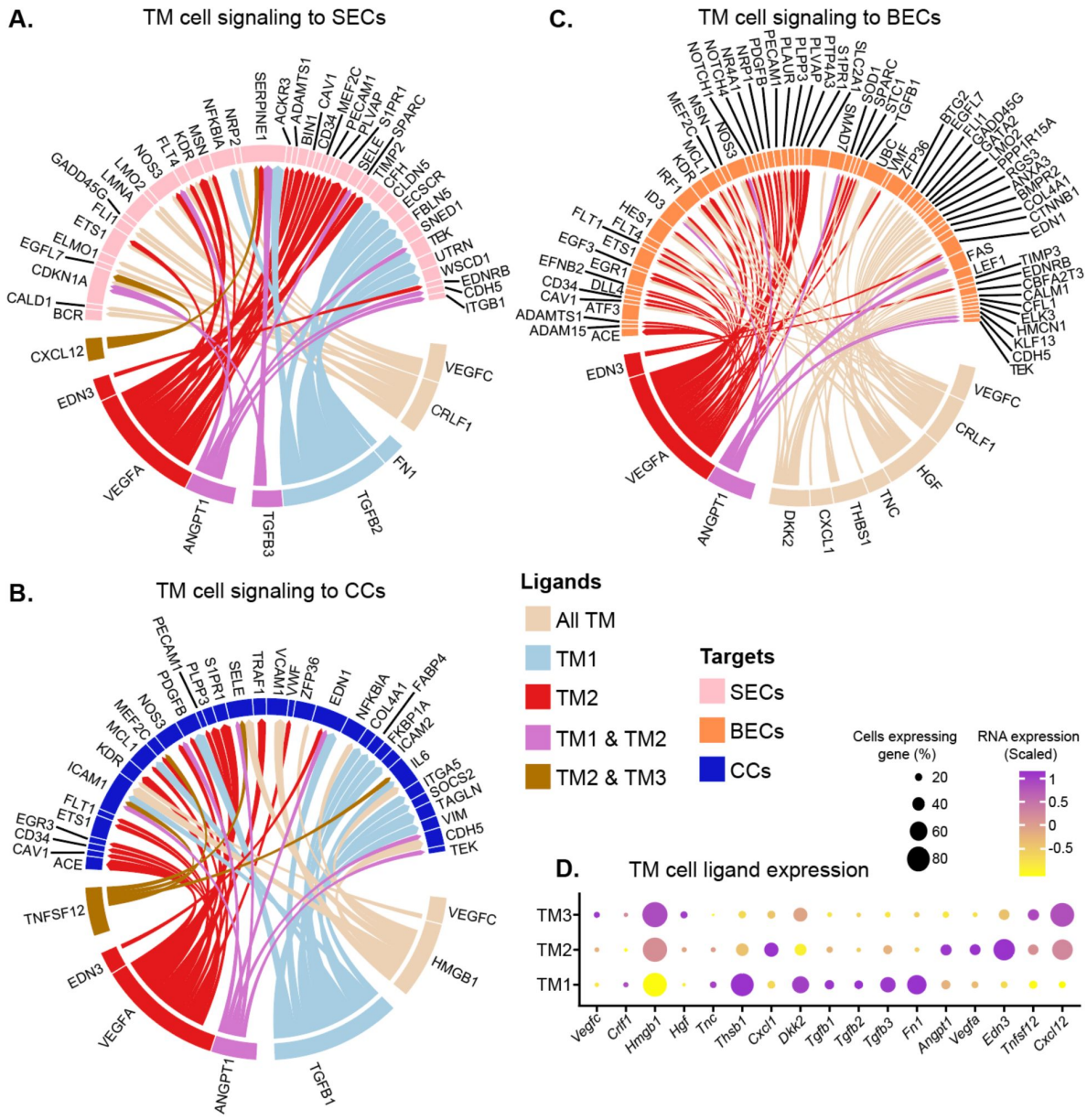

Fig 4.

Signaling interactions directed from TM cells to Schlemm's canal and vascular endothelial cells differ across TM subtypes.

(A) Circos plot showing the top predicted interactions between TM cell ligands and Schlemm's canal endothelial (SEC) target molecules. The top predicted targets in all TM cells are split by their expression across subtypes. TM1 and TM2 participate in more predicted signaling events compared to TM3. TM1-biased ligands include members of the *Tgf-β* and fibronectin signaling families. Various endothelial trophic factors are predominantly expressed in TM2 including endothelin 3, vascular endothelial growth factor A, and angiopoietin 1. See Table S4 for comprehensive list of ligand-target interaction data. (B-C) TM cell ligands that signal to collector channel (CC) endothelial cells (B) or blood endothelial cells (BECs, C). (D) The expression of all ligands predicted to have signaling interactions with SECs, CCs, or BECs, are displayed across TM cell subtypes (Dot plot).

Next, we evaluated the expression of genes implicated in elevated IOP and glaucoma by genome-wide association studies (GWAS). TM1 and TM2 cells had similar expression levels of GWAS genes associated with IOP elevation and primary open-angle glaucoma (POAG) respectively (**S14A Fig**). TM3 cells had slightly less expression of these GWAS genes compared to TM1 and TM2. To better understand the genes driving GWAS gene enrichment in different TM subtypes, we studied pathways that are significantly enriched for GWAS genes (**S14B-C Fig**, see Table S5 for complete list). TM1 cells were the most enriched for genes involved in ECM organization, cell-substrate adhesion, and growth factor stimulus (**S14D Fig**). All 3 TM subtypes had similar expression of GWAS genes associated with hormone stimulus, *Vegf* signaling, and *Rho* kinase signaling. TM3 cells expressed lipid and carbohydrate mitochondrial metabolism pathway genes at higher expression levels and in more cells than did TM1 and TM2 cells (**S14E Fig**). The same was true for actin binding-associated GWAS genes in TM3 cells versus TM1 and TM2. Genetic variation in lipid and carbohydrate mitochondrial metabolism pathways is associated with IOP elevation and glaucoma [61].

Regulation of TM cell gene expression

To better understand the overlap and differences in transcriptional control of TM cell gene expression, we performed single-cell resolution multiome sequencing. Using limbal strip tissue isolated from a separate cohort of mice than those used for scRNA-seq, we simultaneously performed both single nucleus RNA sequencing (snRNA-seq) and snATAC-seq. We thus captured both gene expression and open chromatin data throughout the genome in the same cell. Using the snRNA-seq data, we clustered cells into various cell types. The generated clusters and their marker genes generally agreed with our scRNA-seq analyses (**Fig 5A-B**, **S15A Fig**). Notably, there was a significant correlation between gene expression (RNA-based clustering) and chromatin accessibility (ATAC-based clustering) with adjusted Rand index of 0.20 ($p < 0.001$, permutation test, S15B-D Fig). This included an increase in chromatin accessibility at the promoters of marker genes in their respective TM cell subtypes (**Fig 5C-E**). To discover the key transcriptional regulators within TM cells, we examined the correlation between the expression of each transcription factor (TF) and their chromatin accessibility at predicted binding sites within all TM cells. Various TFs that either activated or repressed transcriptional activity exhibited good correlations with gene expression across TM cells (**Fig 5F**). Such activating TFs include *Tcf21*, *Arid3b*, and *Myc*, while repressing TFs include *Meox2*, *Junb*, and *Sox6*. Notably, *LMX1B*, an important gene in glaucoma GWAS [28, 34–38], is among the most strongly activating TFs in TM cells.

Metabolism-supporting treatment lessens IOP elevation in *Lmx1b*^{V265D} mice

To evaluate the utility of our new TM cell atlas, we used it to examine how *Lmx1b* mutations affect the TM cell transcriptome and to identify potential mechanisms underlying IOP elevation. We selected LMX1B because it causes IOP elevation and glaucoma in humans and was identified as a highly active transcription factor in our TM cell dataset. To do this, we analyzed scRNA-seq data generated for limbal cells from mice with a dominant mutation in *Lmx1b* (*Lmx1b*$^{V265D/+}$), which included 2,491 *Lmx1b* mutant TM cells. These mutant C57BL/6J mice develop early onset IOP elevation [39, 40, 72]. We compared gene expression in *V265D* mutant TM cells after integration with our wild-type data (all data B6 background and postnatal day 60, **Fig 6A**, **S16A Fig**). Results show that *Lmx1b* is minimally expressed in TM1 and TM2 but is highly expressed in TM3 cells (**Fig 6B**). Next, we analyzed DEGs and pathway differences between WT and *V265D/+* cells across each TM cell subtype. Across all TM subtypes, various genes related to ECM function and growth factor signaling were downregulated in mutants, including glycosaminoglycans and insulin growth factor binding proteins (**Fig 6C**, S6 Table for complete list of pathways). Pathways enriched in mutant TM cells were associated with ribosome and calcium signaling. We then examined the differential responses to the *Lmx1b* mutation by analyzing pathways dysregulated in each TM subtype that were not common across all TM cells

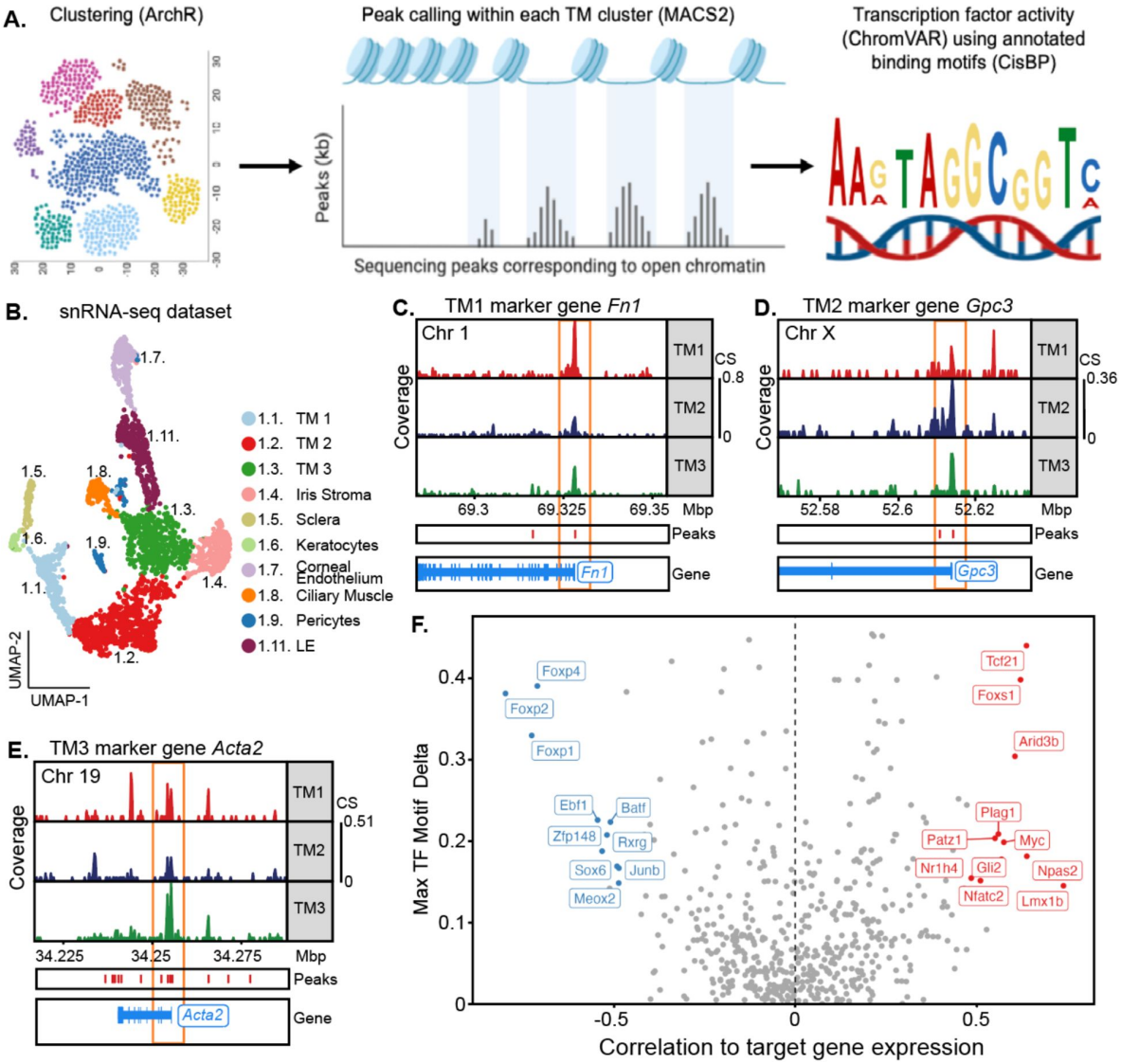

Fig 5.

Transcription factors dictating gene expression in TM cells

(A) A schematic representation of the pipeline used to identify open chromatin sites and active transcription factors (TFs). Individual cells were profiled using both single nucleus (sn) RNA and ATAC sequencing (multiome). TM cell clusters were identified using the snRNA-seq data, while significantly open chromatin regions were identified using the snATAC-seq data. Active TFs were determined based on the odds ratio of TF binding motifs within these open chromatin regions. Schematic created with *BioRender.com* (see *here* and *here*). **(B)** UMAP of subclusters derived from TM cell containing cluster (cluster 1) in the snRNA-seq data. **(C-E)** Example ATAC tracts for the promotor regions of selected marker genes for TM1 (C), TM2 (D), and TM3 (E). Each of these marker genes has greater promoter accessibility in the TM cell subtype in which its RNA expression is enriched (orange box). The aligned marker gene positions are shown. Coverage = normalized ATAC signal reads in transcription start site. CS = coverage scale. **(F)** Correlations between RNA expression levels (snRNA-seq dataset) of each TF and the chromatin accessibility levels (snATAC-seq dataset) of their respective predicted target binding motifs across all TM cell subtypes (see Methods). Select TFs with strong positive (red) or negative correlations (blue) are named.

(**Fig 6D-F**, S16B Fig). *V265D* mutant TM1 cells had a downregulation of collagen synthesis/metabolism gene expression relative to WT cells, particularly in the production and turnover of fibrillar collagens. TM2 cells with *Lmx1b* mutations had upregulation of immune signaling pathways. The highly *Lmx1b* expressing TM3 cells exhibited perturbed mitochondrial metabolism, with a downregulation of genes in complex I and ATP synthase. In addition, mutant TM3 cells showed an upregulation of protein tagging genes. However, there is a downregulation of the polyubiquitin precursor gene (*Ubb*, P = 4.5E-30), indicating a general dysregulation of pathways that tag proteins for degradation. These results document altered mitochondrial function and proteostasis in TM3 cells. Although the documented gene expression changes strongly suggest metabolic and mitochondrial dysfunction, they do not directly prove it. Using electron microscopy to directly evaluate mitochondria in the TM, we found a reduction in total mitochondria number per cell in mutants (P = 0.015, **Figure 6G**). In addition, mitochondria in mutants had increased area and reduced cristae (inner membrane folds) in mutants consistent with mitochondrial swelling and metabolic dysfunction (all P < 0.001 compared to WT, **Figure 6G-H**).

Our findings most strongly implicate perturbed metabolism within TM3 cells as responsible for IOP elevation in an *Lmx1b* glaucoma model. Nicotinamide (NAM) is known to boost nicotinamide adenine dinucleotide (NAD), supporting healthy metabolism/ mitochondrial function [73, 74]. Thus, we hypothesized that the metabolic abnormalities in TM3 cells underlie the IOP elevation that causes glaucoma, and that NAM treatment may protect the *Lmx1b* mutant TM. Beyond *LMX1B*, this hypothesis is relevant more commonly to POAG treatment because metabolism-relevant genes are implicated by GWAS (and their expression is enriched in TM3 cells, S14E Fig). To test our hypothesis, we treated mice by adding NAM to their drinking water starting at postnatal day 2 and continuing into adulthood. Results showed that NAM supplementation significantly protected against anterior chamber deepening (ACD, a symptom of IOP elevation, **Fig 7A-B**) and IOP elevation (**Fig 7C-D**). These results support NAM as a treatment to prevent TM damage and IOP elevation in LMX1B-mediated glaucoma with potential general relevance to POAG.

Discussion

This study provides a comprehensive multimodal analysis of mouse limbal cells that focuses on the TM. We defined three TM cell subtypes with unique marker panels that can be used for their identification across different strains, laboratories, and processing methods. We validated key marker gene expression by IF and ISH, discovering biases for specific TM subtypes to reside in different parts of the TM. For example, TM1 cells have a location bias for the outer, posterior TM while TM3 cells are more abundant in the inner, anterior TM. Importantly, our pathway analyses suggest that the different TM subtypes have overlapping roles. All 3 TM subtypes are enriched in ECM synthesis and ECM metabolism compared to other limbal subtypes. However, there is also compartmentalized enrichment of some processes to specific subtypes. For example, ECM production and turnover, secreted ligand signaling, debris removal, immune surveillance, actin-associated cell contraction and increased metabolic gene activity (as discussed below) are enriched in specific cell-subtypes. Using ATAC-seq data, we discovered key TFs controlling gene expression in TM cells, including LMX1B. Importantly, we implicate LMX1B in metabolic control in TM cells. More specifically, we demonstrate that *Lmx1b* is the most active TM cell TF and is enriched in TM3 cells, while mutation of *Lmx1b* induces prominent mitochondrial defects in TM3 cells. Finally, we show that therapeutically targeting TM3 dysfunction with a mitochondrial/ metabolism supporting nutrient (nicotinamide) protects from IOP elevation in the *Lmx1b* glaucoma model. We also suggest that a TM3-like cell is generally relevant to metabolic pathways in human glaucoma based on enriched expression of human glaucoma GWAS gene in TM3 cells. Together these data provide a wealth of new molecular information about TM cells and suggest a new approach for preventing IOP elevation.

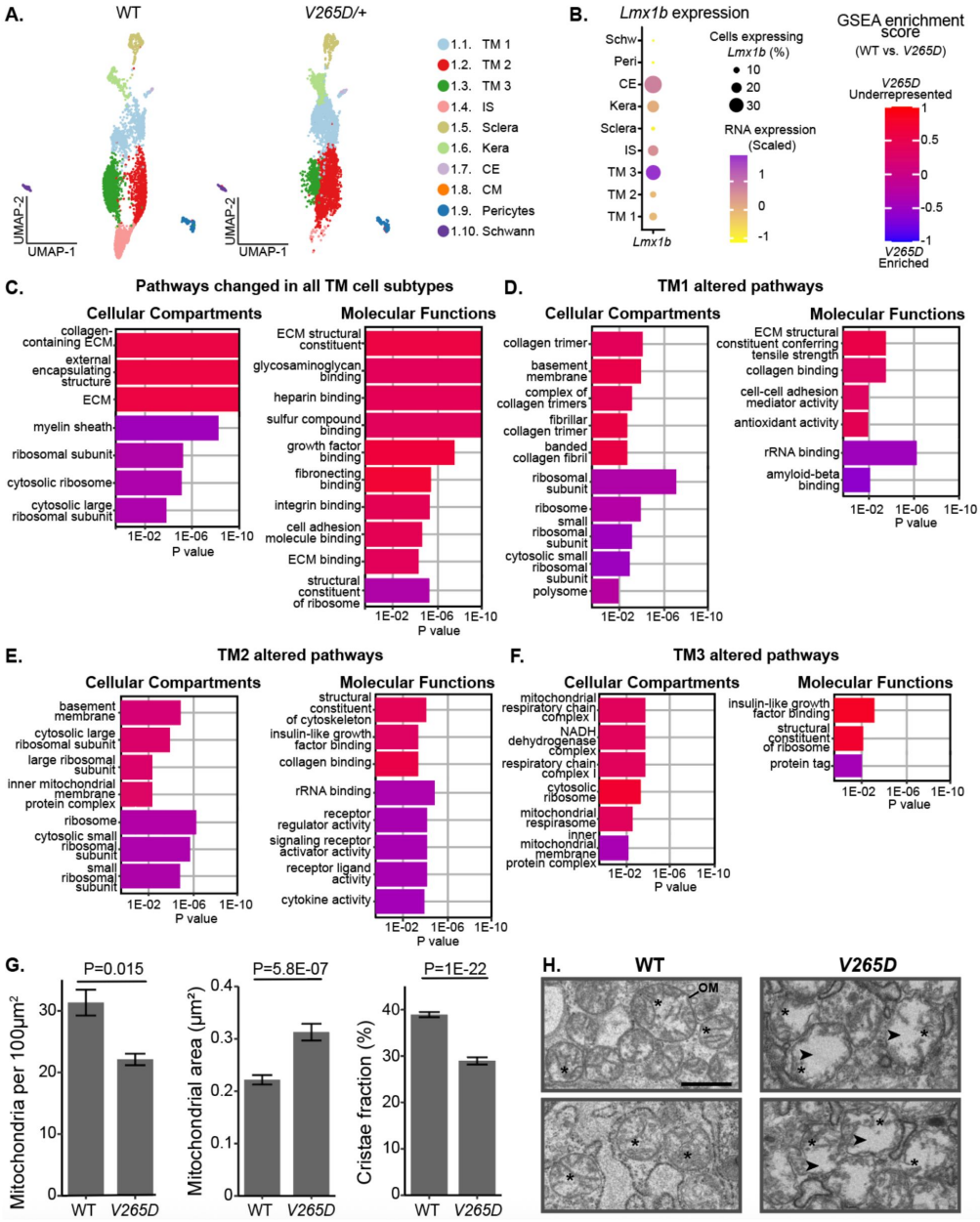

Fig 6.

Differential molecular responses of TM cell subtypes to an *Lmx1b* mutation

(A) UMAPs of limbal cells from WT and *Lmx1b*$^{V265D/+}$ (*V265D*) mutant mice (both genotypes B6 background). **(B)** *Lmx1b* expression across limbal cell types. *Lmx1b* expression is highest in TM3 cells. **(C)** Pathways that are changed in all TM cell subtypes. **(D-F)** Top pathways that are significantly altered when comparing each indicated TM cell subtype across genotypes. Many of these pathways were not significantly changed when comparing all TM cell subtypes as a group, indicating that the *V265D*-induced changes are strongest within each TM cell subtype. *V265D* has a pronounced effect on mitochondrial pathways in TM3 cells but much less so in other TM cells. ECM = extracellular matrix. ECS = extracellular structure. **(G)** Mitochondria in *V265D* mutant TM cells are reduced in number per cell, have increased area, and decreased cristae area (cristae fraction is ratio of area occupied by cristae: total area of mitochondria; shown as bar plots with standard error). A total of 160–180 mitochondria were analyzed across 3 eyes per genotype (approximately 60 mitochondria per eye). Groups were compared using Student's t-test. **(H)** Representative images show mitochondria defined by their outer membranes (OM) and inner membrane folds (cristae). Asterisks indicate a subset of representative cristae for each genotype. Mutant mitochondria exhibit increased area (space enclosed by the OM) and disorganized cristae structure. Arrows highlight regions in mutant mitochondria that lack cristae. Scale bar = 500 nm.

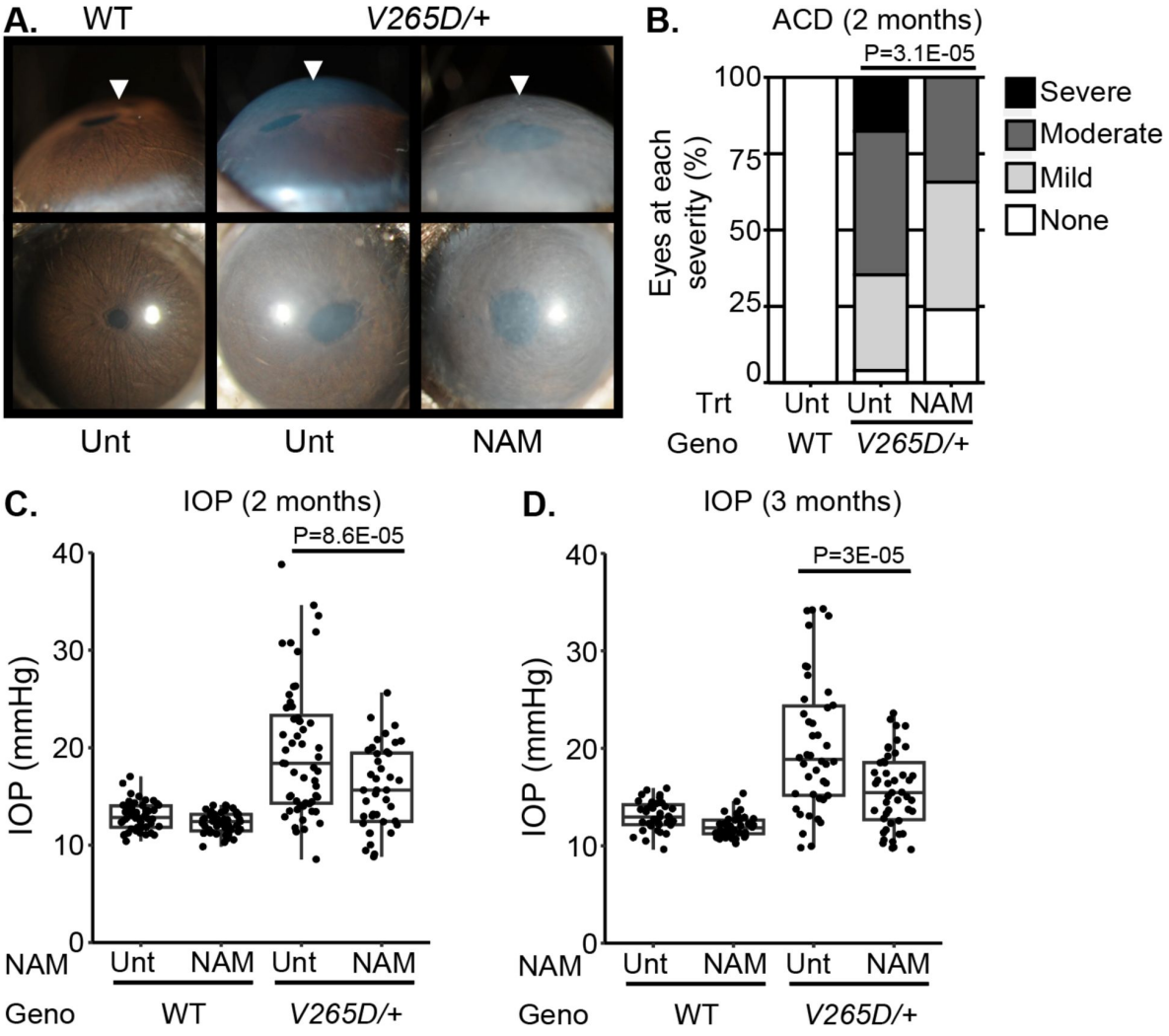

Figure 7

Nicotinamide treatment protects from IOP elevation in *Lmx1b* mutants.

(A) Representative photos of eyes from mice of the indicated genotypes and treatments (UNT = untreated, NAM = nicotinamide treated, 550mg/kg/day provided in drinking water). NAM treatment substantially lessens anterior chamber deepening (ACD), a sensitive indicator of IOP elevation in mice. The WT and NAM-treated mutant eyes have very shallow anterior chambers while the untreated mutant eye has an obviously deepened chamber (arrowheads). **(B)** Distributions of anterior chamber depth based on previously defined scoring system [40]. Groups compared by Fisher's exact test. **(C-D)** Boxplots of IOP (interquartile range and median line) in WT and mutant eyes of both NAM treated and untreated groups. NAM treatment significantly lessens IOP elevation in mutants compared to untreated mutant controls. Groups compared by ANOVA followed by Tukey's honestly significant difference (see Table S7 for additional statistics). n ≥ 35 eyes examined in each WT group and n ≥ 40 in *V265D* mutant groups. Geno = genotype.

Mouse trabecular meshwork subtype classification

Here we provide evidence for three TM cell subtypes in mice that are robust across datasets from different institutions, using different tissue processing and sequencing protocols. Although others [24, 51] subdivided TM cell subtypes beyond the three defined in the present study, at this point we decided against further subdivision (See Figure S5) for the following reasons. We lacked confidence in the higher resolution clustering, as it was not consistent across datasets, did not produce unique marker gene sets, and could have resulted in over-clustering due to stochastic or stress-induced differences between subpopulations of cells. Moreover, the number of reported mouse TM cell clusters in previous studies were inconsistent. Although three TM subtypes were reported by Van Zyl et al. and Ujiie et al. [31, 51], the molecular features of cells in these clusters were not the same across these studies. Differences between studies may be due to batch effects, different computational methods and possibly over-clustering. Most importantly, there was very limited validation by IF, IHC, or other methods in previous studies.

Only the JCT type of TM cell in these previous studies was assessed by means other than scRNA-seq (IF and ISH) [31]. Additionally, Thompson et al. treated cells with Y27632, a ROCK inhibitor, which could alter TM cell transcriptomes. It is also important to point out that both Thompson et al. and Van Zyl et al. used albino mouse strains, which can impact TM cell development and function [75]. Finally, Ujiie et al. sequenced TM cells at 3-4 weeks, which is prior to full maturation of the TM structure [30], while our ongoing developmental studies show substantial molecular maturation of TM cells between P21 and P60.

As Van Zyl et al's data is deposited in the Broad Institute's single-cell portal, we further compared their data with ours. Although both Van Zyl et al. and our current paper identified 3 TM subtypes, our work does not fully agree. Some of the cells named beam A and beam Y by Van Zyl et al. express markers present in our TM2 cell subtype, while others express markers that are absent in TM2 cells but present in our scleral cells. Our IF studies confirm that these discordant markers are not expressed in TM cells, but instead show that they are in fact scleral cells. These scleral cells highly express fibroblast markers including *Mfap5*, *Clec3b*, and *Tnxb*, suggesting they are scleral fibroblasts. Cells initially named uveal cells by Van Zyl et al. (and subsequently by Ujiie et al. and Thompson et al.) express markers of our TM3 cells. Consistent with our gene expression data, our IF shows that these Van Zyl markers are expressed by cells that are primarily located in the TM region that is closer to the cornea and not in the uvea or the TM region adjacent to the uvea. Thus, our current study resolves some previous inconsistencies in classifying mouse TM cell subtypes. It lays a firmer foundation for continued understanding of TM cell types and their biology. Moving ahead, sequencing cells at greater depths will enhance TM cell characterization and improve comparisons between datasets.

Differential roles of specific mouse TM cell subtypes and comparison to human

As a group, all TM cells share various molecular properties that distinguish them from other ocular cells. Our analyses determine the expression of IOP, and glaucoma genes identified by GWAS in TM cell subtypes as well as in other limbal cells. Pathways enriched across all TM cell subtypes based on RNA-seq are largely related to ECM (including collagens, integrins, and glycosaminoglycan pathways), cell-cell signaling, and growth factor signaling. This fits with an essential role of the TM in both ECM synthesis/turnover and in signaling to the SC to maintain IOP [24, 26, 27, 76, 77]. In addition, the expression of genes that we document generally agrees with the literature. For example, the following genes and signaling molecules have been reported in TM cells, WNT signaling [78], TGF-β signaling [79–85], integrin binding [86–88], actin cytoskeletal networks [89], calcification genes [90, 91], and Myocillin [91–94].

Additionally, genes associated with intermediate filaments, which function in determining cell shape and structure and can also act as mechanical stress absorbers [95], are underrepresented in TM cells. Lower levels of intermediate filaments may enable TM cells to alter their shape to respond to changes in IOP.

Mouse TM1 cells closely resemble sequenced human JCT cells. Like human JCT cells, the majority of TM1 cells are located nearest to the SC inner wall, particularly adjacent to the posterior of the mouse SC. Human JCT cells are generally accepted to be embedded in a more diffuse ECM and to not cover the collagenous trabecular beams [2, 10, 11]. In vivo, a proportion of TM1 cells have a shorter, more spherical nuclear morphology, consistent with JCT cell identity. Importantly, the JCT region is critical in determining resistance to AH outflow and in regulating IOP [5, 12, 27, 96]. JCT cells have fibroblast-like properties, including the secretion of ECM proteins and degradation enzymes to support continuous ECM remodeling [2, 76, 97]. The subset of TM1 cells that lie distant from SC have more beam cell-like, elongated nuclear morphology. This suggests that either our TM1 cluster contains more than 1 TM cell subtype or that the morphology of a single TM1 cell subtype is influenced by local environment. This needs to be resolved by future studies. Compared to the other TM cell subtypes, TM1 cell pathways are enriched in both ECM structural molecules, such as collagens and integrins, and TGF-β signaling, which increases ECM production [98]. Notably, excessive TGF-β signaling and ECM production can lead to fibrosis and elevate IOP [82, 99–102]. TGFβ2 has also been shown to cause ocular hypertension both *in vivo* [79–81] and *ex vivo* [82, 83] and is elevated in POAG patients [103, 104]. These data suggest that TM1 cells play an important role in the constant remodeling of the ECM. However, dysregulation of these pathways can be pathogenic.

TM2 cells molecularly resemble previously sequenced human TM beam cells [31, 33]. This includes overlap of expression of top TM2 signature gene expression with sequenced human beam cells. Consistent with a beam cell identity, TM2 cells are located more towards the mid and inner TM than most TM1 cells. TM2 cells have an elongated nuclear morphology, consistent with the previously established beam cell morphology of cells in the regions they occupy [2, 30, 105]. Beam cells have endothelial-like properties, such as maintaining the patency of the AH outflow tract through the production of antithrombotic molecules. Proteases and molecules classically known as antithrombotic and thrombolytic maintain fluid flow through the TM by preventing build-up of protein aggregates to maintain fluid drainage [5, 27]. Such molecules include glycosaminoglycans, like heparin, the serine protease tPA and matrix metalloprotease that are all highly expressed in TM2 cells. Beam cells are also phagocytic and this activity along with turnover of ECM further cleans the TM (called filtering) to enhance fluid drainage [2]. Human Beam cells also participate in antigen presentation and modulation of inflammation through cytokines and major histocompatibility proteins [2, 106], consistent with TM2 cells being enriched for these immune pathways/ molecules. Additionally, our data suggest that signaling from TM2 cells to SC endothelial cells is mediated by soluble molecules including *Vegfa*, *Edn3*, and *Angpt1*, which are critical for SC maintenance and function. This links TM2 cells to ocular development and glaucoma. VEGF receptor and ANGPT signaling genes modulate SC development/ function as well as contribute to developmental and primary open-angle glaucoma [25, 34, 35, 68, 107–109].

TM3 cells also have a location and elongated nuclear morphology resembling beam cells with enriched localization in the inner, anterior TM. TM3 cell-enriched processes include actin binding, and modulation of the actomyosin system, which is known to modulate outflow resistance and IOP [21, 22]. As such, TM3 cells express a large percentage of glaucoma-associated genes involved in actin binding at a high level. Importantly, TM3 cells are enriched for various mitochondrial metabolic and antioxidant pathways, including those associated with IOP elevation and glaucoma [60, 61]. Inhibiting metabolic pathways alters AH outflow resistance [89]. Since maintaining contractile tone is an energy-intensive process [110], this could explain the enrichment of energy metabolism pathways in TM3 cells compared to other TM cells.

TM3 cells have a unique susceptibility to mitochondrial dysfunction

In addition to being enriched in mitochondrial/ energy metabolism processes, TM3 cells express *Lmx1b* at significantly higher levels than both the other TM cell subtypes and other limbal cells. Importantly, in heterozygous mutant *V265D/+* mice, TM3 cells had pronounced gene expression changes that implicate mitochondrial dysfunction, but that were absent or much lower in other cells including TM1 and TM2. In sections of the inner TM (enriched for TM3 cells), we show that the inner membrane folds known as cristae are disrupted or lacking in mutant mitochondria.

Cristae disruptions are well established to disrupt cellular metabolism, impair oxidative phosphorylation, reduce ATP synthesis, alter mitochondrial membrane potential, and elevate ROS production [111–115]. Together, these data suggest that mutation of *Lmx1b* has a primary effect on metabolism in TM3 cells that subsequently leads to IOP elevation and then glaucoma. Relevantly, homozygous conditional knockout of both *Lmx1b* and *Lmx1a* as well as siRNA knockdown of *Lmx1b* alone impact mitochondrial functions in neurons and may contribute to Parkinson's disease [116–118]. Our data extend these published findings by showing that inheritance of a single dominant mutation in *Lmx1b* similarly affects mitochondria in TM cells.

Although our studies show a clear effect of the *Lmx1b* mutation on mitochondria, future studies are needed to determine if LMX1B directly modulates mitochondrial genes in *V265D* mutant TM cells.

In addition to modulating mitochondria, LMX1B was recently identified as a TF that regulates responses to cell stress. This includes promotion of autophagy under stress conditions to enable recycling of cellular resources to maintain cellular functions and enable survival [116]. Thus, mutation of *Lmx1b* may also result in a deficiency of the beneficial autophagic response to stress [116]. Although further experiments are needed, dysfunctional autophagy may further prolong and exacerbate TM cell stress, resulting in more extensive depletion of cellular resources, exacerbated cellular dysfunction, and IOP elevation. Other consequences of the *Lmx1b* mutation that were evident in the *V265D/+* cells may also contribute to IOP elevation, including the overexpression of genes associated with ribosomes and calcium signaling, and depletion of genes involved with ECM synthesis and metabolism. However, these processes were not limited to TM3 cells or even to cell types that express detectable *Lmx1b*, suggesting that they are secondary damaging processes that are subsequent to the initiating, *Lmx1b*-induced perturbations in TM3 cells. Thus, we hypothesize that mitochondrial abnormalities in TM3 cells are of primary importance to IOP elevation in *V265D/+* glaucomatous mice.

Nicotinamide protects against IOP elevation in *Lmx1b*^{V265D}-mutant mice

Based on our findings in TM3 cells, we tested if mitochondrial and metabolic disturbances are important in IOP elevation by administering nicotinamide (NAM). NAM is a form of vitamin B3 that is well-established to boost NAD^+ levels, promote mitochondrial health and energy metabolism, relieve oxidative stress and thus promote cellular resilience [74, 119–125].

Supporting our hypothesis of primary metabolic dysfunction in TM3 cells, NAM treatment strongly protected *V265D/+* mice from IOP elevation. Thus, treatments that support normal metabolism may protect from IOP elevation in individuals with *LMX1B* variants including both developmental glaucoma and POAG patients [28, 34–37, 126–129]. As NAM and other NAD^+ boosting treatments are also known to be directly neuroprotective in glaucoma [74, 130–133], our current data suggest that such treatments will have a double benefit for patients. As mitochondrial

defects are becoming broadly associated with glaucoma risk and progression [134–138], these treatments could have wide-ranging potential to complement and augment existing IOP-lowering therapeutics through a completely distinct mechanism.

Our results provide a thorough molecular characterization of mouse TM cells, providing much needed molecular information on subtype specializations in regulating IOP and the roles of specific subtypes in glaucoma. This comprehensive TM atlas provides a new foundation to guide development of new glaucoma treatments. We validate its utility by implicating metabolic changes in a single TM cell subtype in both mouse and human glaucoma, with success of a metabolic treatment targeting this subtype in a glaucoma model.

Materials and Methods

Animal husbandry and ethics statement

Experimental animals were either C57BL/6J (Stock# 664) or 129/Sj (unique substrain of 129) [40] inbred mice. The *Lmx1b*^{V265D} mutation was discovered in an N-ethyl-N-nitrosourea (ENU) mutagenesis screen [39, 40, 139]. These mice were then backcrossed to the C57BL/6J (Stock #000664) for at least 30 generations. All mice were treated in accordance with the Association for Research in Vision and Ophthalmology's statement on the use of animals in ophthalmic research. The Institutional Animal Care and Use Committee of either Columbia University or Duke University approved all experimental protocols performed at their respective institutions.

Mice were maintained on PicoLab Rodent Diet 20 (5053, 4.5% fat) and provided with reverse osmosis-filtered water. Mutant and control littermates were housed together in cages containing ¼-inch corn cob bedding, covered with polyester filters. The animal facility was maintained at a constant temperature of 22°C with a 14-hour light and 10-hour dark cycle.

Genotyping of the *Lmx1b* allele

Lmx1b^{V265D} and *Lmx1b*$^{+}$ genotypes were determined by direct Sanger sequencing of a specific PCR product. Genomic DNA was PCR amplified with forward primer 5'-CTTTGAGCCATCGGAGCTG-3' and reverse primer 5'-ATCTCCGACCGCTTCCTGAT-3' using the following program: (1) 94 °C for 3 min; (2) 94 °C for 30 s; (3) 57 °C for 30 s; (4) 72 °C for 1 min; (5) repeat steps 2–4 35 times; and (6) 72 °C for 5 min. PCR products were purified and sequenced by the Genewiz (Azenta Life Sciences).

Slit-lamp examination

Anterior eye tissues were initially examined approximately at 2 months of age. Balanced groups of males and females were examined. Photographs were taken with a 40× objective lens.

Phenotypic evaluation included the same disease features found in past studies of *Lmx1b*-mutant mice [39, 40]. Anterior chamber deepening was graded based on a semiquantitative scale of phenotype being not present, mild, moderate, or severe in presentation [40]. Groups were compared statistically by Fisher's exact test. n > 30 eyes examined in each group.

IOP measurement

IOP was measured with the microneedle method as previously described in detail [140, 141]. Prior to cannulation, mice were acclimatized to the procedure room and anesthetized via an intraperitoneal injection of a mixture of ketamine (99 mg/kg; Ketlar, Parke-Davis, Paramus, NJ, USA) and xylazine (9 mg/kg; Rompun, Phoenix Pharmaceutical, St Joseph, MO, USA) immediately prior to IOP assessment, a procedure that does not alter IOP in the experimental window [141]. IOP was measured at both 2 months and 3 months of age in WT and *Lmx1b*$^{V265D/+}$eyes. Balanced

groups of males and females were examined. During each IOP measurement period, eyes of independent WT B6 mice were assessed in parallel with experimental mice as a methodological control to ensure proper calibration and equipment function. *Lmx1b* mutant groups compared by ANOVA followed by Tukey's honestly significant difference. n ≥35 eyes examined in each WT group and n ≥ 40 in *V265D* mutant groups.

NAM administration

Nicotinamide (NAM or niacinamide; Sigma-Aldrich, St. Louis, Missouri) was dissolved in the standard institutional drinking water to a dose of 550 mg/kg/day (low dose) based on the average volume adult mice consume. Untreated groups received the same drinking water without NAM. Water was changed once per week. Treatment was started at postnatal day 2 and continued throughout the experiment. Births were checked daily between 9am-12pm to determine the pup's age.

Sequencing

Preparation of ocular cells

Columbia animals

Eyes were pooled from 4 animals to generate 1 sample (8 eyes total per pool). Two independent samples were processed. Mice were 2 months of age. Sex was balanced in each group.

Duke animals

One sample was generated from a pool of 4 animals (8 eyes total). All mice were male. Mice were 3 months of age.

Dissections

After euthanizing the animals, eyes were enucleated into fresh Dulbecco's Modified Eagle Medium (DMEM; Gibco) and subsequently dissected in DMEM. All dissection tools and surfaces were treated with RNAse zap (Ambion). For dissections, we removed the posterior eye by cutting between the limbus and sclera. The lens was then removed. Finally, we made a small circular cut in the anterior cornea, removing the middle $1/3^{rd}$ of the area. Only limbal tissues were collected and all other tissues were removed. The remaining limbal tissue was minced and prepared for digestion.

Single Cell RNA Sequencing

Single-cell RNA sequencing (Columbia University): Tissues were digested enzymatically using Papain and Deoxyribonuclease I (Worthington Biochemical Corporation, Cat. no. LK003153) for 20 min at 37°C and stopped using Earl's balanced salt solution (EBSS, Thermo Fisher Scientific, Cat no. 24010-043). Cells were triturated using an 18-gauge needle, centrifuged at 300g at 4 °C, washed with cold DMEM, and filtered using a 100 μm Flowmi Cell Strainer (H13680-0040, Bel-Art. Cells were resuspended in cold DMEM and placed on ice immediately. Cells were counted using Countess II automated cell counter and processed for 10x library preparation immediately (see below). All data will be deposited in the Gene Expression Omnibus (GEO) database and single cell portal.

Single-cell RNA sequencing (Duke University): Single cell dissociation was performed using Collagenase IV (Worthington Biochemical Cat. no. LS004188), Dispase II (Sigma Cat. No. D4693) and DNAse I (Roche Cat no. 50225500) for 60 min and then trypsin/EDTA for 10 min at 37°C. Cells were triturated using a 1 ml pipette tip, centrifuged at 300g at 4°C, washed with cold DMEM containing

10% FBS, and filtered using a 70 µm cell strainer (Fisher). Cells were resuspended in cold DMEM containing 5% FBS and placed on ice immediately and sent to Duke Genome Core Facility. Cells were counted using Countess II automated cell counter (the cell viability was 88%) and then immediately processed immediately (see below). All data will be deposited in the Gene Expression Omnibus (GEO) database and single cell portal.

Multiome (Columbia University): Limbal strip samples for multiome analysis were snap-frozen on dry ice immediately following dissection and stored at −80C until processing. To isolate nuclei, tissue was homogenized in 100 µL of chilled lysis buffer (10 mM Tris-HCl, pH 7.4, 10 mM NaCl, 3 mM MgCl2, 0.1% NP40, 0.1% Tween20, and 0.01% digitonin – from [142] supplemented with 1% BSA). Afterwards, samples were incubated for 5 min on ice, gently agitated by pipetting, and incubated for an additional 10 minutes on ice. We then added 1 mL of chilled wash buffer (10 mM Tris-HCl, pH 7.4, 10 mM NaCl, 3 mM MgCl2, 0.1% Tween 20, 1% BSA) to the cells and centrifuged at 500 rcf for 5 min at 4°C. Cells were resuspended in chilled Diluted Nuclei Buffer (PN-2000153, 10x Genomics) and filtered through a 40 µm Flowmi Cell Strainer (H13680-0040, Bel-Art). Cells were resuspended in cold DMEM and placed on ice immediately. An aliquot of nuclei suspension was stained with SYTOX green to count nuclei using Countess II automated cell counter and processed for 10x library preparation immediately (see below). All data will be deposited in the Gene Expression Omnibus (GEO) database and single cell portal.

Single-cell and single-nucleus RNA-seq was performed at the single-cell sequencing core in Columbia Genome Center (Columbia University) or Duke Molecular Genomics Core (MGC, Duke University). Single cells or nuclei were loaded into chromium microfluidic chips with v3 chemistry and barcoded with a 10x chromium controller (10x Genomics). RNA from the barcoded cells was reverse-transcribed, and sequencing libraries were constructed with a Chromium Single Cell v3 reagent kit (10x Genomics). Sequencing at both institutions was performed on NovaSeq 6000 (Illumina).

Sequencing data processing

Single cell and single nucleus sequencing

Raw reads were mapped to the mm10 reference genome by 10x Genomics Cell Ranger pipeline. “Seurat” (Version 4.0.1) [143] was used to conduct all single-cell and single-nucleus sequencing analyses. Briefly, the dataset was filtered to contain cells with at least 200 expressed genes and genes with expression in more than three cells. Cells were also filtered for mitochondrial gene expression (<20% for single-cell and <5% for single-nucleus). The dataset was log-normalized and scaled. Biological incompatibility based on gene expression was used to identify doublets. For the scRNA-seq dataset generated at Columbia scRNA-seq, we performed unsupervised clustering followed by comparison to previous annotations [24, 26, 31–33]. A resolution parameter of 0.03 was used to match these data and previous annotations. Cluster 1 was then subclustered using unsupervised methods with a resolution parameter of 0.3. All cluster identities based on a combination of known marker genes and validation experiments. For additional datasets (Duke scRNA-seq, and Columbia snRNA-seq), parameters were manually adjusted cluster cells based on the Columbia scRNA-seq dataset. Marker genes were identified using Wilcoxon test implemented in Seurat using default parameters.

Multiome

Single-nucleus multiome data were quantified by 10x CellRanger and preprocessed according to integratedSeurat v4 [143] and Signac [144]. We filtered cells which have <500 and >80000 ATAC reads, have <500 and >25000 RNA reads, and have >10% mitochondrial reads. RNA-seq processing was performed using the same methods as scRNA-seq (above). ATAC-seq processing was performed using ArchR (version 1.0.2) [145], where we used default latent semantic

indexing (LSI) approach to derive low-dimensional embedding followed by single-cell neighborhood construction and graph-based clustering using the top 50 LSI dimensions excluding the first dimension. We assigned cell types using similar process based on marker peak accesibility and transferred cell type labels to the ATAC data.

Lmx1b^{V265D} analysis

Data from limbal cells with the *Lmx1b*^{V265D} mutation (C57BL/6J background) were integrated with Wild-Type (WT) cells from the C57BL/6J strain only. Multiple approaches were used for normalizing data for integration in Seurat, including log normalization and SC transform. The relative number of cells in each cell cluster between WT and *V265D* mutant cells changed based on the integration technique. Therefore, we chose not to assess TM or other cell proportions between genotypes. Log normalization was selected for downstream analysis based on the log-transformed integrated WT clusters being more molecularly similar to the WT only clusters compared with the SC transform results.

Statistical data analysis

Hierarchical clustering

TM-containing cells were assessed by hierarchical clustering based on the similarity of the expression of the top 500 marker genes (ranked by P value) of each individual cluster. This analysis filtered out low-expressing genes (expressed in >10% of cells, with a logFC > 0.25 compared to other cells).

GO analysis

Gene ontology and pathway enrichment analysis were performed by comparing the differentially expressed genes in three scenarios:

1. All TM cells versus all other sequenced cells.
2. Each individual TM cell subtype against other TM cell subtypes.
3. WT versus *Lmx1b*$^{V265D/+}$ TM cells.

For comparisons of all TM cells to all sequenced cells, pathway enrichment was compared against a background expression universe of genes expressed in any sequenced cell. For comparisons of individual TM cell subtypes, only genes expressed in trabecular meshwork cells were used as a background (P value cut-off 0.01) [146].

Gene set enrichment analysis (GSEA) was performed using the same set of differentially expressed genes from the above comparisons with the GseGO function. All pathways were assigned an enrichment score (< 0, underrepresented; > 0, enriched). Pathways that were significantly enriched or underrepresented were also analyzed (P value cut-off 0.01). The R package ClusterProfiler was used for analysis [147].

Module score

From genome-wide association studies of IOP elevation [34, 35, 37, 129, 148–154] or primary open-angle glaucoma [28, 36, 38, 155–158], we curated a list of genes associated with the disease. Seurat's AddModuleScore function was applied to assess glaucoma disease risk for each cell type, using default parameters (24 bins for aggregation with 100 control features per analyzed feature).

Predicted ligand-receptor interactions

Predicted ligand-target links between interacting cells were identified using LRLoop [63], which was developed based on NicheNet [64]. Briefly, the expression of genes in cell types is linked to a database of signaling and gene regulatory networks curated from prior information, enabling viable predictions of potential interactions between cell types. These interactions were calculated using target molecules from one cell type and ligands from multiple cell types. The top interactions, regardless of the cell type origin of the ligand, are represented in a Circos plot. Ligands were assigned to an individual TM cell subtype/subtypes based on the following criteria:

1. Exclusively assigned to a TM cell subtype if expressed > 1 transcript per ten thousand in a given cell type and expressed on average 4X more in that subtype compared to all other TM cell subtypes.
2. Assigned to multiple TM cell subtypes if expression is > 1 transcript per ten thousand in multiple cell types and average ligand expression is < 4X between those TM cell subtypes.
3. If ligand expression is low (< 1 transcript per ten thousand) across TM cell subtypes, the ligand is assigned to all subtypes that express the ligand.

Comparison to published datasets

To compare TM cell clusters across datasets, the top 10 marker genes (by P value) for TM cell subtypes in our dataset were compared to published marker genes in other TM cell datasets [24, 31–33, 51]. Comparisons to both human and mouse TM cell data in the Van Zyl et al. dataset were performed using the Broad Institute single-cell browser: *https://singlecell.broadinstitute.org/single_cell/study/SCP780*.

ATAC

To refine ATAC-seq analysis, we applied ArchR [145] to remove any additional doublet cells and iteratively estimated LSI embedding using 500bp peaks tiled across the genome, followed by ArchR clustering and UMAP projection workflows to generate ATAC-seq cell clusters and two-dimensional embeddings (same cluster resolutions as above). Using marker gene expression, clusters were named and related to the single cell cluster identities. Using single-cell RNA-seq data collected earlier with annotated cell types, we projected single-cell ATAC-seq data onto the reference using ArchR's addGeneIntegrationMatrix function with default parameters. The integrated data with RNA-seq defined clusters were used for peak calling with MACS2, followed by marker peak identification (getMarkerFeatures) and TF enrichment (addMotifAnnotations) using the CisBP database [159]. Finally, TF activity was quantified using chromVAR [160] and gene-peak links were inferred using the addPeak2GeneLinks function with default parameters. All significant TFs (VAR > 1) for each TM cell subtype were filtered by average RNA expression within the entire cluster using the Columbia University scRNA-seq data (better read depth than snRNA-seq). All significant TFs with no RNA expression were removed and all TFs with expression > 0.5 counts per 10,000 were prioritized for analysis. For a schematic of the analysis workflow, see **Figure 4A**. We then performed integrative analysis correlating the activity of each TF with its gene expression profile (both directly measured from multiome data and integrated expression data from reference scRNA-sequencing data). We used ArchR's correlateMatrices function, which reports Pearson correlation of normalized counts (TF activity matrix and gene expression / gene integration matrix) across 100 randomly subsampled neighborhoods of cells. We designated influential TFs as those with correlation > 0.5, adjusted p-value of correlation < 0.01, and chromVAR deviation above 75% of all TFs.

ATAC tracts

We chose marker genes (TM1: *Fn1*, TM2: *Gpc3*, TM3: *Acta2*) and plotted accessibility tracks. Motif footprinting analysis was performed using ArchR getFootprints function using CisBP-defined motif positions for RNA-defined cell types with default parameters.

Immunofluorescence and in situ hybridization

Sections with antibody staining

Enucleated adult eyes were fixed for 1 hour at 4°C in 4% paraformaldehyde (PFA, Electron Microscopy Science, Hatfield, PA) prepared in phosphate-buffered saline (1X PBS, 137 mM NaCl, 10 mM phosphate, 2.7 mM KCl, pH 7.4). Following fixation, a small window was made through the optic nerve head so that eyes would not shrivel during dehydration. Eyes were dehydrated in a 30% sucrose (Sigma-Aldrich, St. Louis, Missouri) in 1X PBS at 4°C until eyes sunk to the bottom of a 2 ml glass vial. Once sunken, eyes were embedded in optimal cutting temperature embedding medium (Fisher Scientific, Waltham, MA) and flash frozen on dry ice. Eyes were cryosectioned at 10 μm thickness in the sagittal plane. Sections were evenly spaced throughout the peripheral and central ocular regions.

Sections were washed three times with 1× PBS with 0.3% Triton X-100 for 5 min to quench residual fixation. The sections were then incubated with 10% Donkey serum (Sigma-Aldrich, St. Louis, Missouri) and 0.3% Triton X-100 in 1× PBS (blocking buffer) at room temperature for 1 h to block nonspecific binding of antibody and to permeabilize the tissue. The sections were then incubated with primary antibodies (see S8 Table) in 200 μl blocking buffer overnight at 4°C. The sections were then washed three times for 5 m with 1× PBS with 0.3% Triton X-100. Primary antibodies were detected with the appropriate species-specific secondary antibody (all Alexa 488, 594, or 647 at 1:1000 dilution, Life Technologies, Grand Island, NY) diluted in 1× PBS with 0.3% Triton X-100 for 2 h at room temperature. The secondary detection solution also had DAPI at 1:1000 (Thermo Scientific, Waltham, MA) to label nuclei. The immunostained sections were washed three times for 5 m in 1× PBS with 0.3% Triton X-100. Sections were then cover-slipped using Flouromount (Sigma, St. Louis, MO).

Tyramide signal amplification (TSA)

We performed a TSA reaction for a subset of antibodies (S8 Table). TSA was performed on slides containing serial transverse cryosections of enucleated mouse eyes using the Akoya Biosciences TSA Plus Cyanine 3 detection kit (NEL744001KT). Freshly cut sections were allowed to come to room temperature and were then quenched for 10 minutes in a 1% hydrogen peroxide, 10% methanol in 0.01M phosphate buffered saline solution (1X PBS). The slides were rinsed in 1X PBS and allowed to block for 1 hour at room temperature in a blocking solution of 10% donkey serum, 0.3% Triton-X 100 in 1X PBS. Primaries for TSA were diluted 1:100 in blocking solution and approximately 200 microliters were added to the slides overnight at 4 degrees Celsius. The slides were then rinsed using a 0.3% Triton-X 100 in 1X PBS solution before being blocked in Tris-NaCl-blocking (TNB) buffer for 1 hour at room temperature. Approximately 200 microliters of Horseradish peroxidase conjugated secondaries diluted 1:200 in TNB buffer were applied to the slides for 2 hours at room temperature. The slides were subsequently rinsed in Tris-NaCl-Tween (TNT) buffer. TSA Plus Working Solution was made by diluting the TSA Plus Stock Solution 1:50 in 1X Amplification Diluent. The TSA Plus Working Solution was added at a volume of 200 microliters for 7 minutes at room temperature. The slides were then washed in TNT buffer and approximately 200 microliters of non-amplified primaries for counterstaining diluted 1:200 in 10% donkey serum, 0.3% Triton-X 100 in 1X PBS blocking solution was applied overnight at 4 degrees Celsius. Secondary antibody detection and mounting were performed as above.

in situ hybridization

We used the RNAscope® Multiplex Fluorescent Reagent Kit v2-Mm (Advanced Cell Diagnostics a Bio Techne Brand, Newark, CA). Probes for mouse *Lypd1* (#318361-C2), *Inmt* (#486371-C2), *Edn3* (#505841-C1), *Acta2* (α-SMA) (#319531-C3), and *Myoc* (#460981-C1) (also purchased from ACD Bio) were used. Fluorescent dyes Opal 690 (FP1497001KT) and Opal 620 (FP1495001KT) (Akoya Biosciences, Marlborough, MA) were used with each of these probes. Briefly, eyes from 3-month-old C57BL/6J were enucleated and fixed in 4% PFA for 24 h at 4°C. A window was made to the back of the eye cup, lens removed, and the anterior cup placed in 30% sucrose overnight at 4°C. Tissue was cryopreserved in OCT and placed at −80°C. Sections were cut at 12 µm thickness using SuperFrost Plus slides (Fisher Scientific, Hampton, NH).. RNAscope® was performed over two days as per manufacturer's protocol.

Whole mounts

Enucleated eyes were fixed for 2 hours at 4°C in 4% paraformaldehyde (PFA, Electron Microscopy Science, Hatfield, PA) prepared in phosphate-buffered saline (1× PBS, 137 mM NaCl, 10 mM phosphate, 2.7 mM KCl, pH 7.4). The postnatal eyes were dissected out following fixation. The anterior part of the eye was cut just posterior to the limbus (transition zone between cornea and sclera) as described in Kizhatil et al. [25]. Briefly, the iris, lens, ciliary body, and thin strip of retina were carefully removed to obtain the anterior eye cup. The anterior cup includes the cornea, limbus, and a small portion of retinal pigmented epithelium. Four centripetal cuts were made to relax the eye-cup and facilitate eventual mounting onto a slide after immunofluorescence.

Anterior eye cups were rinsed multiple times with 1× PBS. The eye cups were incubated with 3% bovine serum albumin and 1% Triton X-100 in 1× PBS (blocking buffer) at room temperature for 1 h in 2 ml glass vials to block nonspecific binding of antibody and to permeabilize the tissue. The anterior cups were then incubated with primary antibodies (S8 Table) in 200 µl blocking buffer for 2 days, with rocking, at 4°C. The anterior cups were then washed three times over a 3-h period with 1× PBS. The primary antibodies were detected with the appropriate species-specific secondary antibody (all Alexa 488, 594, or 647 at 1:1,000 dilution, Life Technologies, Grand Island, NY) diluted in blocking buffer, which also had DAPI to label nuclei. The immunostained eye cups were washed three times over a 3-h period in 1× PBS. Eye cups were then whole-mounted on slides in Fluoromount (Sigma, St. Louis, MO).

Microscopy of drainage structures

Sections

Microscopy of sectioned postnatal eye slides was performed using an LSM SP8 confocal microscope (Leica) and 40×1.1 NA water immersion objective.

In situ

Images were taken using a Nikon Eclipse 90i confocal laser-scanning microscope (Melville). Z-stack images of 1 µm thickness, using the 40X objective lens, were taken of each section and converted into maximum projection images that were used for analysis.

Whole mounts

Microscopy was performed using an LSM SP8 confocal microscope (Leica) using a 63×1.4 NA glycerol immersion objective. The Mark and Find mode was used to automate collection of images, generating a folder full of Z stacks (Z = 0.3 µm) at various individual overlapping positions around the limbus. We examined n = 6 eyes total. We imaged a certain distance around the ocular circumference, with an equal representation from each ocular quadrant (1.5-2.5 mm total).

Postprocessing of whole-mount images

3D rendering

We followed the guidelines detailed in Kizhatil et al for visualizing SC and TM in 3D. Individual confocal Z stacks (.lsm files) were processed directly using Imaris 9.5 (Oxford Instruments, Carteret, NJ). The maximum intensity projection setting in Surpass mode of Imaris was used for 3D rendering. Controls and experimental image sets were treated identically.

Images were oriented so that structures of interest were visible. For whole-mounted eyes, multiposition Z stacks generated using the Mark and Find setting on the confocal microscope were first imported into Imaris and converted into Imaris files (.ims files). The resulting Imaris files were then stitched to generate a comprehensive Z stack encompassing the limbus using ImarisStitcher 9.5 (BitPlane AG, Zurich, Switzerland). The stitch was exported as an Imaris file and processed appropriately. For sections, images were taken in the Z-plane in focus. When making figures, the snapshot feature of Imaris was used to collect images at high resolution (1024×1024 pixels, 300 dpi).

TM marker location analysis

We defined the TM as the region between the inner wall of Schlemm's canal (SC, outer TM) and the anterior chamber (inner TM), extending from the anterior edge of the pars plana (posterior TM) to the posterior edge of Descemet's membrane of the corneal endothelium (anterior TM).

The SC was defined using a panel of validated markers that varied to allow for different antibody species and different secondary antibodies to be used in conjunction with the SC markers (See Table S8 for list of antibodies) [25]. Sections were only included in the scoring analysis if they met the following criteria:

1. Absence of obvious sectioning artifacts or abnormalities in the SC or TM region.
2. Distinguishability of all landmarks defining the TM.
3. Acceptably low background signal and absence of staining for non-specific or non-biological entities within the section.

For each section, the TM was segmented and analyzed in two separate ways. The anterior-posterior distance was measured, and the TM was divided in half along this axis at the midway point (S7C-D Fig). Using the surface feature in Imaris, the area of individual marker staining was measured, and the total area in both the anterior and posterior zones was calculated. Because markers are expressed at different levels, we normalized across markers by calculating the percent of individual marker expression in the anterior and posterior halves within each section. These percentage values in anterior and posterior halves were compared both within markers and across all markers of a given TM cell subtype by Student's t-test. The same analysis was repeated for the inner-outer halves by measuring the inner-outer TM distance at the midpoint of the TM (anterior-posterior axis) and dividing the TM in half at this value. A total of 130-160 sections were examined for markers of each individual TM cell subtype. These sections were from 10-12 individual eyes per cluster. All eyes were from WT mice of C57BL/6J background and between 3-6 months of age.

Additional analysis was performed by selecting a subset of examined sections with staining for select markers (TM1: MYOC antibody, TM2: CRYM antibody, *Inmt in situ*, TM3: α-SMA antibody). These sections were of exceptionally high quality and had: 1) Anterior-posterior TM length between 125-200 μm. 2) Inner-outer TM distance is between 15-30 μm.

With these selected sections, we subdivided the TM into eight different zones along both inner/outer and anterior/posterior axes (Figure S7F). For each individual section, we used Imaris to measure the anterior-posterior distance and divide the TM into three equal sectors (anterior, central, and posterior. Within each sector, the average depth of the TM was measured in Imaris.

This calculation was used to divide the central and posterior sectors into three zones each (inner, intermediate, and outer). Because the anterior TM depth is thinner, we divided the anterior sector into two zones (inner and outer). In total, there were eight distinct zones.

The percent of total marker area was calculated for each of the eight zones for each individual section as described above. Percent of marker area in each zone was compared as shown in **Figure 2** by one-way ANOVA followed by Tukey's honestly significant difference test.

Scleral cell marker analysis

For CD34 and LY6C1 expression, we examined greater than 60 sections from 4 eyes (CD34) and 3 eyes (LY6C1) respectively. The observed locations of these markers within the iridocorneal angle are described.

Whole mount marker location analysis

To analyze the expression of markers within the TM, we segmented the TM based on anatomy. Because various anatomical features including the pars plana were removed during the whole mount process, we used the SC (marked by PECAM) as the major anterior-posterior landmark. The TM was defined as the group of cells inner to the SC and not outside the anterior or posterior boundary of the SC.

Nuclear morphology

Anterior segment whole-mounts were used to examine nuclear morphology in 3D (TM1: MYOC, TM3: α-SMA, all antibodies). The TM was segmented as described above and the 'Surface' feature in Imaris used to demarcate TM cell nuclei. Nuclei that were analyzed were immediately adjacent to the immunolabeled TM marker and had to be well spaced from other nuclei. To ensure accuracy we used manual inspection to exclude: 1) Nuclei that were very close to other nuclei or groups of nuclei and 2) nuclei of cells that were labeled with a Schlemm's canal endothelial cell marker (PECAM) and/ or that projected into the lumen of SC. The 'Sphericity' tool was used to determine the degree of sphericity in Imaris. For each cell subtype, we assessed a total 60 nuclei from 6 eyes, assessing the first 10 randomly selected nuclei that met our inclusion criteria in each eye. Groups were compared by Student's t-test.

Electron microscopy

Mice were euthanized, and eyes were enucleated into DBG buffer containing 1X Dulbecco's phosphate-buffered saline with 5.5 mM D-glucose (Sigma-Aldrich). Eyes were immediately dissected in DBG buffer to generate anterior segment eye cups, with centripetal relaxing cuts in the cornea to allow flattening (see Figure S1). The tissue was fixed at room temperature for 30 minutes in a solution of 0.8% paraformaldehyde, 1.2% glutaraldehyde, and 0.08 M phosphate buffer (Smith-Rudt). Following fixation, each anterior segment was mounted on a slide and flattened under a coverslip overnight at 4 °C. A 1 g weight was placed on top of the coverslip to aid in flattening the limbal region. The eyes were then washed three times in 1X PBS for 15 minutes each and stored in PBS under the same slide/coverslip setup to maintain flattening until embedding. Before further processing, individual limbal strips of the four quadrants of each were dissected from the surrounding cornea and sclera (see Figure S1). These strips were post-fixed in 2% aqueous osmium tetroxide, rinsed in PBS, and dehydrated for epoxy resin embedding using EMBED 812 (Electron Microscopy Sciences). Embedding was performed while preserving the

orientation of the limbal strip, with the TM (inner side) and cornea / sclera (outer side) clearly maintained. Embedded strips were imaged using computed tomography to locate the tissue, confirm TM orientation and flattening for *en face* sectioning, and to guide the sectioning process. Ultrathin, 70 nm, *enface* sections of the inner side of the limbal strip were taken using a Leica ultramicrotome (inner TM is the most superficial tissue being sectioned). Sections were placed onto formvar coated slot grids then stained en grid using a combination of 5% Uranyl Acetate and Reynold's lead citrate (Reynold's 1963) for 17 and 7 minutes, respectively. Large mosaic regions of the TM were imaged at 5,000× magnification (2.18nm/px) using a JEOL 1400FLASH TEM operating at 80 kV, equipped with a Gatan OneView camera. Mosaics were then computationally reconstructed using custom nornir-buildscripts (*https://nornir.github.io/*) and initially visualized in the Software suite Viking (*http://connectomes.utah.edu*)

From each TM section, 20 cells with sampled nucei were randomly selected from evenly spaced regions throughout the imaged area (approximately 25,000 μm² per eye). In the perinuclear area of each selected cell, up to 3 (typically 2-3) mitochondria were randomly selected and analyzed. The perimeter of the mitochondrial outer membrane (area) and inner membrane (cristae) were traced in ImageJ according to established protocols [161, 162]. The percentage of cristae area compared to the whole mitochondrial area was calculated (cristae fraction) for each mitochondrion. The number of mitochondria were counted in the perinuclear region of each analyzed cell. This number was normalized to an area of 100 μm² and averaged across cells.

As each en face section sampled a large area of the TM. 3 sections from different eyes were examined for each genotype. All mice were 14 days old. A total of 178 mitochondria from WT eyes and 161 from *V265D* eyes were analyzed. Groups were compared by Student's t-test.

Acknowledgements

The authors would like to thank the members of the Simon John Laboratory for experimental and technical assistance, Drs. Krish Kizhatil and Chi Zhang for reading and editing the manuscript, the Institute of Comparative Medicine and Devanshi Ragha at Columbia University for animal and veterinary care, the JP Sulzberger Columbia Genome Center and Duke University Molecular Genomics Core for assistance with genomics studies, and the P30EY019007 Columbia Shared Resources grant for histological experiments.

Additional information

Funding

This project was supported by National Eye Institute grant EY032507 (to S.W.M.J). Partial support was provided by EY011721, EY032062, and EY018606 (to SWMJ), Brightfocus grants CG2020004 (to S.W.M.J.), and G2021007 (to R.B.), startup funds at Columbia University including the Precision Medicine Initiative, and the New York Fund for Innovation in Research and Scientific Talent (NYFIRST; EMPIRE CU19-2660). At Duke, the work was also supported by NEI grants EY028608, EY022359 (to WDS). Supported also came from Vision Core grants P30EY019007 (Columbia University), P30EY005722 (Duke University), The Glaucoma Foundation (Columbia University) and an unrestricted departmental award from Research to Prevent Blindness (Columbia University and Duke University). The content is solely the responsibility of the authors and does not necessarily represent the official views of the National Institutes of Health. SWMJ is the Robert Burch III Professor of Ophthalmic Sciences.

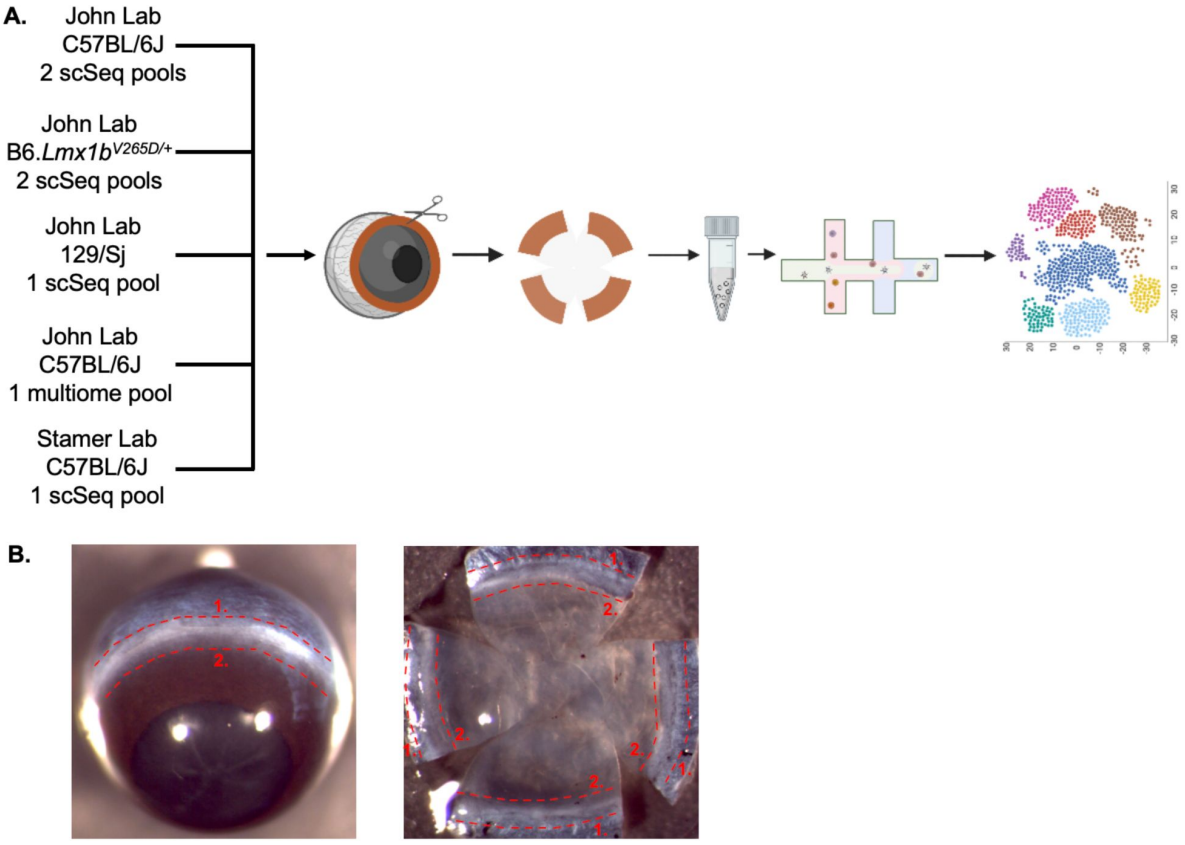

S1 Fig.

Schematic of datasets and pipeline.

(A) Each pool included limbal tissue from 8 eyes. The mouse strains and lab where data were generated are shown (Columbia University, John Lab or Duke, Stamer lab). Individual eyes were dissected to isolate strips of limbal tissue, which are enriched for TM cells in comparison to dissecting the anterior segment as a whole. Limbal strips were then minced and pooled for further processing. Individual cells were sequenced using the 10X Genomics pipeline (see Methods) for sc-RNA-Seq or multiome (snRNA-seq and scATAC-seq). Schematic created with BioRender.com. **(B)** (Left) The limbal region of the enucleated eye is outlined with red dotted lines. The posterior portion of the eye is first removed by making a cut along line1. After lens removal, a second cut is made through the anterior cornea and iris along line 2, generating a limbal strip. This strip is then minced prior to dissociation. (Right) A dissected anterior eye cup (with the lens removed) is shown to indicate the interior surface of the limbus between lines 1 and 2. Centripetal cuts were made in the cornea of this specimen to flatten it for ease of imaging. Although we do not flatten limbal strips used for RNA-seq, this view provides additional context. Schematic created with *BioRender.com/8h40kmb*.

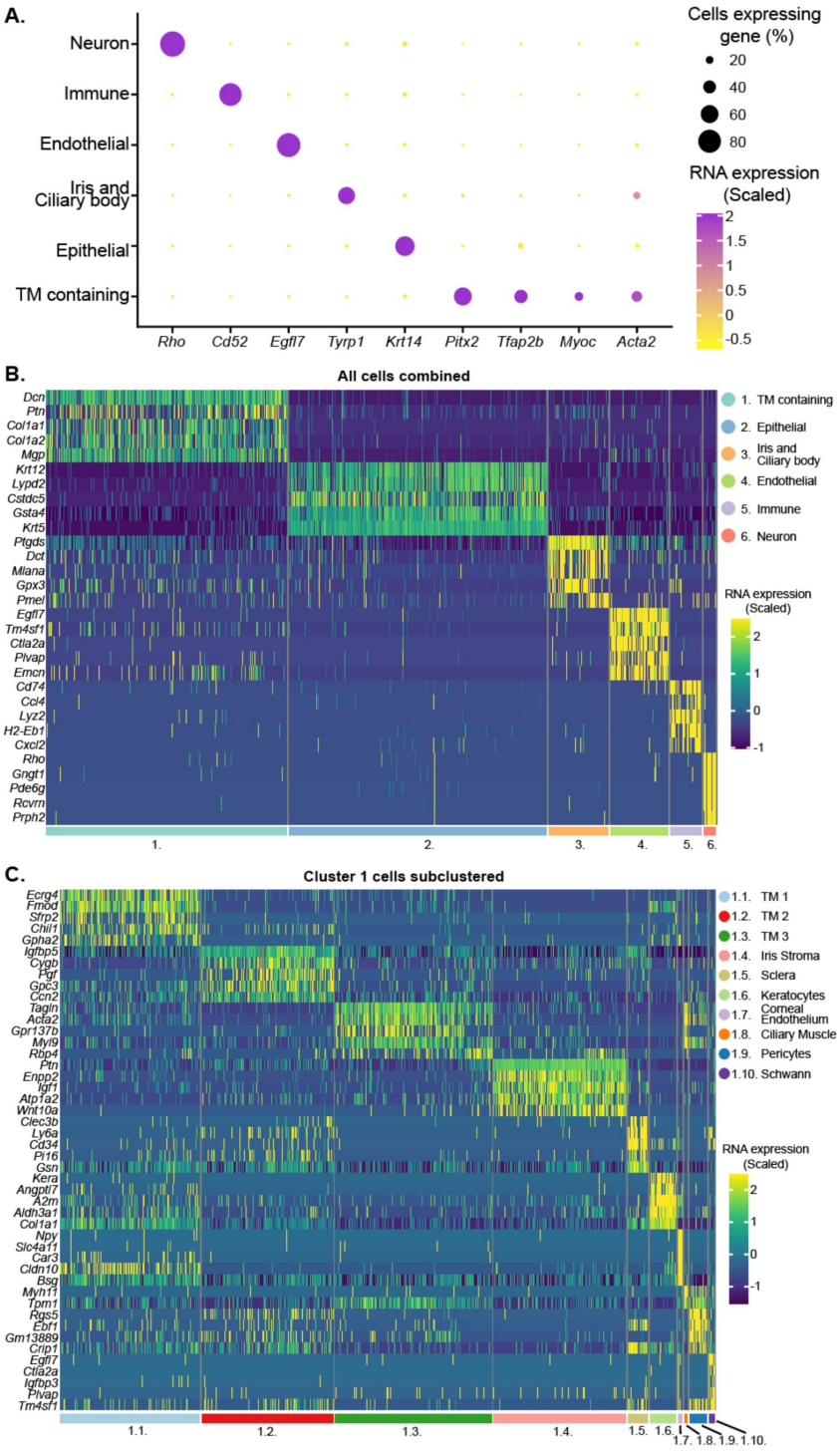

S2 Fig.

Limbal cell cluster marker genes.

(A) The expression levels of various anterior segment cell type marker genes in the integrated B6 and 129 data are depicted on a dot plot. These marker genes are generally accepted to be specific to individual cell types. Epithelial cells (*Krt14*); neurons (*Rho*); endothelial cells (*Egfl7*); ciliary body and iris cells (*Tyrp1*); and immune cells (*Cd52*). Cluster 1 expressed multiple TM marker genes including *Myoc*, *Acta2* (encodes α-SMA), *Pitx2*, and *Tfap2b*. Although some of the neurons may be limbal, it is possible that others are retinal contamination. **(B-C)** Heatmaps of differentially expressed genes across all limbal tissue cell clusters (B) and across the subclusters of cluster 1 (C).

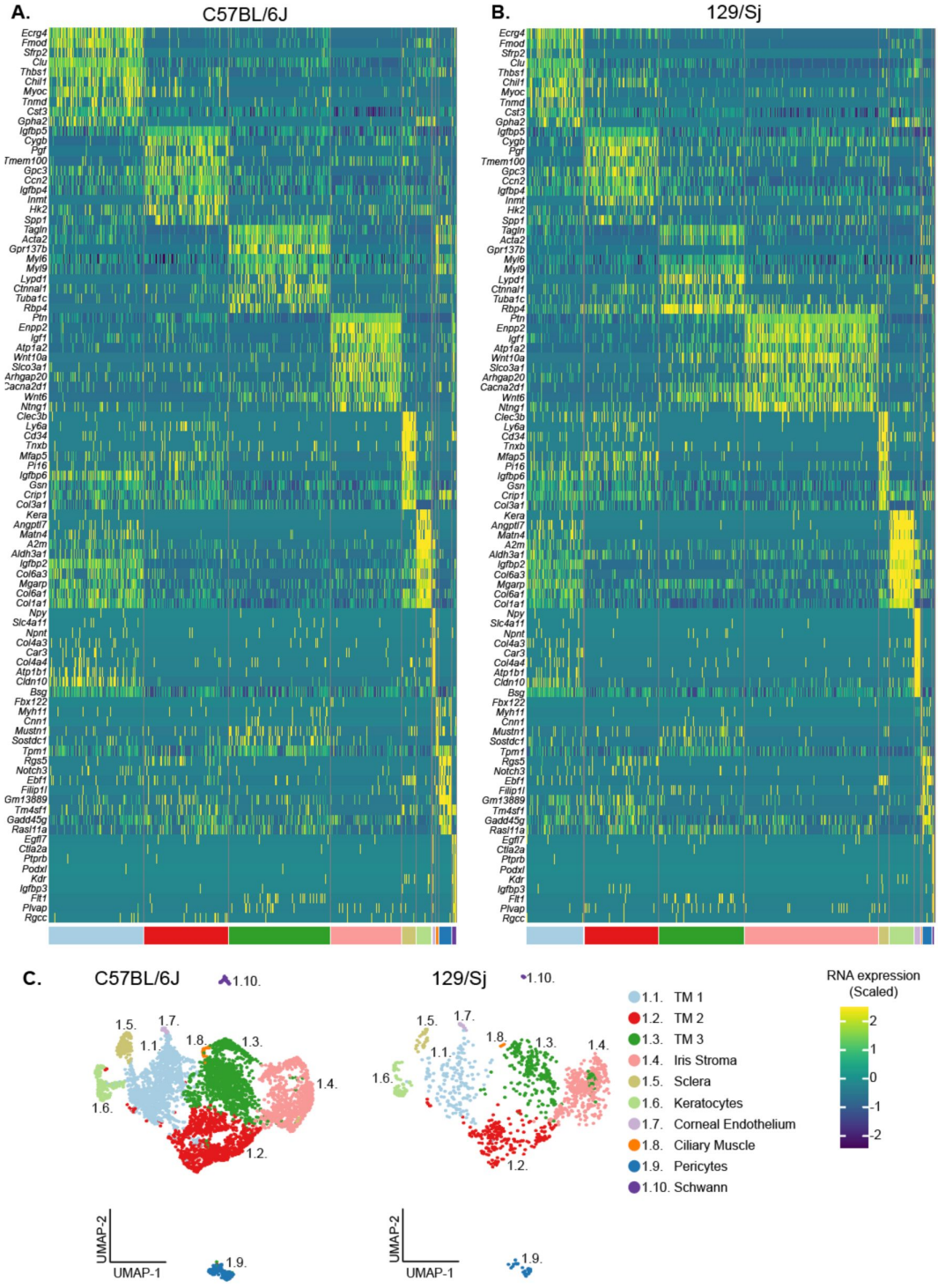

S3 Fig.

Transcriptomic similarities between strain B6 and strain 129.

(A-B) The 129/Sj (129) and C57BL/6J (B6) strains exhibit significant overlap in marker gene expression. Heatmaps display the expression of the top 10 gene markers for each subcluster of cluster 1. The expression patterns are very similarity across strains. **(C)** UMAP representations of subclusters derived from cluster 1 separated by strain.

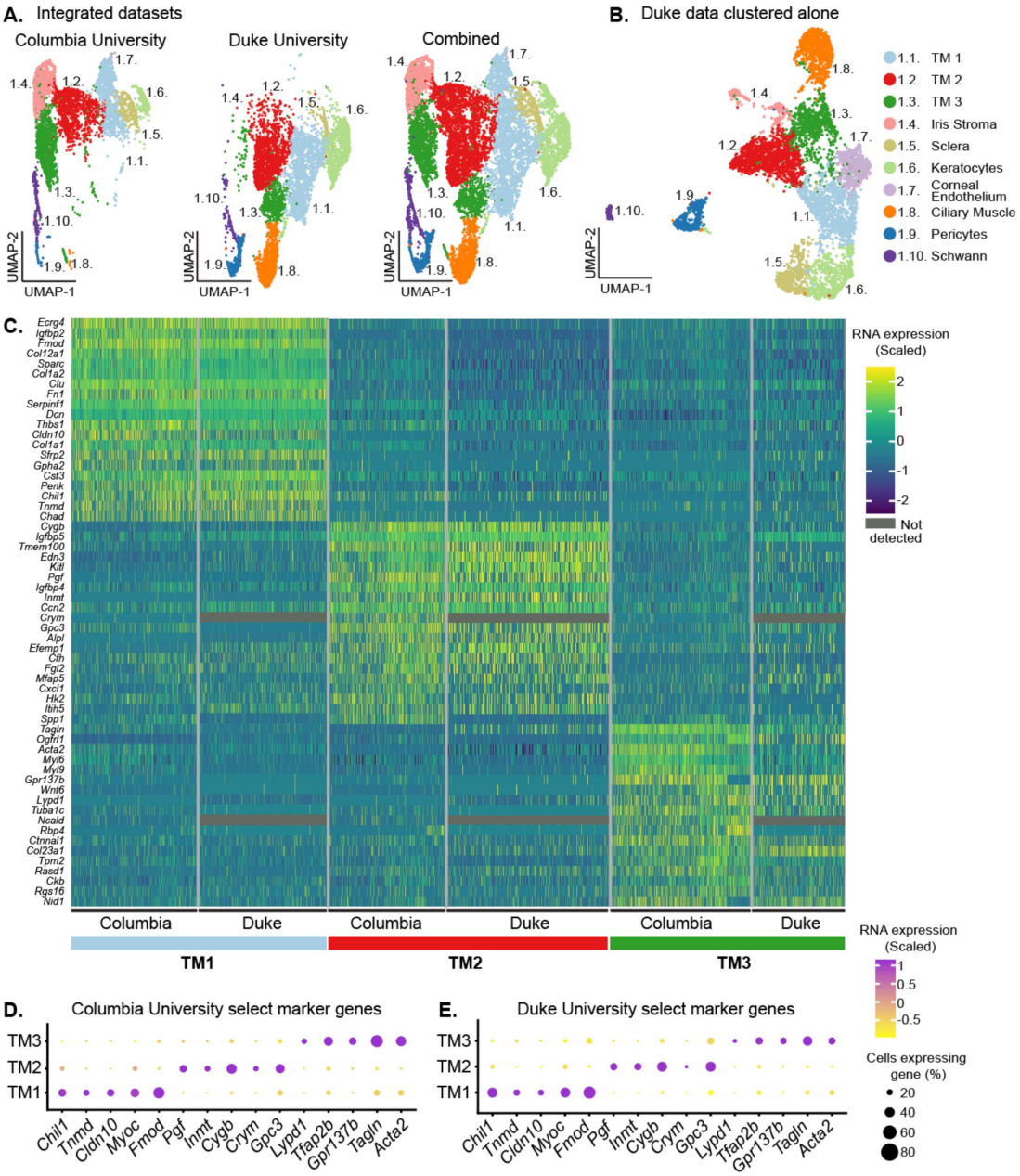

S4 Fig.

An independent B6 scRNA-seq dataset corroborates TM cell clusters.

(A) UMAPs of the integrated Columbia University and Duke University datasets. Cells from the different institutions occupy largely different but adjacent UMAP coordinates with some overlap, indicating batch effects. The difference was largest for TM3, but the marker genes were still conserved. Because tissue processing techniques can alter gene expression [52], the heatmap variation between institutes likely reflects differences in processing techniques (Methods) and suggests that TM3 cells are more susceptible to these effects than other cell types. **(B)** Analysis of Duke University data alone independently validates our findings presented in **Figure 1** from Columbia University, including the presence of 3 TM cell clusters. **(C)**. A heatmap comparing the top 20 marker genes of each TM cell subcluster for the Columbia (C57BL/6J strain only) and Duke datasets. Overall, there is strong overlap of TM cell gene expression between datasets. Discrepancies include certain marker genes (eg. *Crym*) in the Columbia dataset that are not detected in the Duke dataset. These differences are associated with lower sequencing depth in the Duke data, and other technical factors/batch effects. **(D-E)** Dot plots showing similar TM subtype marker gene expression in the two datasets.

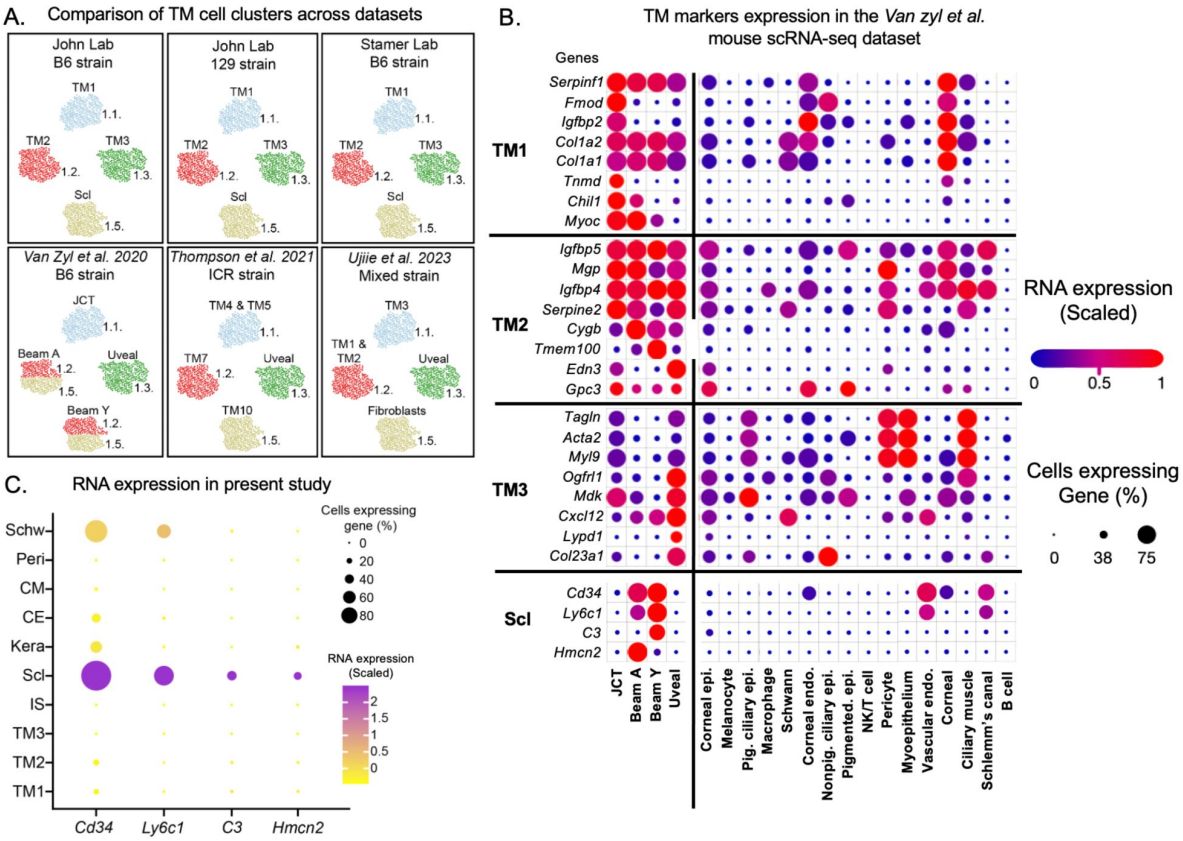

S5 Fig.

Comparison of our TM cells to published mouse datasets

(A) Diagrammatic representation of TM and scleral cell clusters across different mouse scRNA-seq datasets. **Upper panels** diagrammatically represent the current study. **Lower panels** represent the indicated studies. All diagrams based on marker gene expression in the cells that were clustered together. Despite some naming differences, matches for the 3 TM cell types that we identify in the current paper are evident in the previous studies. Although previous studies named additional TM subtypes, we did not subcluster to the same degree to ensure that subtype differences are robust. Previous studies had limited if any validation for some cell types. Based on our current characterization and immunofluorescent localization studies (**Figures 2**, S6, S8, & S9) some of the cells previously labeled TM beam cells are scleral (possibly fibroblasts). The marker gene expression for these previously named TM beam cells is highest in 'Fibroblasts' rather than TM cells in human scRNA-seq data, further supporting a scleral identity. In addition, cells previously named as uveal cells are a TM cell type. The cells are color-coded based on their molecular identities to match the current study. Current study subcluster identity numbers are shown. **(B)** Dot plot of TM cell subtype markers identified in the present study (left) using the dataset and cell type assignments (bottom) of Van Zyl et al. Based on these markers, our TM subtypes match their data as follows: TM1= JCT, TM2 = Beam A and Beam Y, and TM3 = Uveal). Scleral markers that we found are enriched in the Van Zyl Beam A and Y cells, which appear to be a mix of different cell types. **(C)** Expression of the Van Zyl Beam A and Y cell markers that are enriched in sclera in our combined B6 and 129 dataset (the same expression pattern was evident in all Columbia and Duke datasets in the current study). See Figure S6 for IF showing expression of these markers in Sclera but not TM.

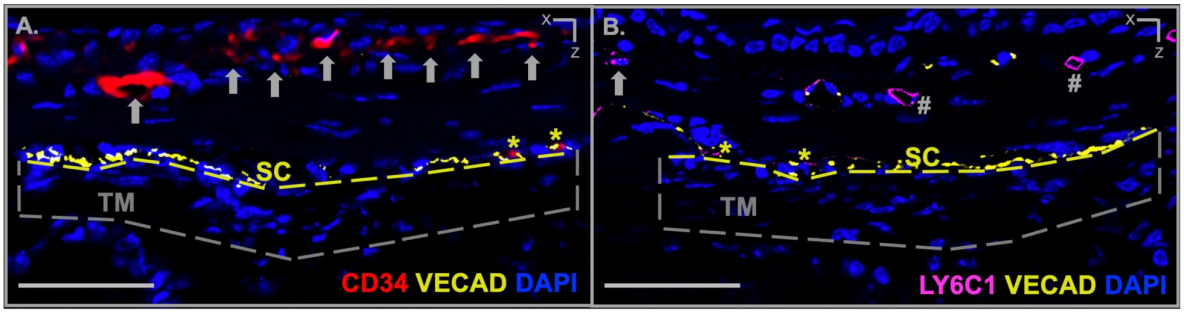

S6 Fig.

Immunostaining demonstrates expression of specific marker genes in sclera but not TM.

(**A**) CD34 is expressed in cells of the sclera/corneoscleral transition zone (arrows). No CD34 staining was found in the TM (> 60 sections from 4 eyes). **(B)** LY6C1 is expressed in both vascular (based on morphology and the vascular endothelial cell marker, VECAD, hash marks) and nonvascular (arrow) cells in the sclera. LY6C1 is not found in the TM. The TM is encompassed within the dashed box while the yellow dashed line marks the inner wall of SC (see Figure S7). CD34 and LY6C1 were expressed in SC endothelial cells (yellow asterisks). Scale bars = 50 μm.

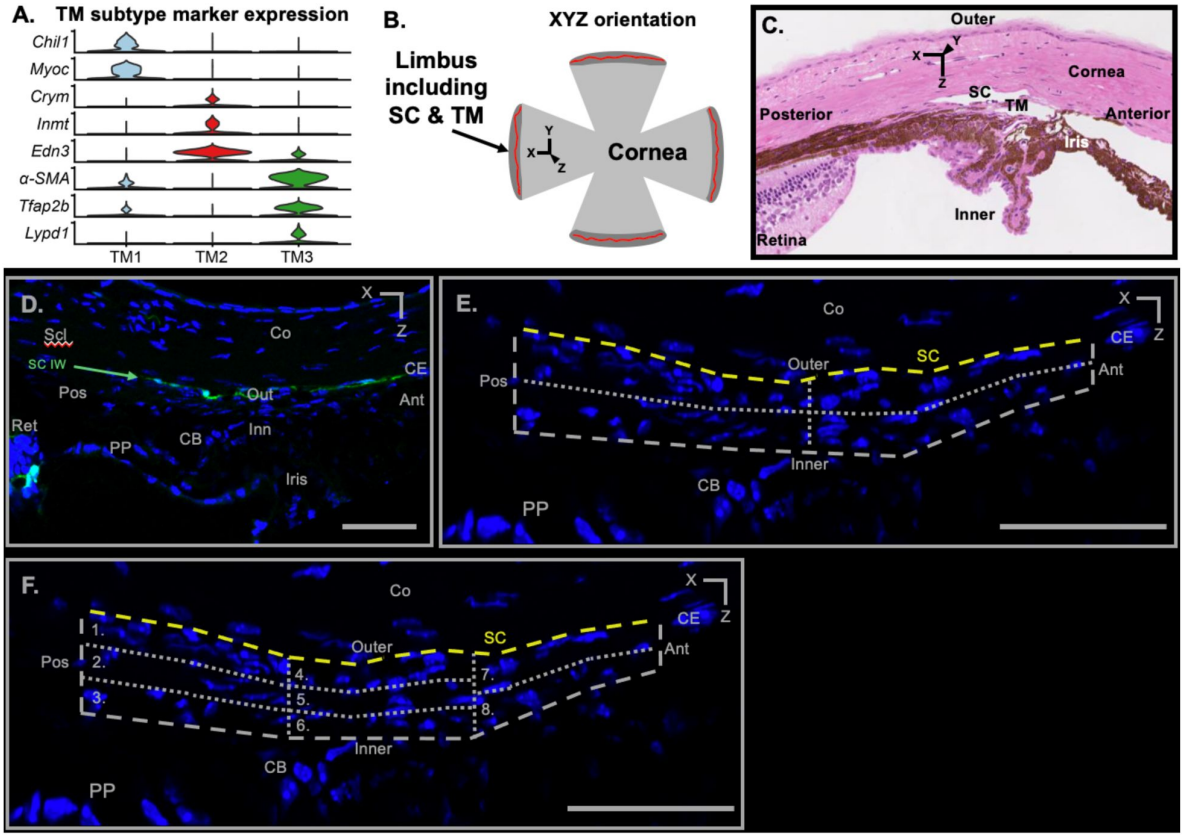

S7 Fig.

Assessing zonal distribution of TM cell subtypes.

(A) Violin plot showing expression of signature genes that were used to localize TM cell subtypes. **(B-C)** Diagram of flat-mounted anterior segment (B) and *hematoxylin and eosin-stained s*agittal section (C) indicating the X, Y and Z axis as used throughout this paper as previously reported (Kizhatil et al., 2014). **(D-E)** Schlemm's canal (SC) inner wall was identified based on anatomy and the expression of *Prox*-GFP (green) and other endothelial cell markers. The pars plana (PP) and corneal endothelium (CE) were identified based on anatomy and DAPI staining. The posterior boundary of the TM begins just anterior to the PP and was typically aligned with the most posterior portion of SC. The anterior TM ends where the corneal endothelium begins. This typically aligned with the most anterior portion of SC. The outer boundary of the TM was immediately internal to the inner wall of SC. The inner-most TM was where the TM cells end abutting the anterior chamber. Using these boundaries, the anterior-posterior and inner-outer axis of the TM were measured. Based on these measurements for each eye, the TM was divided in half along both the inner-outer and anterior-posterior axes. (**F**) For more refined analysis, the anterior-posterior distance was then divided into thirds to generate posterior, central, and anterior regions. Each of these regions was then equally divided into their subregions as shown. Because the anterior TM is thinner, it was divided into two zones. These divisions generate 8 TM zones. All scale bars: 50 μm.

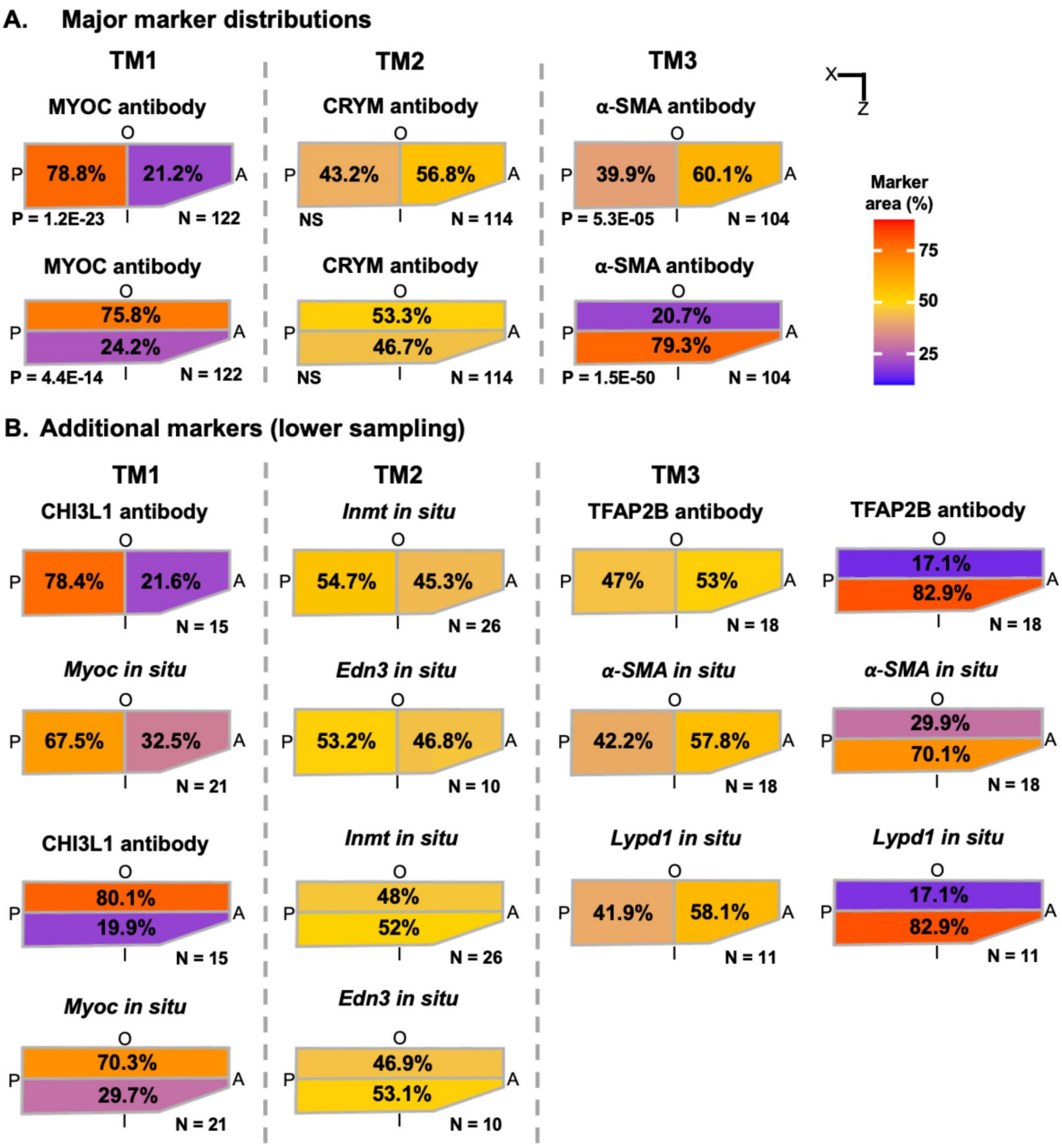

S8 Fig.

Distribution of TM cell subtypes by marker.

(A) Schematic representation of major marker distributions from **Figure 2**. **(B)** Additional markers for a given TM cell subtype had similar patterns of localization (see Figure S9 for example staining). However, these markers were not sampled deeply enough to perform statistical analysis. A: anterior TM, I: inner TM, O: outer TM, P: posterior TM.

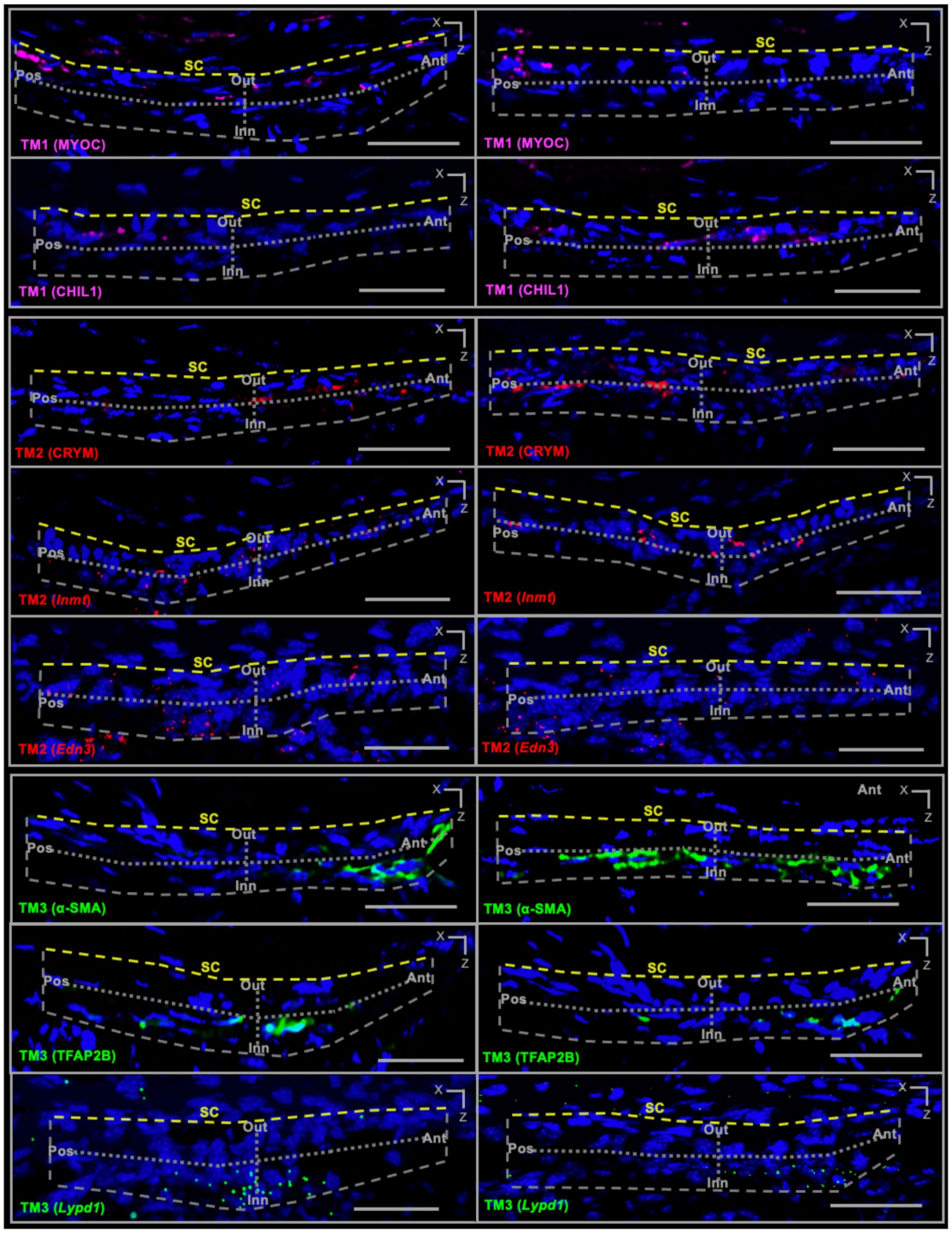

S9 Fig.

Additional examples of TM subtype marker localization.

Although there is variability in expression between sections, the aggregate of all sections reveals the biased distributions of TM cell subtypes as summarized in **Figures 2**. Here we focus on TM expression. However, some of the markers are also expressed outside of the TM. For examples, *Edn3* is expressed in vasculature, while both *Lypd1* and *Inmt* are expressed at low levels in scleral and iris cells (but are higher in TM cells). All scale bars: 50 μm. Markers assessed by IF: MYOC, CHIL1, CRYM, α-SMA, TFAP2B. Markers assessed by ISH: *Inmt*, *Edn3*, *Lypd1*. All scale bars: 50 μm.

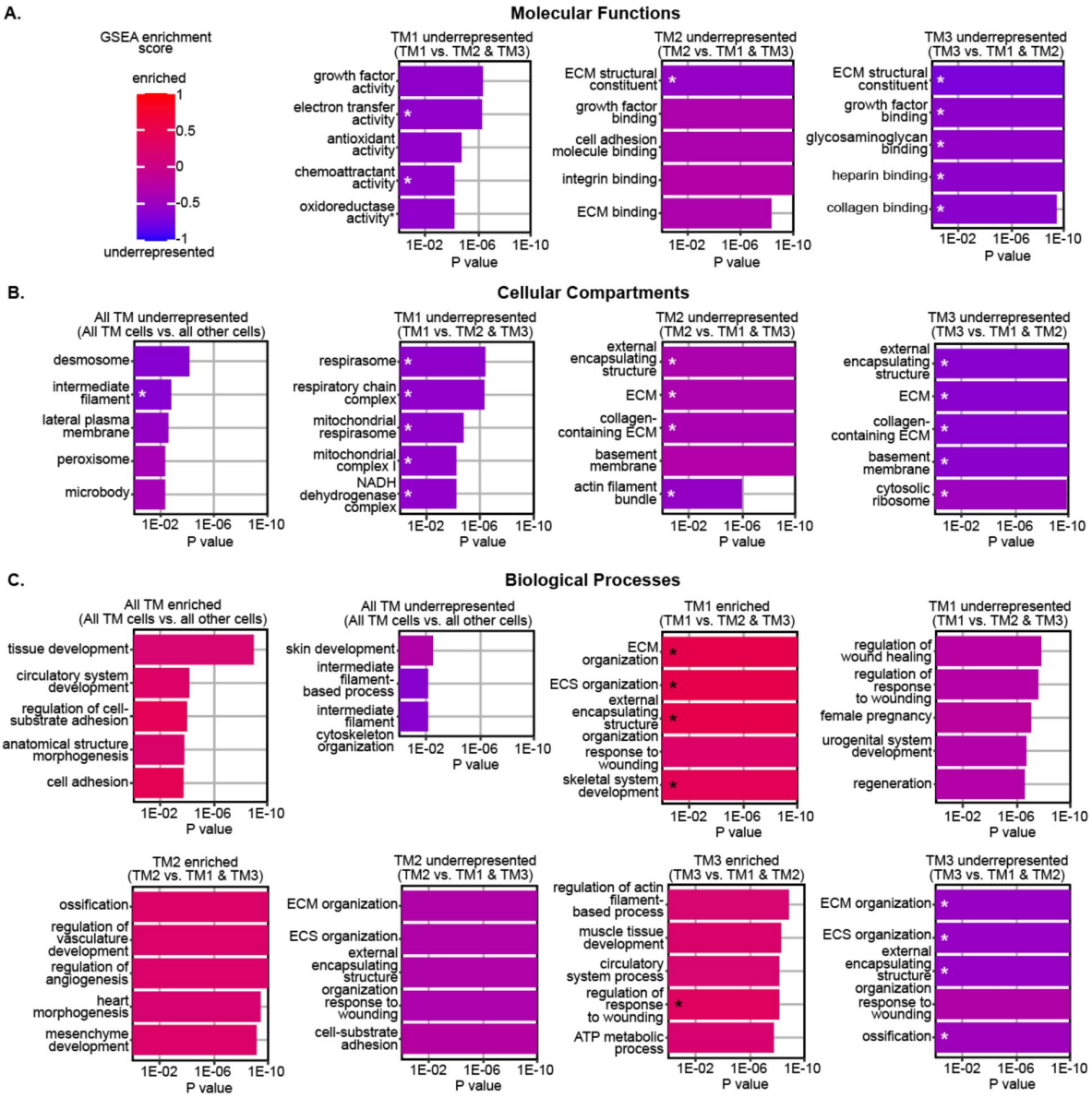

S10 Fig.

TM cell pathway analysis.

(A-C) Additional analyses showing the most significant pathways (by gene ontology (GO) analysis. Pathways are further separated into enriched or underrepresented categories based on gene set enrichment analysis (GSEA) score. Asterisks indicate pathways that are significantly enriched or underrepresented based on GSEA score. ECM = extracellular matrix. ECS = extracellular structure.

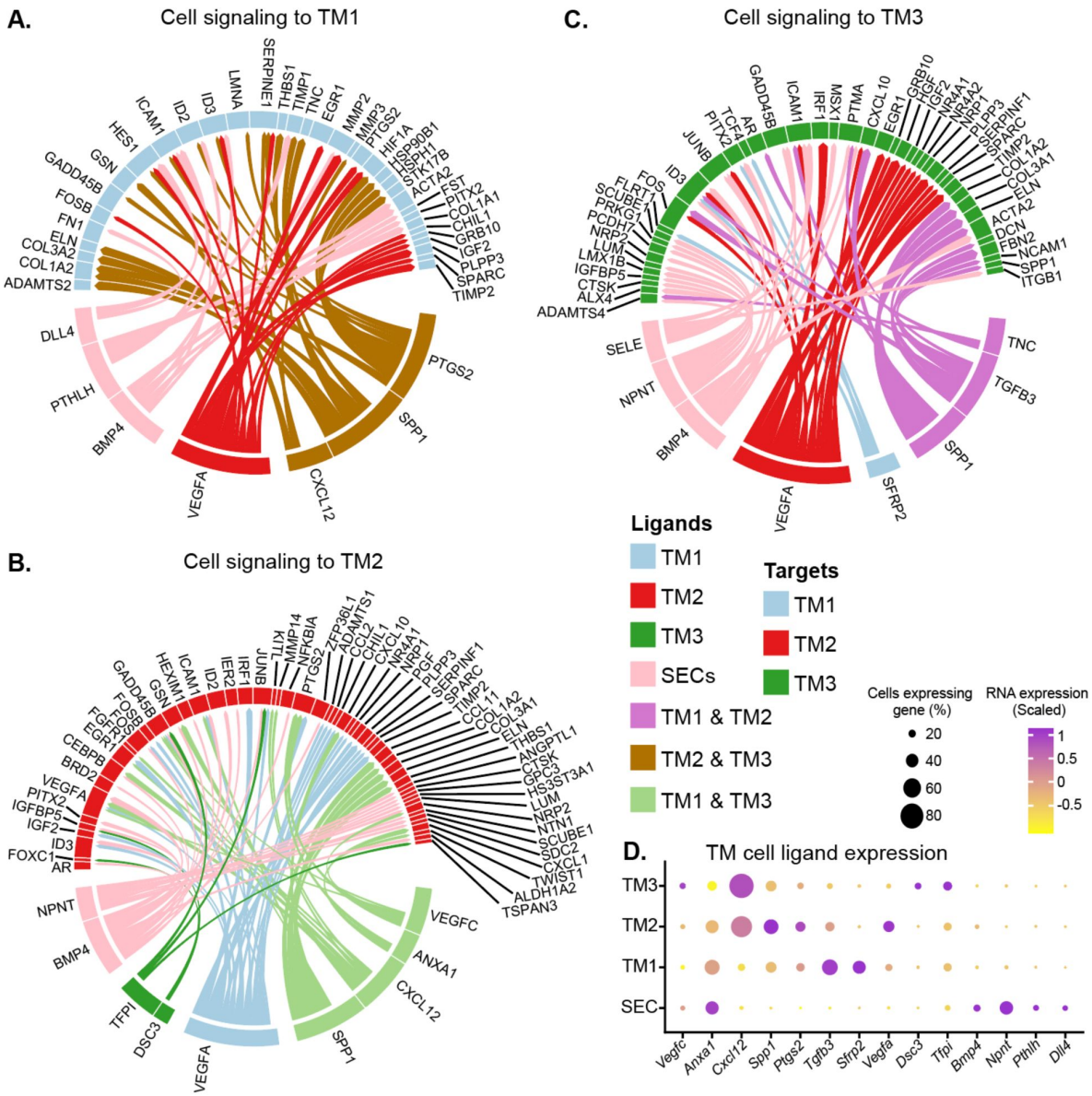

S11 Fig.

TM-TM and SEC-TM signaling.

(A-C) Analyses showing the top predicted interactions between TM and Schlemm's canal endothelial (SEC) ligands and individual TM cell target molecules (Circos plots). The three plots show target molecules in each individual TM cell subtype respectively. **(D)** The expression of all ligands predicted to have signaling interactions with TM cell subtypes (Dot plot).

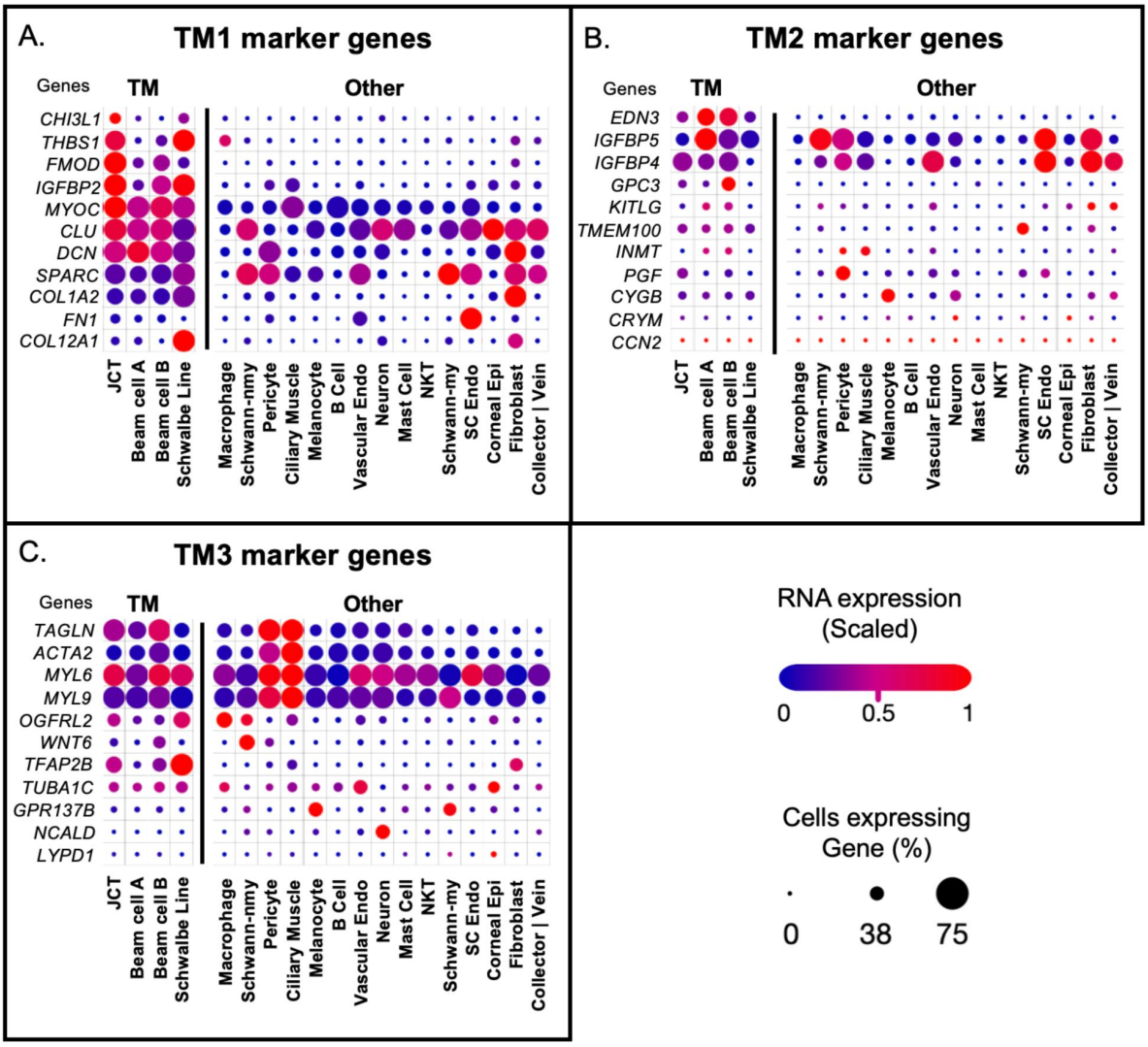

S12 Fig.

Mouse TM subtype marker expression in human TM cells.

(A-C) Dot plots of the expression of the top 11 marker genes for each of our mouse TM cell subtypes that have human orthologues expressed in the Van Zyl et al human dataset. TM1 marker genes generally have higher expression in the human JCT cluster than in any other cluster of cells. Other than EDN3, TM2 and TM3 marker genes do not show a strong enrichment for the annotated TM cells compared to other cells. Among TM cells, TM2 marker genes are more enriched in beam A and beam B cells. TM3 markers are mostly expressed in relatively equal levels across all the human TM cells. Schwalbe's line cells are also similar to TM. The anterior insertion of the TM is near Schwalbe's line, where TM stem cells are reported to reside. Therefore, the Schwalbe's line cells maybe TM stem cells.

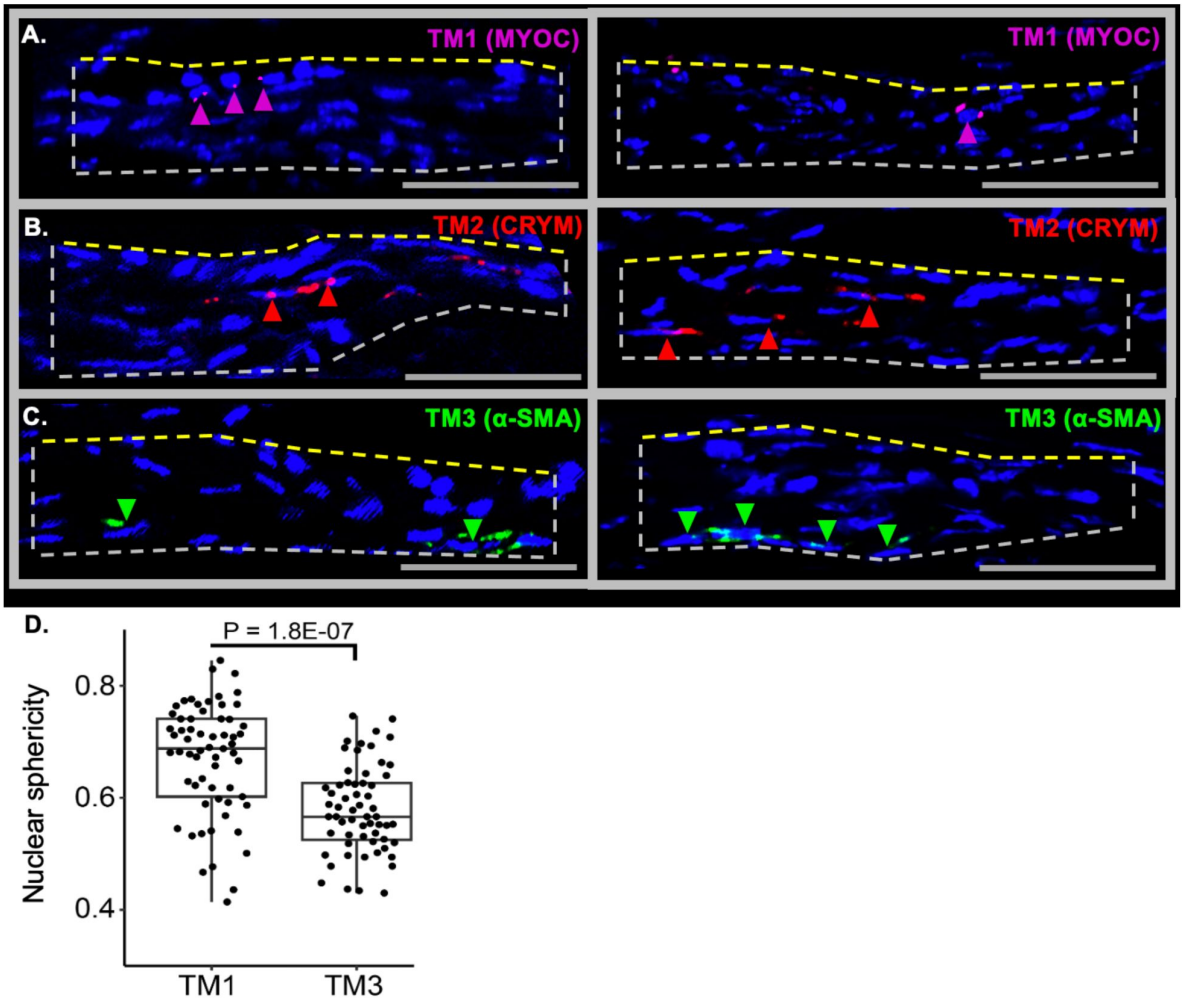

S13 Fig.

Nuclear morphology of each TM subtype.

(A-C) 2D section view of TM cell subtype nuclei. TM1 nuclei adjacent to the SC appear shorter than TM2 and TM3 nuclei and lack the typical elongated, endothelial-like morphology of beam cells. This shorter morphology gives TM1 nuclei a more spherical appearance. All scale bars: 50 μm. **(D)** To rigorously assess whether TM1 nuclei are more spherical, we analyzed their reconstructed 3D shapes from whole mounts images by confocal microscopy, comparing them to TM3 nuclei using the 'Sphericity' tool in Imaris. The data show that TM1 cells indeed have more spherical nuclei, consistent with a JCT identity. However, some TM1 cells exhibit more elongated nuclei, especially when located further from the SC. A higher sphericity score indicates a more rounded nucleus (with a completely spherical shape scoring 1). We characterized 60 randomly selected nuclei for each TM cell subtype. Groups were compared using Student's t-test.

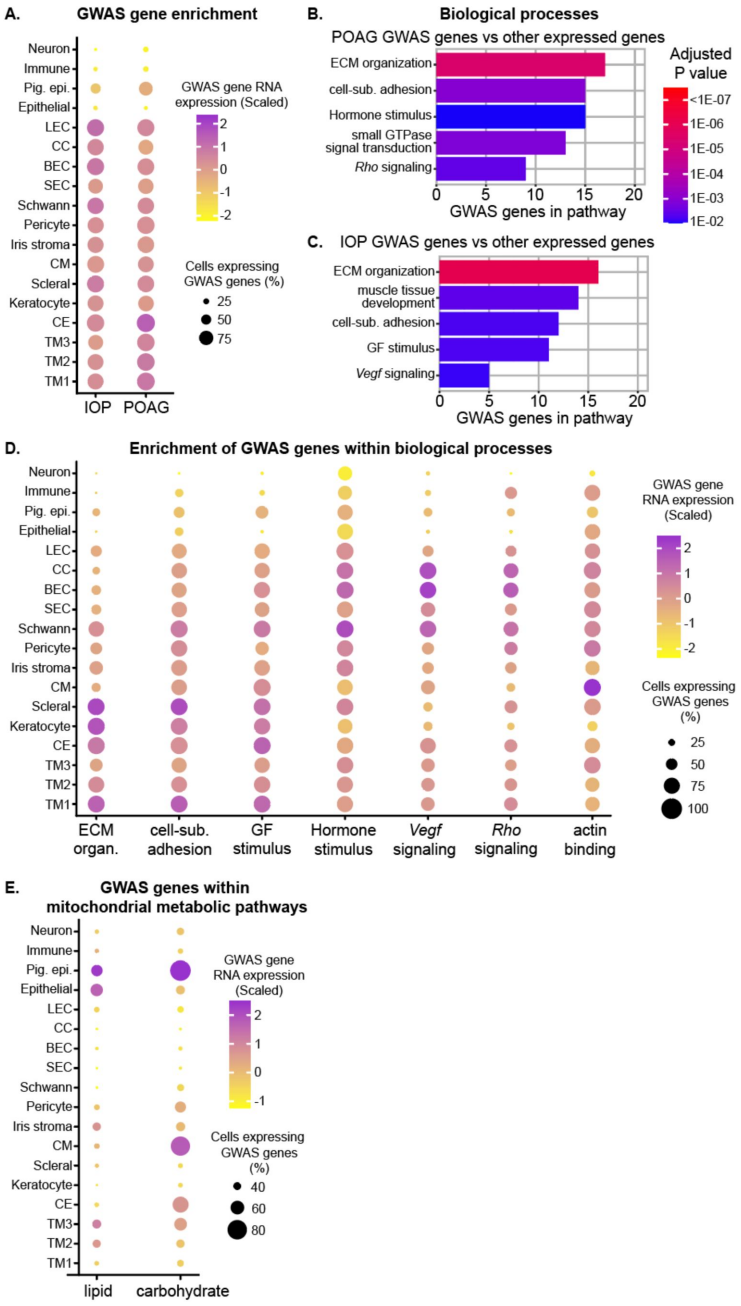

S14 Fig

GWAS gene expression in limbal cells.

(A) Expression of genes implicated in risk for IOP elevation (left) and primary open-angle glaucoma (POAG, right) in humans GWAS plotted against mouse limbal cell type. There is similar GWAS gene expression across TM cell subtypes and other limbal cell types. TM1 and TM2 have a slightly higher expression of GWAS genes compared to TM3. **(B-C)** Pathway analysis (Gene ontology, GO) shows enrichment of biological pathways for the POAG (B) or IOP (C) genes vs other expressed genes considering all cell types (see Table S5 for full list of GWAS gene-enriched pathways). **(D)** Enriched biological pathways among POAG GWAS genes within the indicated cell types. **(E)** Cell type enrichment of lipid and carbohydrate metabolism pathway genes that are significantly associated with POAG (Khawaja et al.). ECM organ. = extracellular matrix organization, cell-sub. = cell-substrate adhesion, Hormone stimulus = cellular response to hormone stimulus, small GTPase signal transduction = regulation of small GTPase mediated signal transduction, *Rho* signaling = regulation of Rho protein signal transduction, GF stimulus = regulation of cellular response to growth factor stimulus, *Vegf* signaling = vascular endothelial growth factor receptor signaling pathway.

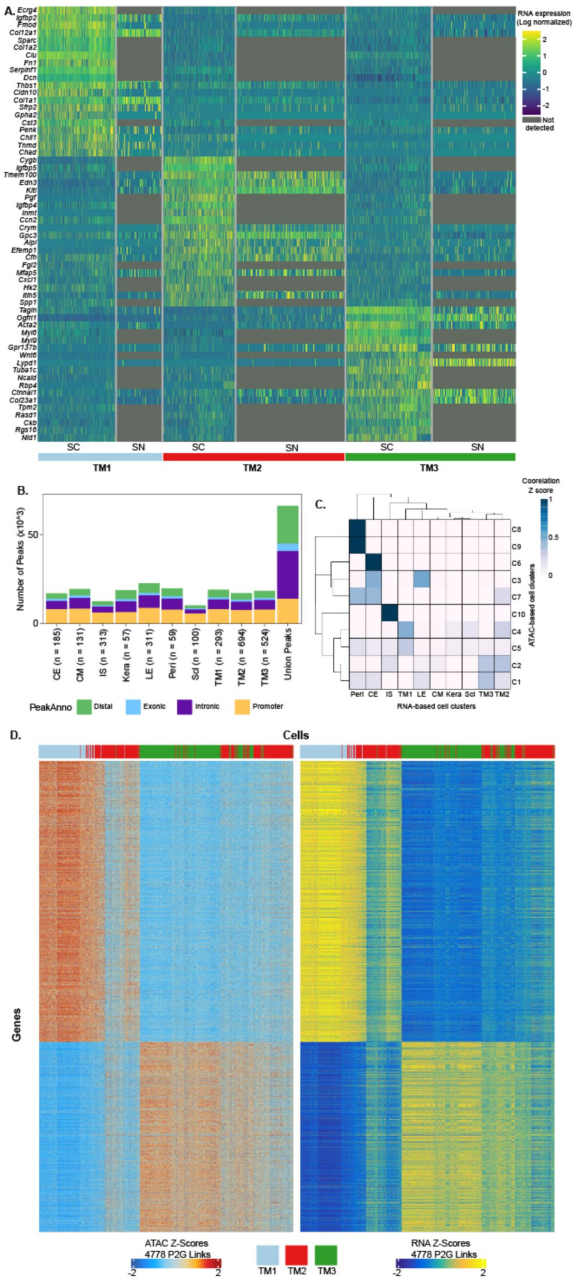

S15 Fig.

Analysis of ATAC dataset

(A) Overlap of marker gene expression for each TM cell subtype between single-cell (sc) and single-nucleus (sn) RNA sequencing (RNA-seq). Other than the expected technical drop out of genes (no detected expression) in the snRNA-seq dataset, there is general agreement. **(B)** Localization of significantly open chromatin regions (snATAC-seq). **(C)** Confusion matrix of clusters identified by snRNA-seq and snATAC-seq after separately clustering each data type using unbiased dimensional reduction. Colors indicate the fraction of cells identified in each ATAC cluster (row) which are also identified in each RNA cell type (columns), where darker colors represent stronger correspondence between RNA and ATAC clusters. There is a significant correlation between gene expression (RNA-based clustering) and chromatin accessibility (ATAC-based clustering) with adjusted Rand index of 0.20 ($p < 0.001$, permutation test). **(D)** Heatmaps comparing the open chromatin score at a gene promoter (left panel, snATAC-seq) to the RNA expression (right panel, snRNA-seq). Individual genes are represented on the y-axis and individual cells are plotted on the x-axis (only TM cells included). The consistent heatmap patterns indicate a strong overlap between promoter chromatin states and RNA expression for individual genes across cell types, validating the quality of these multiome datasets.

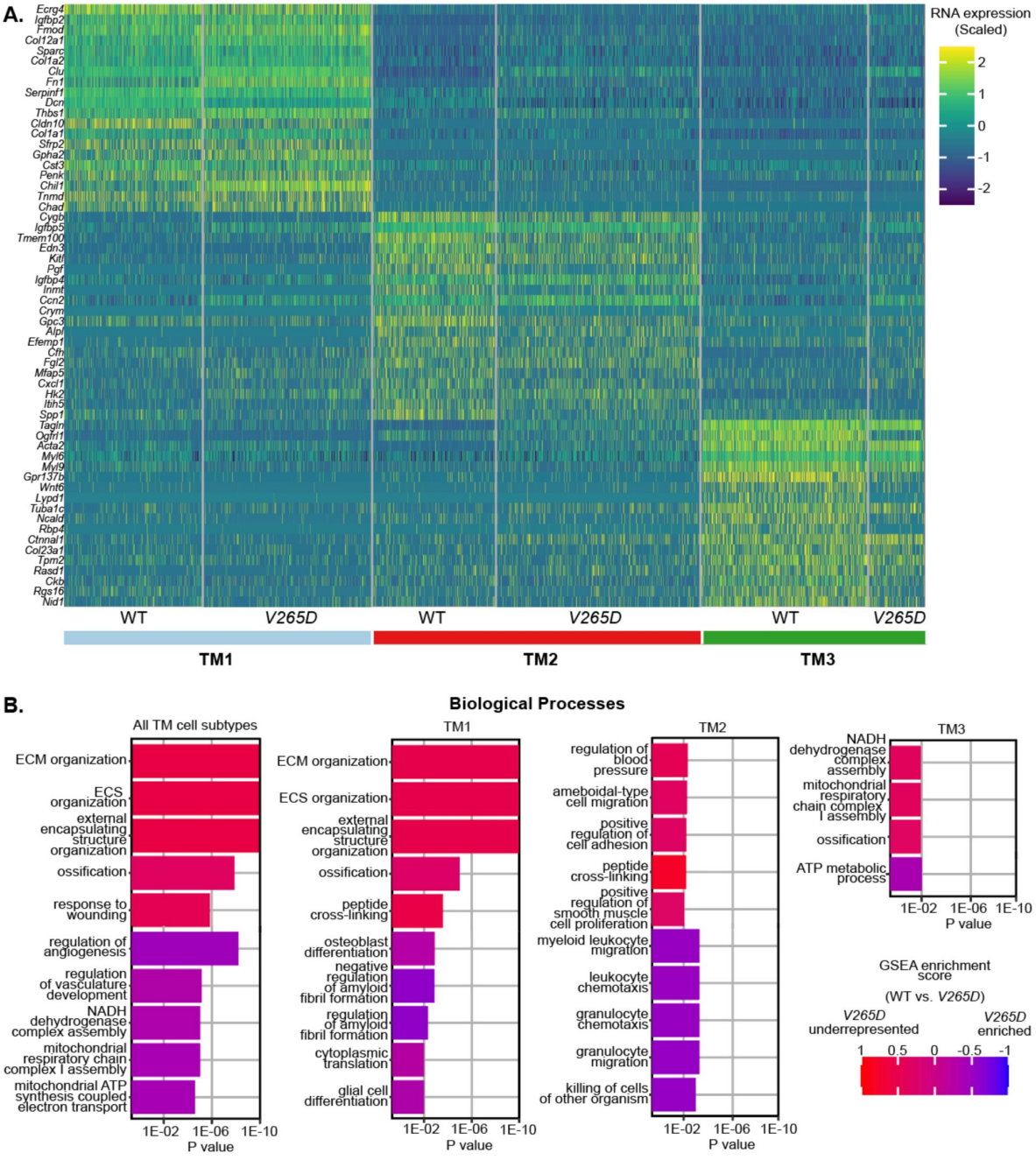

S16 Fig.

Further pathway analyses of *Lmx1b*^{V265D} vs WT.

(A) Heatmaps comparing marker genes for all TM cell subtypes across genotype. **(B)** The top 10 *V265D* upregulated and downregulated biological processes for the indicated comparisons across genotype are shown (all scRNA-seq data, Adjusted P values, axis cut of at 1E-10). ECM = extracellular matrix. ECS = extracellular structure.

References

1. Quigley HA, Broman AT (2006) **The number of people with glaucoma worldwide in 2010 and 2020** *Br J Ophthalmol* **90**:262–7 https://doi.org/10.1136/bjo.2005.081224 | PubMed | Google Scholar

2. Stamer WD, Clark AF (2017) **The many faces of the trabecular meshwork cell** *Exp Eye Res* **158**:112–23 https://doi.org/10.1016/j.exer.2016.07.009 | PubMed | Google Scholar

3. Keller KE, Peters DM. (2022) **Pathogenesis of glaucoma: Extracellular matrix dysfunction in the trabecular meshwork-A review** *Clin Exp Ophthalmol* **50**:163–82 https://doi.org/10.1111/ceo.14027 | PubMed | Google Scholar

4. Buffault J, Labbe A, Hamard P, Brignole-Baudouin F, Baudouin C (2020) **The trabecular meshwork: Structure, function and clinical implications. A review of the literature** *J Fr Ophtalmol* **43**:e217–e30 https://doi.org/10.1016/j.jfo.2020.05.002 | PubMed | Google Scholar

5. Acott TS, Kelley MJ (2008) **Extracellular matrix in the trabecular meshwork** *Exp Eye Res* **86**:543–61 https://doi.org/10.1016/j.exer.2008.01.013 | PubMed | Google Scholar

6. Fuchshofer R, Welge-Lussen U, Lutjen-Drecoll E, Birke M (2006) **Biochemical and morphological analysis of basement membrane component expression in corneoscleral and cribriform human trabecular meshwork cells** *Invest Ophthalmol Vis Sci* **47**:794–801 https://doi.org/10.1167/iovs.05-0292 | PubMed | Google Scholar

7. Yue BY (1996) **The extracellular matrix and its modulation in the trabecular meshwork** *Surv Ophthalmol* **40**:379–90 https://doi.org/10.1016/s0039-6257(96)80066-x | PubMed | Google Scholar

8. Vittal V, Rose A, Gregory KE, Kelley MJ, Acott TS (2005) **Changes in gene expression by trabecular meshwork cells in response to mechanical stretching** *Invest Ophthalmol Vis Sci* **46**:2857–68 https://doi.org/10.1167/iovs.05-0075 | PubMed | Google Scholar

9. Abu-Hassan DW, Acott TS, Kelley MJ. (2014) **The Trabecular Meshwork: A Basic Review of Form and Function** *J Ocul Biol* **2** https://doi.org/10.13188/2334-2838.1000017 | PubMed | Google Scholar

10. Vranka JA, Kelley MJ, Acott TS, Keller KE (2015) **Extracellular matrix in the trabecular meshwork: intraocular pressure regulation and dysregulation in glaucoma** *Exp Eye Res* **133**:112–25 https://doi.org/10.1016/j.exer.2014.07.014 | PubMed | Google Scholar

11. Keller KE, Acott TS (2013) **The Juxtacanalicular Region of Ocular Trabecular Meshwork: A Tissue with a Unique Extracellular Matrix and Specialized Function** *J Ocul Biol* **1**:3 PubMed | Google Scholar

12. Johnson M (2006) **What controls aqueous humour outflow resistance?** *Exp Eye Res* **82**:545–57 https://doi.org/10.1016/j.exer.2005.10.011 | PubMed | Google Scholar

13. Tian B, Gabelt BT, Geiger B, Kaufman PL (2009) **The role of the actomyosin system in regulating trabecular fluid outflow** *Exp Eye Res* **88**:713–7 https://doi.org/10.1016/j.exer.2008

.08.008 | PubMed | Google Scholar

14. Tamm ER (2009) **The trabecular meshwork outflow pathways: structural and functional aspects** *Exp Eye Res* **88**:648–55 https://doi.org/10.1016/j.exer.2009.02.007 | PubMed | Google Scholar

15. Overby DR, Stamer WD, Johnson M (2009) **The changing paradigm of outflow resistance generation: towards synergistic models of the JCT and inner wall endothelium** *Exp Eye Res* **88**:656–70 https://doi.org/10.1016/j.exer.2008.11.033 | PubMed | Google Scholar

16. Zhang M, Rao PV (2005) **Blebbistatin, a novel inhibitor of myosin II ATPase activity, increases aqueous humor outflow facility in perfused enucleated porcine eyes** *Invest Ophthalmol Vis Sci* **46**:4130–8 https://doi.org/10.1167/iovs.05-0164 | PubMed | Google Scholar

17. Thieme H, Nuskovski M, Nass JU, Pleyer U, Strauss O, Wiederholt M (2000) **Mediation of calcium-independent contraction in trabecular meshwork through protein kinase C and rho-A** *Invest Ophthalmol Vis Sci* **41**:4240–6 PubMed | Google Scholar

18. Rao PV, Deng P, Sasaki Y, Epstein DL (2005) **Regulation of myosin light chain phosphorylation in the trabecular meshwork: role in aqueous humour outflow facility** *Exp Eye Res* **80**:197–206 https://doi.org/10.1016/j.exer.2004.08.029 | PubMed | Google Scholar

19. Syriani E, Cuesto G, Abad E, Pelaez T, Gual A, Pintor J, et al. (2009) **Effects of platelet-derived growth factor on aqueous humor dynamics** *Invest Ophthalmol Vis Sci* **50**:3833–9 https://doi.org/10.1167/iovs.08-2924 | PubMed | Google Scholar

20. Tian B, Kaufman PL (2005) **Effects of the Rho kinase inhibitor Y-27632 and the phosphatase inhibitor calyculin A on outflow facility in monkeys** *Exp Eye Res* **80**:215–25 https://doi.org/10.1016/j.exer.2004.09.002 | PubMed | Google Scholar

21. Rao PV, Deng PF, Kumar J, Epstein DL (2001) **Modulation of aqueous humor outflow facility by the Rho kinase-specific inhibitor Y-27632** *Invest Ophthalmol Vis Sci* **42**:1029–37 PubMed | Google Scholar

22. Yu M, Chen X, Wang N, Cai S, Li N, Qiu J, et al. (2008) **H-1152 effects on intraocular pressure and trabecular meshwork morphology of rat eyes** *J Ocul Pharmacol Ther* **24**:373–9 https://doi.org/10.1089/jop.2008.0029 | PubMed | Google Scholar

23. Wang K, Li G, Read AT, Navarro I, Mitra AK, Stamer WD, et al. (2018) **The relationship between outflow resistance and trabecular meshwork stiffness in mice** *Sci Rep* **8**:5848 https://doi.org/10.1038/s41598-018-24165-w | PubMed | Google Scholar

24. Thomson BR, Liu P, Onay T, Du J, Tompson SW, Misener S, et al. (2021) **Cellular crosstalk regulates the aqueous humor outflow pathway and provides new targets for glaucoma therapies** *Nat Commun* **12**:6072 https://doi.org/10.1038/s41467-021-26346-0 | PubMed | Google Scholar

25. Kizhatil K, Ryan M, Marchant JK, Henrich S, John SW (2014) **Schlemm's canal is a unique vessel with a combination of blood vascular and lymphatic phenotypes that forms by a novel developmental process** *PLoS Biol* **12**:e1001912 https://doi.org/10.1371/journal.pbio.1001912 | PubMed | Google Scholar

26. Balasubramanian R, Kizhatil K, Li T, Tolman N, Bhandari A, Clark G, et al. (2024) **Transcriptomic profiling of Schlemm's canal cells reveals a lymphatic-biased identity and three major**

cell states *bioRxiv* https://doi.org/10.1101/2023.08.31.555823 | PubMed | Google Scholar

27. Stamer WD, Acott TS (2012) **Current understanding of conventional outflow dysfunction in glaucoma** *Curr Opin Ophthalmol* **23**:135–43 https://doi.org/10.1097/ICU.0b013e32834ff23e | PubMed | Google Scholar

28. Gharahkhani P, Jorgenson E, Hysi P, Khawaja AP, Pendergrass S, Han X, et al. (2021) **Genome-wide meta-analysis identifies 127 open-angle glaucoma loci with consistent effect across ancestries** *Nat Commun* **12**:1258 https://doi.org/10.1038/s41467-020-20851-4 | PubMed | Google Scholar

29. Chen L, Zhao Y, Zhang H (2016) **Comparative Anatomy of the Trabecular Meshwork, the Optic Nerve Head and the Inner Retina in Rodent and Primate Models Used for Glaucoma Research** *Vision (Basel)* **1** https://doi.org/10.3390/vision1010004 | PubMed | Google Scholar

30. Smith RS, Zabaleta A, Savinova OV, John SW (2001) **The mouse anterior chamber angle and trabecular meshwork develop without cell death** *BMC Dev Biol* **1** https://doi.org/10.1186/1471-213x-1-3 | PubMed | Google Scholar

31. van Zyl T, Yan W, McAdams A, Peng YR, Shekhar K, Regev A, et al. (2020) **Cell atlas of aqueous humor outflow pathways in eyes of humans and four model species provides insight into glaucoma pathogenesis** *Proc Natl Acad Sci U S A* **117**:10339–49 https://doi.org/10.1073/pnas.2001250117 | PubMed | Google Scholar

32. van Zyl T, Yan W, McAdams AM, Monavarfeshani A, Hageman GS, Sanes JR (2022) **Cell atlas of the human ocular anterior segment: Tissue-specific and shared cell types** *Proc Natl Acad Sci U S A* **119**:e2200914119 https://doi.org/10.1073/pnas.2200914119 | PubMed | Google Scholar

33. Patel G, Fury W, Yang H, Gomez-Caraballo M, Bai Y, Yang T, et al. (2020) **Molecular taxonomy of human ocular outflow tissues defined by single-cell transcriptomics** *Proc Natl Acad Sci U S A* **117**:12856–67 https://doi.org/10.1073/pnas.2001896117 | PubMed | Google Scholar

34. Khawaja AP, Cooke Bailey JN, Wareham NJ, Scott RA, Simcoe M, Igo RP, et al. (2018) **Genome-wide analyses identify 68 new loci associated with intraocular pressure and improve risk prediction for primary open-angle glaucoma** *Nat Genet* **50**:778–82 https://doi.org/10.1038/s41588-018-0126-8 | PubMed | Google Scholar

35. MacGregor S, Ong JS, An J, Han X, Zhou T, Siggs OM, et al. (2018) **Genome-wide association study of intraocular pressure uncovers new pathways to glaucoma** *Nat Genet* **50**:1067–71 https://doi.org/10.1038/s41588-018-0176-y | PubMed | Google Scholar

36. Choquet H, Paylakhi S, Kneeland SC, Thai KK, Hoffmann TJ, Yin J, et al. (2018) **A multiethnic genome-wide association study of primary open-angle glaucoma identifies novel risk loci** *Nat Commun* **9**:2278 https://doi.org/10.1038/s41467-018-04555-4 | PubMed | Google Scholar

37. Gao XR, Huang H, Nannini DR, Fan F, Kim H (2018) **Genome-wide association analyses identify new loci influencing intraocular pressure** *Hum Mol Genet* **27**:2205–13 https://doi.org/10.1093/hmg/ddy111 | PubMed | Google Scholar

38. Shiga Y, Akiyama M, Nishiguchi KM, Sato K, Shimozawa N, Takahashi A, et al. (2018) **Genome-wide association study identifies seven novel susceptibility loci for primary open-angle glaucoma** *Hum Mol Genet* **27**:1486–96 https://doi.org/10.1093/hmg/ddy053 | PubMed | Google Scholar

39. Cross SH, Macalinao DG, McKie L, Rose L, Kearney AL, Rainger J, et al. (2014) **A dominant-negative mutation of mouse Lmx1b causes glaucoma and is semi-lethal via LDB1-mediated dimerization [corrected]** *PLoS Genet* **10**:e1004359 https://doi.org/10.1371/journal.pgen.1004359 | PubMed | Google Scholar

40. Tolman NG, Balasubramanian R, Macalinao DG, Kearney AL, MacNicoll KH, Montgomery CL, et al. (2021) **Genetic background modifies vulnerability to glaucoma-related phenotypes in Lmx1b mutant mice** *Dis Model Mech* **14** https://doi.org/10.1242/dmm.046953 | PubMed | Google Scholar

41. Akula M, Taiyab A, Deschamps P, Yee S, Ball AK, Williams T, et al. (2020) **AP-2beta is required for formation of the murine trabecular meshwork and Schlemm's canal** *Exp Eye Res* **195** https://doi.org/10.1016/j.exer.2020.108042 | PubMed | Google Scholar

42. Ostojic J, Grozdanic S, Syed NA, Hargrove MS, Trent JT, et al. (2008) **3rd, Kuehn MH, Neuroglobin and cytoglobin distribution in the anterior eye segment: a comparative immunohistochemical study** *J Histochem Cytochem* **56**:863–72 https://doi.org/10.1369/jhc.2008.951392 | PubMed | Google Scholar

43. de Kater AW, Shahsafaei A, Epstein DL (1992) **Localization of smooth muscle and nonmuscle actin isoforms in the human aqueous outflow pathway** *Invest Ophthalmol Vis Sci* **33**:424–9 PubMed | Google Scholar

44. Patel SP, Parker MD (2015) **SLC4A11 and the Pathophysiology of Congenital Hereditary Endothelial Dystrophy** *Biomed Res Int* **2015**:475392 https://doi.org/10.1155/2015/475392 | PubMed | Google Scholar

45. Lopez IA, Rosenblatt MI, Kim C, Galbraith GC, Jones SM, Kao L, et al. (2009) **Slc4a11 gene disruption in mice: cellular targets of sensorineuronal abnormalities** *J Biol Chem* **284**:26882–96 https://doi.org/10.1074/jbc.M109.008102 | PubMed | Google Scholar

46. Liu CY, Birk DE, Hassell JR, Kane B, Kao WW (2003) **Keratocan-deficient mice display alterations in corneal structure** *J Biol Chem* **278**:21672–7 https://doi.org/10.1074/jbc.M301169200 | PubMed | Google Scholar

47. Toyono T, Usui T, Yokoo S, Taketani Y, Nakagawa S, Kuroda M, et al. (2015) **Angiopoietin-like 7 is an anti-angiogenic protein required to prevent vascularization of the cornea** *PLoS One* **10**:e0116838 https://doi.org/10.1371/journal.pone.0116838 | PubMed | Google Scholar

48. Monje PV, Sant D, Wang G (2018) **Phenotypic and Functional Characteristics of Human Schwann Cells as Revealed by Cell-Based Assays and RNA-SEQ** *Mol Neurobiol* **55**:6637–60 https://doi.org/10.1007/s12035-017-0837-3 | PubMed | Google Scholar

49. Stratton JA, Kumar R, Sinha S, Shah P, Stykel M, Shapira Y, et al. (2017) **Purification and Characterization of Schwann Cells from Adult Human Skin and Nerve** *eNeuro* **4** https://doi.org/10.1523/ENEURO.0307-16.2017 | PubMed | Google Scholar

50. Nitzan E, Pfaltzgraff ER, Labosky PA, Kalcheim C (2013) **Neural crest and Schwann cell progenitor-derived melanocytes are two spatially segregated populations similarly regulated by Foxd3** *Proc Natl Acad Sci U S A* **110**:12709–14 https://doi.org/10.1073/pnas.1306287110 | PubMed | Google Scholar

51. Ujiie N, Norden PR, Fang R, Beckmann L, Cai Z, Kweon J, et al. (2023) **Differential roles of FOXC2 in the trabecular meshwork and Schlemm's canal in glaucomatous pathology** *Life*

Sci Alliance **6** https://doi.org/10.26508/lsa.202201721 | PubMed | Google Scholar

52. van den Brink SC, Sage F, Vertesy A, Spanjaard B, Peterson-Maduro J, Baron CS, et al. (2017) **Single-cell sequencing reveals dissociation-induced gene expression in tissue subpopulations** *Nat Methods* **14**:935–6 https://doi.org/10.1038/nmeth.4437 | PubMed | Google Scholar

53. Desronvil T, Logan-Wyatt D, Abdrabou W, Triana M, Jones R, Taheri S, et al. (2010) **Distribution of COL8A2 and COL8A1 gene variants in Caucasian primary open angle glaucoma patients with thin central corneal thickness** *Mol Vis* **16**:2185–91 PubMed | Google Scholar

54. Ali M, McKibbin M, Booth A, Parry DA, Jain P, Riazuddin SA, et al. (2009) **Null mutations in LTBP2 cause primary congenital glaucoma** *Am J Hum Genet* **84**:664–71 https://doi.org/10.1016/j.ajhg.2009.03.017 | PubMed | Google Scholar

55. Roberts AL, Mavlyutov TA, Perlmutter TE, Curry SM, Harris SL, Chauhan AK, et al. (2020) **Fibronectin extra domain A (FN-EDA) elevates intraocular pressure through Toll-like receptor 4 signaling** *Sci Rep* **10**:9815 https://doi.org/10.1038/s41598-020-66756-6 | PubMed | Google Scholar

56. Knepper PA, Farbman AI, Telser AG (1981) **Aqueous outflow pathway glycosaminoglycans** *Exp Eye Res* **32**:265–77 https://doi.org/10.1016/0014-4835(81)90032-4 | PubMed | Google Scholar

57. Knepper PA, McLone DG (1985) **Glycosaminoglycans and outflow pathways of the eye and brain** *Pediatr Neurosci* **12**:240–51 https://doi.org/10.1159/000120258 | PubMed | Google Scholar

58. Knepper PA, Goossens W, Hvizd M, Palmberg PF (1996) **Glycosaminoglycans of the human trabecular meshwork in primary open-angle glaucoma** *Invest Ophthalmol Vis Sci* **37**:1360–7 PubMed | Google Scholar

59. Aumailley M. (2013) **The laminin family** *Cell Adh Migr* **7**:48–55 https://doi.org/10.4161/cam.22826 | PubMed | Google Scholar

60. Aboobakar IF, Kinzy TG, Zhao Y, Fan B, Pasquale LR, Qassim A, et al. (2023) **Mitochondrial TXNRD2 and ME3 Genetic Risk Scores Are Associated with Specific Primary Open-Angle Glaucoma Phenotypes** *Ophthalmology* **130**:756–63 https://doi.org/10.1016/j.ophtha.2023.02.018 | PubMed | Google Scholar

61. Khawaja AP, Cooke Bailey JN, Kang JH, Allingham RR, Hauser MA, Brilliant M, et al. (2016) **Assessing the Association of Mitochondrial Genetic Variation With Primary Open-Angle Glaucoma Using Gene-Set Analyses** *Invest Ophthalmol Vis Sci* **57**:5046–52 https://doi.org/10.1167/iovs.16-20017 | PubMed | Google Scholar

62. Zhang ZQ, Xie Z, Chen SY, Zhang X (2023) **Mitochondrial dysfunction in glaucomatous degeneration** *Int J Ophthalmol* **16**:811–23 https://doi.org/10.18240/ijo.2023.05.20 | PubMed | Google Scholar

63. Xin Y, Lyu P, Jiang J, Zhou F, Wang J, Blackshaw S, et al. (2022) **LRLoop: a method to predict feedback loops in cell-cell communication** *Bioinformatics* **38**:4117–26 https://doi.org/10.1093/bioinformatics/btac447 | PubMed | Google Scholar

64. Browaeys R, Saelens W, Saeys Y (2020) **NicheNet: modeling intercellular communication by linking ligands to target genes** *Nat Methods* **17**:159–62 https://doi.org/10.1038/s41592-019-0667-5 | PubMed | Google Scholar

65. Shibuya M (2011) **Vascular Endothelial Growth Factor (VEGF) and Its Receptor (VEGFR) Signaling in Angiogenesis: A Crucial Target for Anti- and Pro-Angiogenic Therapies** *Genes Cancer* **2**:1097–105 https://doi.org/10.1177/1947601911423031 | PubMed | Google Scholar

66. Saharinen P, Eklund L, Alitalo K (2017) **Therapeutic targeting of the angiopoietin-TIE pathway** *Nat Rev Drug Discov* **16**:635–61 https://doi.org/10.1038/nrd.2016.278 | PubMed | Google Scholar

67. Genovesi S, Giussani M, Orlando A, Lieti G, Viazzi F, Parati G (2022) **Relationship between endothelin and nitric oxide pathways in the onset and maintenance of hypertension in children and adolescents** *Pediatr Nephrol* **37**:537–45 https://doi.org/10.1007/s00467-021-05144-2 | PubMed | Google Scholar

68. Thomson BR, Grannonico M, Liu F, Liu M, Mendapara P, Xu Y, et al. (2020) **Angiopoietin-1 Knockout Mice as a Genetic Model of Open-Angle Glaucoma** *Transl Vis Sci Technol* **9**:16 https://doi.org/10.1167/tvst.9.4.16 | PubMed | Google Scholar

69. Fujimoto T, Inoue T, Maki K, Inoue-Mochita M, Tanihara H (2016) **Vascular Endothelial Growth Factor-A Increases the Aqueous Humor Outflow Facility** *PLoS One* **11**:e0161332 https://doi.org/10.1371/journal.pone.0161332 | PubMed | Google Scholar

70. Reina-Torres E, Wen JC, Liu KC, Li G, Sherwood JM, Chang JY, et al. (2017) **VEGF as a Paracrine Regulator of Conventional Outflow Facility** *Invest Ophthalmol Vis Sci* **58**:1899–908 https://doi.org/10.1167/iovs.16-20779 | PubMed | Google Scholar

71. Comes N, Borras T (2009) **Individual molecular response to elevated intraocular pressure in perfused postmortem human eyes** *Physiol Genomics* **38**:205–25 https://doi.org/10.1152/physiolgenomics.90261.2008 | PubMed | Google Scholar

72. Zhang C, Simon M, Lim H, Tolman NG, Horbal L, Juarez FA, et al. (2024) **IOP-induced blood-retinal barrier compromise contributes to RGC death in glaucoma** *bioRxiv* https://doi.org/10.1101/2024.10.15.618539 | PubMed | Google Scholar

73. Schondorf DC, Ivanyuk D, Baden P, Sanchez-Martinez A, De Cicco S, Yu C, et al. (2018) **The NAD+ Precursor Nicotinamide Riboside Rescues Mitochondrial Defects and Neuronal Loss in iPSC and Fly Models of Parkinson's Disease** *Cell Rep* **23**:2976–88 https://doi.org/10.1016/j.celrep.2018.05.009 | PubMed | Google Scholar

74. Williams PA, Harder JM, Foxworth NE, Cochran KE, Philip VM, Porciatti V, et al. (2017) **Vitamin B(3) modulates mitochondrial vulnerability and prevents glaucoma in aged mice** *Science* **355**:756–60 https://doi.org/10.1126/science.aal0092 | PubMed | Google Scholar

75. Libby RT, Smith RS, Savinova OV, Zabaleta A, Martin JE, Gonzalez FJ, et al. (2003) **Modification of ocular defects in mouse developmental glaucoma models by tyrosinase** *Science* **299**:1578–81 https://doi.org/10.1126/science.1080095 | PubMed | Google Scholar

76. Keller KE, Aga M, Bradley JM, Kelley MJ, Acott TS (2009) **Extracellular matrix turnover and outflow resistance** *Exp Eye Res* **88**:676–82 https://doi.org/10.1016/j.exer.2008.11.023 | PubMed | Google Scholar

77. Fuchshofer R, Tamm ER (2009) **Modulation of extracellular matrix turnover in the trabecular meshwork** *Exp Eye Res* **88**:683–8 https://doi.org/10.1016/j.exer.2009.01.005 | PubMed | Google Scholar

78. Wang WH, McNatt LG, Pang IH, Millar JC, Hellberg PE, Hellberg MH, et al. (2008) **Increased expression of the WNT antagonist sFRP-1 in glaucoma elevates intraocular pressure** *J Clin Invest* **118**:1056–64 https://doi.org/10.1172/JCI33871 | PubMed | Google Scholar

79. McDowell CM, Tebow HE, Wordinger RJ, Clark AF (2013) **Smad3 is necessary for transforming growth factor-beta2 induced ocular hypertension in mice** *Exp Eye Res* **116**:419–23 https://doi.org/10.1016/j.exer.2013.10.017 | PubMed | Google Scholar

80. Shepard AR, Millar JC, Pang IH, Jacobson N, Wang WH, Clark AF (2010) **Adenoviral gene transfer of active human transforming growth factor-beta2 elevates intraocular pressure and reduces outflow facility in rodent eyes** *Invest Ophthalmol Vis Sci* **51**:2067–76 https://doi.org/10.1167/iovs.09-4567 | PubMed | Google Scholar

81. Rudzitis CN, Lakk M, Singh A, Redmon SN, Kirdajova D, Tseng YT, et al. (2025) **TRPV4 activation by TGFbeta2 enhances cellular contractility and drives ocular hypertension** *eLife* **14** https://doi.org/10.7554/eLife.104894 | PubMed | Google Scholar

82. Fleenor DL, Shepard AR, Hellberg PE, Jacobson N, Pang IH, Clark AF (2006) **TGFbeta2-induced changes in human trabecular meshwork: implications for intraocular pressure** *Invest Ophthalmol Vis Sci* **47**:226–34 https://doi.org/10.1167/iovs.05-1060 | PubMed | Google Scholar

83. Gottanka J, Chan D, Eichhorn M, Lutjen-Drecoll E, Ethier CR (2004) **Effects of TGF-beta2 in perfused human eyes** *Invest Ophthalmol Vis Sci* **45**:153–8 https://doi.org/10.1167/iovs.03-0796 | PubMed | Google Scholar

84. Wordinger RJ, Fleenor DL, Hellberg PE, Pang IH, Tovar TO, Zode GS, et al. (2007) **Effects of TGF-beta2, BMP-4, and gremlin in the trabecular meshwork: implications for glaucoma** *Invest Ophthalmol Vis Sci* **48**:1191–200 https://doi.org/10.1167/iovs.06-0296 | PubMed | Google Scholar

85. Mody AA, Millar JC, Clark AF (2021) **ID1 and ID3 are Negative Regulators of TGFbeta2-Induced Ocular Hypertension and Compromised Aqueous Humor Outflow Facility in Mice** *Invest Ophthalmol Vis Sci* **62**:3 https://doi.org/10.1167/iovs.62.6.3 | PubMed | Google Scholar

86. Gagen D, Faralli JA, Filla MS, Peters DM (2014) **The role of integrins in the trabecular meshwork** *J Ocul Pharmacol Ther* **30**:110–20 https://doi.org/10.1089/jop.2013.0176 | PubMed | Google Scholar

87. Faralli JA, Filla MS, Peters DM (2019) **Effect of alphavbeta3 Integrin Expression and Activity on Intraocular Pressure** *Invest Ophthalmol Vis Sci* **60**:1776–88 https://doi.org/10.1167/iovs.18-26038 | PubMed | Google Scholar

88. Yang YF, Sun YY, Peters DM, Keller KE (2022) **The Effects of Mechanical Stretch on Integrins and Filopodial-Associated Proteins in Normal and Glaucomatous Trabecular Meshwork Cells** *Front Cell Dev Biol* **10** https://doi.org/10.3389/fcell.2022.886706 | PubMed | Google Scholar

89. Bermudez JY, Montecchi-Palmer M, Mao W, Clark AF (2017) **Cross-linked actin networks (CLANs) in glaucoma** *Exp Eye Res* **159**:16–22 https://doi.org/10.1016/j.exer.2017.02.010 | PubMed | Google Scholar

90. Xue W, Comes N, Borras T (2007) **Presence of an established calcification marker in trabecular meshwork tissue of glaucoma donors** *Invest Ophthalmol Vis Sci* **48**:3184–94 https://doi.org/10.1167/iovs.06-1403 | PubMed | Google Scholar

91. Borras T, Comes N (2009) **Evidence for a calcification process in the trabecular meshwork** *Exp Eye Res* **88**:738–46 https://doi.org/10.1016/j.exer.2008.11.027 | PubMed | Google Scholar

92. Saccuzzo EG, Youngblood HA, Lieberman RL. (2023) **Myocilin misfolding and glaucoma: A 20-year update** *Prog Retin Eye Res* **95** https://doi.org/10.1016/j.preteyeres.2023.101188 | PubMed | Google Scholar

93. Fingert JH, Stone EM, Sheffield VC, Alward WL. (2002) **Myocilin glaucoma** *Surv Ophthalmol* **47**:547–61 https://doi.org/10.1016/s0039-6257(02)00353-3 | PubMed | Google Scholar

94. Sharma R, Grover A. (2021) **Myocilin-associated Glaucoma: A Historical Perspective and Recent Research Progress** *Mol Vis* **27**:480–93 PubMed | Google Scholar

95. Herrmann H, Bar H, Kreplak L, Strelkov SV, Aebi U (2007) **Intermediate filaments: from cell architecture to nanomechanics** *Nat Rev Mol Cell Biol* **8**:562–73 https://doi.org/10.1038/nrm2197 | PubMed | Google Scholar

96. Ethier CR (2002) **The inner wall of Schlemm's canal** *Exp Eye Res* **74**:161–72 https://doi.org/10.1006/exer.2002.1144 | PubMed | Google Scholar

97. Acott TS, Kingsley PD, Samples JR, Van Buskirk EM (1988) **Human trabecular meshwork organ culture: morphology and glycosaminoglycan synthesis** *Invest Ophthalmol Vis Sci* **29**:90–100 PubMed | Google Scholar

98. Munger JS, Sheppard D (2011) **Cross talk among TGF-beta signaling pathways, integrins, and the extracellular matrix** *Cold Spring Harb Perspect Biol* **3**:a005017 https://doi.org/10.1101/cshperspect.a005017 | PubMed | Google Scholar

99. Meng XM, Nikolic-Paterson DJ, Lan HY (2016) **TGF-beta: the master regulator of fibrosis** *Nat Rev Nephrol* **12**:325–38 https://doi.org/10.1038/nrneph.2016.48 | PubMed | Google Scholar

100. Frangogiannis N (2020) **Transforming growth factor-beta in tissue fibrosis** *J Exp Med* **217**:e20190103 https://doi.org/10.1084/jem.20190103 | PubMed | Google Scholar

101. Biernacka A, Dobaczewski M, Frangogiannis NG (2011) **TGF-beta signaling in fibrosis** *Growth Factors* **29**:196–202 https://doi.org/10.3109/08977194.2011.595714 | PubMed | Google Scholar

102. Fuchshofer R, Tamm ER (2012) **The role of TGF-beta in the pathogenesis of primary open-angle glaucoma** *Cell Tissue Res* **347**:279–90 https://doi.org/10.1007/s00441-011-1274-7 | PubMed | Google Scholar

103. Tripathi RC, Li J, Chan WF, Tripathi BJ (1994) **Aqueous humor in glaucomatous eyes contains an increased level of TGF-beta 2** *Exp Eye Res* **59**:723–7 https://doi.org/10.1006/exer.1994.1158 | PubMed | Google Scholar

104. Min SH, Lee TI, Chung YS, Kim HK (2006) **Transforming growth factor-beta levels in human aqueous humor of glaucomatous, diabetic and uveitic eyes** *Korean J Ophthalmol* **20**:162–5 https://doi.org/10.3341/kjo.2006.20.3.162 | PubMed | Google Scholar

105. Overby DR, Bertrand J, Schicht M, Paulsen F, Stamer WD, Lutjen-Drecoll E (2014) **The structure of the trabecular meshwork, its connections to the ciliary muscle, and the effect of pilocarpine on outflow facility in mice** *Invest Ophthalmol Vis Sci* **55**:3727–36 https://doi.org/10.1167/iovs.13-13699 | PubMed | Google Scholar

106. Shifera AS, Trivedi S, Chau P, Bonnemaison LH, Iguchi R, Alvarado JA (2010) **Constitutive secretion of chemokines by cultured human trabecular meshwork cells** *Exp Eye Res* **91**:42–7 https://doi.org/10.1016/j.exer.2010.04.001 | PubMed | Google Scholar

107. Souma T, Tompson SW, Thomson BR, Siggs OM, Kizhatil K, Yamaguchi S, et al. (2016) **Angiopoietin receptor TEK mutations underlie primary congenital glaucoma with variable expressivity** *J Clin Invest* **126**:2575–87 https://doi.org/10.1172/JCI85830 | PubMed | Google Scholar

108. Kabra M, Zhang W, Rathi S, Mandal AK, Senthil S, Pyatla G, et al. (2017) **Angiopoietin receptor TEK interacts with CYP1B1 in primary congenital glaucoma** *Hum Genet* **136**:941–9 https://doi.org/10.1007/s00439-017-1823-6 | PubMed | Google Scholar

109. Aspelund A, Tammela T, Antila S, Nurmi H, Leppanen VM, Zarkada G, et al. (2014) **The Schlemm's canal is a VEGF-C/VEGFR-3-responsive lymphatic-like vessel** *J Clin Invest* **124**:3975–86 https://doi.org/10.1172/JCI75395 | PubMed | Google Scholar

110. DeWane G, Salvi AM, DeMali KA (2021) **Fueling the cytoskeleton - links between cell metabolism and actin remodeling** *J Cell Sci* **134** https://doi.org/10.1242/jcs.248385 | PubMed | Google Scholar

111. Baker N, Patel J, Khacho M (2019) **Linking mitochondrial dynamics, cristae remodeling and supercomplex formation: How mitochondrial structure can regulate bioenergetics** *Mitochondrion* **49**:259–68 https://doi.org/10.1016/j.mito.2019.06.003 | PubMed | Google Scholar

112. Jenkins BC, Neikirk K, Katti P, Claypool SM, Kirabo A, McReynolds MR, et al. (2024) **Mitochondria in disease: changes in shapes and dynamics** *Trends Biochem Sci* **49**:346–60 https://doi.org/10.1016/j.tibs.2024.01.011 | PubMed | Google Scholar

113. Golombek M, Tsigaras T, Schaumkessel Y, Hansch S, Weidtkamp-Peters S, Anand R, et al. (2024) **Cristae dynamics is modulated in bioenergetically compromised mitochondria** *Life Sci Alliance* **7** https://doi.org/10.26508/lsa.202302386 | PubMed | Google Scholar

114. Huang C, Deng K, Wu M (2023) **Mitochondrial cristae in health and disease** *Int J Biol Macromol* **235** https://doi.org/10.1016/j.ijbiomac.2023.123755 | PubMed | Google Scholar

115. Jezek P, Jaburek M, Holendova B, Engstova H, Dlaskova A (2023) **Mitochondrial Cristae Morphology Reflecting Metabolism, Superoxide Formation, Redox Homeostasis, and Pathology** *Antioxid Redox Signal* **39**:635–83 https://doi.org/10.1089/ars.2022.0173 | PubMed | Google Scholar

116. Jimenez-Moreno N, Kollareddy M, Stathakos P, Moss JJ, Anton Z, Shoemark DK, et al. (2023) **ATG8-dependent LMX1B-autophagy crosstalk shapes human midbrain dopaminergic**

neuronal resilience *J Cell Biol* **222** https://doi.org/10.1083/jcb.201910133 | PubMed | Google Scholar

117. Doucet-Beaupre H, Gilbert C, Profes MS, Chabrat A, Pacelli C, Giguere N, et al. (2016) **Lmx1a and Lmx1b regulate mitochondrial functions and survival of adult midbrain dopaminergic neurons** *Proc Natl Acad Sci U S A* **113**:E4387–96 https://doi.org/10.1073/pnas.1520387113 | PubMed | Google Scholar

118. Bergman O, Hakansson A, Westberg L, Belin AC, Sydow O, Olson L, et al. (2009) **Do polymorphisms in transcription factors LMX1A and LMX1B influence the risk for Parkinson's disease?** *J Neural Transm (Vienna)* **116**:333–8 https://doi.org/10.1007/s00702-009-0187-z | PubMed | Google Scholar

119. Jang SY, Kang HT, Hwang ES (2012) **Nicotinamide-induced mitophagy: event mediated by high NAD+/NADH ratio and SIRT1 protein activation** *J Biol Chem* **287**:19304–14 https://doi.org/10.1074/jbc.M112.363747 | PubMed | Google Scholar

120. Verdin E (2015) **NAD(+) in aging, metabolism, and neurodegeneration** *Science* **350**:1208–13 https://doi.org/10.1126/science.aac4854 | PubMed | Google Scholar

121. Mouchiroud L, Houtkooper RH, Moullan N, Katsyuba E, Ryu D, Canto C, et al. (2013) **The NAD(+)/Sirtuin Pathway Modulates Longevity through Activation of Mitochondrial UPR and FOXO Signaling** *Cell* **154**:430–41 https://doi.org/10.1016/j.cell.2013.06.016 | PubMed | Google Scholar

122. Gomes AP, Price NL, Ling AJ, Moslehi JJ, Montgomery MK, Rajman L, et al. (2013) **Declining NAD(+) induces a pseudohypoxic state disrupting nuclear-mitochondrial communication during aging** *Cell* **155**:1624–38 https://doi.org/10.1016/j.cell.2013.11.037 | PubMed | Google Scholar

123. Imai S, Guarente L. (2014) **NAD+ and sirtuins in aging and disease** *Trends Cell Biol* **24**:464–71 https://doi.org/10.1016/j.tcb.2014.04.002 | PubMed | Google Scholar

124. Song SB, Park JS, Jang SY, Hwang ES (2021) **Nicotinamide Treatment Facilitates Mitochondrial Fission through Drp1 Activation Mediated by SIRT1-Induced Changes in Cellular Levels of cAMP and Ca(2)** *Cells* **10** https://doi.org/10.3390/cells10030612 | PubMed | Google Scholar

125. Kang HT, Hwang ES (2009) **Nicotinamide enhances mitochondria quality through autophagy activation in human cells** *Aging Cell* **8**:426–38 https://doi.org/10.1111/j.1474-9726.2009.00487.x | PubMed | Google Scholar

126. Sweeney E, Fryer A, Mountford R, Green A, McIntosh I (2003) **Nail patella syndrome: a review of the phenotype aided by developmental biology** *J Med Genet* **40**:153–62 https://doi.org/10.1136/jmg.40.3.153 | PubMed | Google Scholar

127. Chen H, Lun Y, Ovchinnikov D, Kokubo H, Oberg KC, Pepicelli CV, et al. (1998) **Limb and kidney defects in Lmx1b mutant mice suggest an involvement of LMX1B in human nail patella syndrome** *Nat Genet* **19**:51–5 https://doi.org/10.1038/ng0598-51 | PubMed | Google Scholar

128. Vollrath D, Jaramillo-Babb VL, Clough MV, McIntosh I, Scott KM, Lichter PR, et al. (1998) **Loss-of-function mutations in the LIM-homeodomain gene, LMX1B, in nail-patella syndrome** *Hum Mol Genet* **7**:1091–8 https://doi.org/10.1093/hmg/7.7.1091 | PubMed | Google Scholar

129. Choquet H, Thai KK, Yin J, Hoffmann TJ, Kvale MN, Banda Y, et al. (2017) **A large multi-ethnic genome-wide association study identifies novel genetic loci for intraocular pressure** *Nat Commun* **8**:2108 https://doi.org/10.1038/s41467-017-01913-6 | PubMed | Google Scholar

130. Hui F, Tang J, Williams PA, McGuinness MB, Hadoux X, Casson RJ, et al. (2020) **Improvement in inner retinal function in glaucoma with nicotinamide (vitamin B3) supplementation: A crossover randomized clinical trial** *Clin Exp Ophthalmol* **48**:903–14 https://doi.org/10.1111/ceo.13818 | PubMed | Google Scholar

131. Williams PA, Harder JM, Foxworth NE, Cardozo BH, Cochran KE, John SWM (2017) **Nicotinamide and WLD(S) Act Together to Prevent Neurodegeneration in Glaucoma** *Front Neurosci* **11** https://doi.org/10.3389/fnins.2017.00232 | PubMed | Google Scholar

132. Williams PA, Harder JM, Cardozo BH, Foxworth NE, John SWM (2018) **Nicotinamide treatment robustly protects from inherited mouse glaucoma** *Commun Integr Biol* **11**:e1356956 https://doi.org/10.1080/19420889.2017.1356956 | PubMed | Google Scholar

133. De Moraes CG, John SWM, Williams PA, Blumberg DM, Cioffi GA, Liebmann JM (2022) **Nicotinamide and Pyruvate for Neuroenhancement in Open-Angle Glaucoma: A Phase 2 Randomized Clinical Trial** *JAMA Ophthalmol* **140**:11–8 https://doi.org/10.1001/jamaophthalmol.2021.4576 | PubMed | Google Scholar

134. Abu-Amero KK, Morales J, Bosley TM (2006) **Mitochondrial abnormalities in patients with primary open-angle glaucoma** *Invest Ophthalmol Vis Sci* **47**:2533–41 https://doi.org/10.1167/iovs.05-1639 | PubMed | Google Scholar

135. Faro V Lo, Nolte IM, Ten Brink JB, Snieder H, Jansonius NM, Bergen AA (2021) **Mitochondrial Genome Study Identifies Association Between Primary Open-Angle Glaucoma and Variants in MT-CYB, MT-ND4 Genes and Haplogroups** *Front Genet* **12**:781189 https://doi.org/10.3389/fgene.2021.781189 | PubMed | Google Scholar

136. Petriti B, Rabiolo A, Chau KY, Williams PA, Montesano G, Lascaratos G, et al. (2024) **Peripheral blood mononuclear cell respiratory function is associated with progressive glaucomatous vision loss** *Nat Med* **30**:2362–70 https://doi.org/10.1038/s41591-024-03068-6 | PubMed | Google Scholar

137. Venkatesan A, Bernstein AM (2025) **Protein misfolding and mitochondrial dysfunction in glaucoma** *Front Cell Dev Biol* **13** https://doi.org/10.3389/fcell.2025.1595121 | PubMed | Google Scholar

138. Venkatesan A, Ridilla M, Castro N, Wolosin JM, Henty-Ridilla JL, Knox BE, et al. (2025) **Mitochondrial and microtubule defects in Exfoliation Glaucoma** *Free Radic Biol Med* **233**:226–39 https://doi.org/10.1016/j.freeradbiomed.2025.03.046 | PubMed | Google Scholar

139. Thaung C, West K, Clark BJ, McKie L, Morgan JE, Arnold K, et al. (2002) **Novel ENU-induced eye mutations in the mouse: models for human eye disease** *Hum Mol Genet* **11**:755–67 https://doi.org/10.1093/hmg/11.7.755 | PubMed | Google Scholar

140. John SW, Hagaman JR, MacTaggart TE, Peng L, Smithes O (1997) **Intraocular pressure in inbred mouse strains** *Invest Ophthalmol Vis Sci* **38**:249–53 PubMed | Google Scholar

141. Savinova OV, Sugiyama F, Martin JE, Tomarev SI, Paigen BJ, Smith RS, et al. (2001) **Intraocular pressure in genetically distinct mice: an update and strain survey** *BMC Genet* **2** https://doi.org/10.1186/1471-2156-2-12 | PubMed | Google Scholar

142. Corces MR, Trevino AE, Hamilton EG, Greenside PG, Sinnott-Armstrong NA, Vesuna S, et al. (2017) **An improved ATAC-seq protocol reduces background and enables interrogation of frozen tissues** *Nat Methods* **14**:959–62 https://doi.org/10.1038/nmeth.4396 | PubMed | Google Scholar

143. Hao Y, Hao S, Andersen-Nissen E, Mauck WM, Zheng S, Butler A, et al. (2021) **Integrated analysis of multimodal single-cell data** *Cell* **184**:3573–87 https://doi.org/10.1016/j.cell.2021.04.048 | PubMed | Google Scholar

144. Stuart T, Srivastava A, Madad S, Lareau CA, Satija R (2021) **Single-cell chromatin state analysis with Signac** *Nat Methods* **18**:1333–41 https://doi.org/10.1038/s41592-021-01282-5 | PubMed | Google Scholar

145. Granja JM, Corces MR, Pierce SE, Bagdatli ST, Choudhry H, Chang HY, et al. (2021) **ArchR is a scalable software package for integrative single-cell chromatin accessibility analysis** *Nat Genet* **53**:403–11 https://doi.org/10.1038/s41588-021-00790-6 | PubMed | Google Scholar

146. Timmons JA, Szkop KJ, Gallagher IJ (2015) **Multiple sources of bias confound functional enrichment analysis of global-omics data** *Genome Biol* **16**:186 https://doi.org/10.1186/s13059-015-0761-7 | PubMed | Google Scholar

147. Yu G, Wang LG, Han Y, He QY (2012) **clusterProfiler: an R package for comparing biological themes among gene clusters** *Omics* **16**:284–7 https://doi.org/10.1089/omi.2011.0118 | PubMed | Google Scholar

148. van Koolwijk LM, Ramdas WD, Ikram MK, Jansonius NM, Pasutto F, Hysi PG, et al. (2012) **Common genetic determinants of intraocular pressure and primary open-angle glaucoma** *PLoS Genet* **8**:e1002611 https://doi.org/10.1371/journal.pgen.1002611 | PubMed | Google Scholar

149. Hysi PG, Cheng CY, Springelkamp H, Macgregor S, Bailey JNC, Wojciechowski R, et al. (2014) **Genome-wide analysis of multi-ancestry cohorts identifies new loci influencing intraocular pressure and susceptibility to glaucoma** *Nat Genet* **46**:1126–30 https://doi.org/10.1038/ng.3087 | PubMed | Google Scholar

150. Springelkamp H, Iglesias AI, Mishra A, Hohn R, Wojciechowski R, Khawaja AP, et al. (2017) **New insights into the genetics of primary open-angle glaucoma based on meta-analyses of intraocular pressure and optic disc characteristics** *Hum Mol Genet* **26**:438–53 https://doi.org/10.1093/hmg/ddw399 | PubMed | Google Scholar

151. Blue Mountains Eye S (2013) **Wellcome Trust Case Control C. Genome-wide association study of intraocular pressure identifies the GLCCI1/ICA1 region as a glaucoma susceptibility locus** *Hum Mol Genet* **22**:4653–60 https://doi.org/10.1093/hmg/ddt293 | PubMed | Google Scholar

152. Nag A, Venturini C, Small KS, International Glaucoma Genetics C, Young TL, Viswanathan AC, et al. (2014) **A genome-wide association study of intra-ocular pressure suggests a novel**

association in the gene FAM125B in the TwinsUK cohort *Hum Mol Genet* **23**:3343–8 https://doi.org/10.1093/hmg/ddu050 | PubMed | Google Scholar

153. Springelkamp H, Iglesias AI, Cuellar-Partida G, Amin N, Burdon KP, van Leeuwen EM, et al. (2015) **ARHGEF12 influences the risk of glaucoma by increasing intraocular pressure** *Hum Mol Genet* **24**:2689–99 https://doi.org/10.1093/hmg/ddv027 | PubMed | Google Scholar

154. Ozel AB, Moroi SE, Reed DM, Nika M, Schmidt CM, Akbari S, et al. (2014) **Genome-wide association study and meta-analysis of intraocular pressure** *Hum Genet* **133**:41–57 https://doi.org/10.1007/s00439-013-1349-5 | PubMed | Google Scholar

155. Bonnemaijer PWM, Iglesias AI, Nadkarni GN, Sanyiwa AJ, Hassan HG, Cook C, et al. (2018) **Genome-wide association study of primary open-angle glaucoma in continental and admixed African populations** *Hum Genet* **137**:847–62 https://doi.org/10.1007/s00439-018-1943-7 | PubMed | Google Scholar

156. Verma SS, Gudiseva HV, Chavali VRM, Salowe RJ, Bradford Y, Guare L, et al. (2024) **A multi-cohort genome-wide association study in African ancestry individuals reveals risk loci for primary open-angle glaucoma** *Cell* **187**:464–80 https://doi.org/10.1016/j.cell.2023.12.006 | PubMed | Google Scholar

157. Bailey JN, Loomis SJ, Kang JH, Allingham RR, Gharahkhani P, Khor CC, et al. (2016) **Genome-wide association analysis identifies TXNRD2, ATXN2 and FOXC1 as susceptibility loci for primary open-angle glaucoma** *Nat Genet* **48**:189–94 https://doi.org/10.1038/ng.3482 | PubMed | Google Scholar

158. Craig JE, Han X, Qassim A, Hassall M, Cooke Bailey JN, Kinzy TG, et al. (2020) **Multitrait analysis of glaucoma identifies new risk loci and enables polygenic prediction of disease susceptibility and progression** *Nat Genet* **52**:160–6 https://doi.org/10.1038/s41588-019-0556-y | PubMed | Google Scholar

159. Weirauch MT, Yang A, Albu M, Cote AG, Montenegro-Montero A, Drewe P, et al. (2014) **Determination and inference of eukaryotic transcription factor sequence specificity** *Cell* **158**:1431–43 https://doi.org/10.1016/j.cell.2014.08.009 | PubMed | Google Scholar

160. Schep AN, Wu B, Buenrostro JD, Greenleaf WJ (2017) **chromVAR: inferring transcription-factor-associated accessibility from single-cell epigenomic data** *Nat Methods* **14**:975–8 https://doi.org/10.1038/nmeth.4401 | PubMed | Google Scholar

161. Lam J, Katti P, Biete M, Mungai M, AshShareef S, Neikirk K, et al. (2021) **A Universal Approach to Analyzing Transmission Electron Microscopy with ImageJ** *Cells* **10** https://doi.org/10.3390/cells10092177 | PubMed | Google Scholar

162. Neikirk K, Lopez EG, Marshall AG, Alghanem A, Krystofiak E, Kula B, et al. (2023) **Call to action to properly utilize electron microscopy to measure organelles to monitor disease** *Eur J Cell Biol* **102**:151365 https://doi.org/10.1016/j.ejcb.2023.151365 | PubMed | Google Scholar

Author information

Nicholas Tolman[¶]
Department of Ophthalmology, Columbia University Irving Medical Center, New York, United States

[¶]These authors contributed equally to this work.

Taibo Li[¶]
Department of Biomedical Engineering, Johns Hopkins University, Baltimore, United States

[¶]These authors contributed equally to this work.

Revathi Balasubramanian[¶]
Department of Ophthalmology, Columbia University Irving Medical Center, New York, United States

[¶]These authors contributed equally to this work.

Guorong Li
Department of Ophthalmology, Duke University, Durham, United States

Rebecca Pfeiffer
Department of Ophthalmology, University of Pittsburgh, Pittsburgh, United States

Violet Bupp-Chickering
Department of Ophthalmology, Columbia University Irving Medical Center, New York, United States

Ruth A Kelly
Department of Ophthalmology, Duke University, Durham, United States

Marina Simón
Department of Ophthalmology, Columbia University Irving Medical Center, New York, United States

John Peregrin
Department of Ophthalmology, Columbia University Irving Medical Center, New York, United States

Christa Montgomery
Department of Ophthalmology, Columbia University Irving Medical Center, New York, United States

Bryan Jones
Department of Ophthalmology, University of Pittsburgh, Pittsburgh, United States

W Daniel Stamer
Department of Ophthalmology, Duke University, Durham, United States

For correspondence: william.stamer@duke.edu

Jiang Qian
Department of Ophthalmology, Johns Hopkins School of Medicine, Baltimore, United States

For correspondence: jiang.qian@jhmi.edu

Simon WM John
Department of Ophthalmology, Columbia University Irving Medical Center, New York, United States, Zuckerman Mind Brain Behavior Institute, Columbia University, New York, United States
ORCID iD: 0000-0002-4319-0356

For correspondence: sj2967@cumc.columbia.edu

Editors

Reviewing Editor
Audrey Bernstein
State University of New York Upstate Medical University, Syracuse, United States of America

Senior Editor
Lois Smith
Boston Children's Hospital, Boston, United States of America

Reviewer #1 (Public review):

Summary:

This study provides a comprehensive single-cell and multiomic characterization of trabecular meshwork (TM) cells in the mouse eye, a structure critical to intraocular pressure (IOP) regulation and glaucoma pathogenesis. Using scRNA-seq, snATAC-seq, immunofluorescence, and in situ hybridization, the authors identify three transcriptionally and spatially distinct TM cell subtypes. The study further demonstrates that mitochondrial dysfunction specifically in one subtype (TM3) contributes to elevated IOP in a genetic mouse model of glaucoma carrying a mutation in the transcription factor Lmx1b. Importantly, treatment with nicotinamide (vitamin B3), known to support mitochondrial health, prevents IOP elevation in this model. The authors also link their findings to human datasets, suggesting the existence of analogous TM3-like cells with potential relevance to human glaucoma.

Strengths:

The study is methodologically rigorous, integrating single-cell transcriptomic and chromatin accessibility profiling with spatial validation and in vivo functional testing. The identification of TM subtypes is consistent across mouse strains and institutions, providing robust evidence of conserved TM cell heterogeneity. The use of a glaucoma model to show subtype-specific vulnerability-combined with a therapeutic intervention-gives the study strong mechanistic and translational significance. The inclusion of chromatin accessibility data adds further depth by implicating active transcription factors such as LMX1B, a gene known to be associated with glaucoma risk. The integration with human single-cell datasets enhances the potential relevance of the findings to human disease.

Weaknesses:

Although the LMX1B transcription factor is implicated as a key regulator in TM3 cells, its role in directly controlling mitochondrial gene expression is not fully explored. Additional analysis of motif accessibility or binding enrichment near relevant target genes could substantiate this mechanistic link. The therapeutic effect of vitamin B3 is clearly demonstrated phenotypically, but the underlying cellular and molecular mechanisms remain somewhat underdeveloped-for instance, changes in mitochondrial function, oxidative stress markers, or NAD+ levels are not directly measured. While the human relevance of TM3 cells is suggested through marker overlap, more quantitative approaches, such as cell identity mapping or gene signature scoring in human datasets, would strengthen the translational connection.

Overall, this is a compelling and carefully executed study that offers significant advances in our understanding of TM cell biology and its role in glaucoma. The integration of multimodal data, disease modeling, and therapeutic testing represents a valuable contribution to the field. With additional mechanistic depth, the study has the potential to become a foundational resource for future research into IOP regulation and glaucoma treatment.

https://doi.org/10.7554/eLife.107161.2.sa2

Reviewer #3 (Public review):

Summary:

In this study, the authors perform multimodal single-cell transcriptomic and epigenomic profiling of 9,394 mouse TM cells, identifying three transcriptionally distinct TM subtypes with validated molecular signatures. TM1 cells are enriched for extracellular matrix genes, TM2 for secreted ligands supporting Schlemm's canal, and TM3 for contractile and mitochondrial/metabolic functions. The transcription factor LMX1B, previously linked to glaucoma, shows the highest expression in TM3 cells and appears to regulate mitochondrial pathways. In Lmx1bV265D mutant mice, TM3 cells exhibit transcriptional signs of mitochondrial dysfunction associated with elevated IOP. Notably, vitamin B3 treatment significantly mitigates IOP elevation, suggesting a potential therapeutic avenue.
This is an excellent and collaborative study involving investigators from two institutions, offering the most detailed single-cell transcriptomic and epigenetic profiling of the mouse limbal tissues-including both TM and Schlemm's canal (SC), from wild-type and Lmx1bV265D mutant mice. The study defines three TM subtypes and characterizes their distinct molecular signatures, associated pathways, and transcriptional regulators. The authors also compare their dataset with previously published murine and human studies, including those by Van Zyl et al., providing valuable cross-species insights.

Strengths:

(1) Comprehensive dataset with high single-cell resolution

(2) Use of multiple bioinformatic and cross-comparative approaches

(3) Integration of 3D imaging of TM and SC for anatomical context

(4) Convincing identification and validation of three TM subtypes using molecular markers.

Weaknesses:

(1) Insufficient evidence linking mitochondrial dysfunction to TM3 cells in Lmx1bV265D mice: While the identification of TM3 cells as metabolically specialized and Lmx1b-enriched is compelling, the proposed link between Lmx1b mutation and mitochondrial dysfunction remains underdeveloped. It is unclear whether mitochondrial defects are a primary

consequence of Lmx1b-mediated transcriptional dysregulation or a secondary response to elevated IOP. Although authors have responded to this, the manuscript is not sufficiently altered to address these points. I would like to suggest that authors tone down mitochondrial connection with Lmx1b from the title and abstract, and clearly discuss that these events are associated, and future work is needed to dissect the role of mitochondria in this pathway. Furthermore, the protective effects of nicotinamide (NAM) are interpreted as evidence of mitochondrial involvement, but no direct mitochondrial measurements (e.g., immunostaining, electron microscopy, OCR assays) are provided. It is essential to validate mitochondrial dysfunction in TM3 cells using in vivo functional assays to support the central conclusion of the paper. Without this, the claim that mitochondrial dysfunction drives IOP elevation in Lmx1bV265D mice remains speculative. Alternatively, authors should consider revising their claims that mitochondrial dysfunction in these mice is a central driver of TM dysfunction.

(2) Mechanism of NAM-mediated protection is unclear: The manuscript states that NAM treatment prevents IOP elevation in Lmx1bV265D mice via metabolic support, yet no data are shown to confirm that NAM specifically rescues mitochondrial function. Do NAM-treated TM3 cells show improved mitochondrial integrity? Are reactive oxygen species (ROS) reduced? Does NAM also protect RGCs from glaucomatous damage? Addressing these points would clarify whether the therapeutic effects of NAM are indeed mitochondrial.

https://doi.org/10.7554/eLife.107161.2.sa1

Author response:

The following is the authors' response to the original reviews.

> ***Reviewer #1 (Public review):***
>
> *Summary:*
>
> *This study provides a comprehensive single-cell and multiomic characterization of trabecular meshwork (TM) cells in the mouse eye, a structure critical to intraocular pressure (IOP) regulation and glaucoma pathogenesis. Using scRNA-seq, snATAC-seq, immunofluorescence, and in situ hybridization, the authors identify three transcriptionally and spatially distinct TM cell subtypes. The study further demonstrates that mitochondrial dysfunction, specifically in one subtype (TM3), contributes to elevated IOP in a genetic mouse model of glaucoma carrying a mutation in the transcription factor Lmx1b. Importantly, treatment with nicotinamide (vitamin B3), known to support mitochondrial health, prevents IOP elevation in this model. The authors also link their findings to human datasets, suggesting the existence of analogous TM3-like cells with potential relevance to human glaucoma.*
>
> *Strengths:*
>
> *The study is methodologically rigorous, integrating single-cell transcriptomic and chromatin accessibility profiling with spatial validation and in vivo functional testing. The identification of TM subtypes is consistent across mouse strains and institutions, providing robust evidence of conserved TM cell heterogeneity. The use of a glaucoma model to show subtype-specific vulnerability, combined with a therapeutic intervention-gives the study strong mechanistic and translational significance. The inclusion of chromatin accessibility data adds further depth by implicating active transcription factors such as LMX1B, a gene known to be associated with glaucoma risk. The integration with human single-cell datasets enhances the potential relevance of the findings to human disease.*

We thank the reviewers for their thorough reading of our manuscript and helpful comments.

> *Weaknesses:*
>
> *(1) Although the LMX1B transcription factor is implicated as a key regulator in TM3 cells, its role in directly controlling mitochondrial gene expression is not fully explored. Additional analysis of motif accessibility or binding enrichment near relevant target genes could substantiate this mechanistic link.*

We show that the Lmx1b mutation induces mitochondrial dysfunction with mitochondrial gene expression changes but agree with the referee in that we do not show direct regulation of mitochondrial genes by LMX1B. Emerging data suggest that LMX1B regulates the expression of mitochondrial genes in other cell types [1, 2] making the direct link reasonable. Future work that is beyond the scope of the current paper will focus on sequencing cells at earlier timepoints to help distinguish gene expression changes associated with the V265D mutation from those secondary to ongoing disease and elevated IOP. Additional studies, including ATAC seq at more ages, ChIP-seq and/or Cut and Run/Tag (in TM cells) will be necessary to directly investigate LMX1B target genes.

As we studied adult mice, mitochondrial gene expression changes could be secondary to other disease induced stresses. Because we did not intend to say we have shown a direct link, we have now added a sentence to the discussion ensure clarity.

Lines 932-934: “Although our studies show a clear effect of the Lmx1b mutation on mitochondria, future studies are needed to determine if LMX1B directly modulates mitochondrial genes in V265D mutant TM cells”

> *(2) The therapeutic effect of vitamin B3 is clearly demonstrated phenotypically, but the underlying cellular and molecular mechanisms remain somewhat underdeveloped - for instance, changes in mitochondrial function, oxidative stress markers, or NAD+ levels are not directly measured.*

We agree that further experiments towards a fuller mechanistic understanding of vitamin B3’s therapeutic effects are needed. Such experiments are planned but are beyond the scope of this paper, which is already very large (7 Figures and 16 Supplemental Figures).

> *(3) While the human relevance of TM3 cells is suggested through marker overlap, more quantitative approaches, such as cell identity mapping or gene signature scoring in human datasets, would strengthen the translational connection.*

We appreciate the reviewer’s suggestion and agree that additional quantitative analyses will further strengthen the translational relevance of TM3 cells. It is not yet clear if humans have a direct TM3 counterpart or if TM cell roles are compartmentalized differently between human cell types. We are currently limited in our ability to perform these comparative analyses. Specifically, we were unable to obtain permission to use the underlying dataset from Patel et al., and our access to the Van Zyl et al. dataset was through the Single Cell Portal, which does not support more complex analyses (ex. cell identity mapping or gene signature scoring). Differences between human studies themselves also affect these comparisons. Future work aimed at resolving differences and standardizing human TM cell annotations, as well as cross species comparisons are needed (working groups exist and this ongoing effort supports 3 human TM cell subtypes as also reported by Van Zyl). This is beyond what we are currently able to do for this paper. We present a comprehensive assessment using readily available published resources.

Reviewer #2 (Public review):

Summary:

This elegant study by Tolman and colleagues provides fundamental findings that substantially advance our knowledge of the major cell types within the limbus of the mouse eye, focusing on the aqueous humor outflow pathway. The authors used single-cell and single-nuclei RNAseq to very clearly identify 3 subtypes of the trabecular meshwork (TM) cells in the mouse eye, with each subtype having unique markers and proposed functions. The U. Columbia results are strengthened by an independent replication in a different mouse strain at a separate laboratory (Duke). Bioinformatics analyses of these expression data were used to identify cellular compartments, molecular functions, and biological processes. Although there were some common pathways among the 3 subtypes of TM cells (e.g., ECM metabolism), there also were distinct functions. For example:

TM1 cell expression supports heavy engagement in ECM metabolism and structure, as well as TGFb2 signaling.

TM2 cells were enriched in laminin and pathways involved in phagocytosis, lysosomal function, and antigen expression, as well as End3/VEGF/angiopoietin signaling.

TM3 cells were enriched in actin binding and mitochondrial metabolism.

They used high-resolution immunostaining and in situ hybridization to show that these 3 TM subtypes express distinct markers and occupy distinct locations within the TM tissue. The authors compared their expression data with other published scRNAseq studies of the mouse as well as the human aqueous outflow pathway. They used ATAC-seq to map open chromatin regions in order to predict transcription factor binding sites. Their results were also evaluated in the context of human IOP and glaucoma risk alleles from published GWAS data, with interesting and meaningful correlations. Although not discussed in their manuscript, their expression data support other signaling pathways/ proteins/ genes that have been implicated in glaucoma, including: TGFb2, BMP signaling (including involvement of ID proteins), MYOC, actin cytoskeleton (CLANs), WNT signaling, etc.

In addition to these very impressive data, the authors used scRNAseq to examine changes in TM cell gene expression in the mouse glaucoma model of mutant Lmxb1-induced ocular hypertension. In man, LMX1B is associated with Nail-Patella syndrome, which can include the development of glaucoma, demonstrating the clinical relevance of this mouse model. Among the gene expression changes detected, TM3 cells had altered expression of genes associated with mitochondrial metabolism. The authors used their previous experience using nicotinamide to metabolically protect DBA2/J mice from glaucomatous damage, and they hypothesized that nicotinamide supplementation of mutant Lmx1b mice would help restore normal mitochondrial metabolism in the TM and prevent Lmx1b-mediated ocular hypertension. Adding nicotinamide to the drinking water significantly prevented Lmxb1 mutant mice from developing high intraocular pressure. This is a laudable example of dissecting the molecular pathogenic mechanisms responsible for a disease (glaucoma) and then discovering and testing a potential therapy that directly intervenes in the disease process and thereby protects from the disease.

Strengths:

There are numerous strengths in this comprehensive study including:

> *Deep scRNA sequencing that was confirmed by an independent dataset in another mouse strain at another university.*
>
> *Identification and validation of molecular markers for each mouse TM cell subset along with localization of these subsets within the mouse aqueous outflow pathway.*
>
> *Rigorous bioinformatics analysis of these data as well as comparison of the current data with previously published mouse and human scRNAseq data.*
>
> *Correlating their current data with GWAS glaucoma and IOP "hits".*
>
> *Discovering gene expression changes in the 3 TM subgroups in the mouse mutant Lmx1b model of glaucoma.*
>
> *Further pursuing the indication of dysfunctional mitochondrial metabolism in TM3 cells from Lmx1b mutant mice to test the efficacy of dietary supplementation with nicotinamide. The authors nicely demonstrate the disease modifying efficacy of nicotinamide in preventing IOP elevation in these Lmx1b mutant mice, preventing the development of glaucoma. These results have clinical implications for new glaucoma therapies.*

We thank the reviewer for these generous and thoughtful comments on the strengths of this study.

> *Weaknesses:*
>
> *(1) Occasional over-interpretation of data. The authors have used changes in gene expression (RNAseq) to implicate functions and signaling pathways. For example: they have not directly measured "changes in metabolism", "mitochondrial dysfunction" or "activity of Lmx1b".*

We thank the reviewer for this feedback. We did not intend to overstate and agree. Our gene expression changes support, but do not by themselves prove, metabolic disturbances. We had felt that this was obvious and did not want to clutter the text. We have revised the manuscript to clarify that our conclusions about metabolic changes and LMX1B activity are based on gene expression patterns rather than direct functional assays and have added EM data (see below under “Recommendations for the authors”).

We have also added the following to the results:

Lines 715-721: “Although the documented gene expression changes strongly suggest metabolic and mitochondrial dysfunction, they do not directly prove it. Using electron microscopy to directly evaluate mitochondria in the TM, we found a reduction in total mitochondria number per cell in mutants ($P = 0.015$, Figure 6G). In addition, mitochondria in mutants had increased area and reduced cristae (inner membrane folds) in mutants consistent with mitochondrial swelling and metabolic dysfunction (all $P < 0.001$ compared to WT, Figure 6G-H).”

More detailed EM and metabolic studies are underway but are beyond the scope of this paper.

> *(2) In their very thorough data set, there is enrichment of or changes in gene expression that support other pathways that have been previously reported to be associated with glaucoma (such as TGFb2, BMP signaling, actin cytoskeletal organization (CLANs), WNT signaling, ossification, etc. that appears to be a lost opportunity to further enhance the significance of this work.*

We appreciate the reviewer's suggestions for enhancing the relevance of our work, we had not initially discussed this due to length concerns. We have now incorporated some of this information into the manuscript (see below under "Recommendations for the authors").

> ***Reviewer #3 (Public review):***
>
> *Summary: In this study, the authors perform multimodal single-cell transcriptomic and epigenomic profiling of 9,394 mouse TM cells, identifying three transcriptionally distinct TM subtypes with validated molecular signatures. TM1 cells are enriched for extracellular matrix genes, TM2 for secreted ligands supporting Schlemm's canal, and TM3 for contractile and mitochondrial/metabolic functions. The transcription factor LMX1B, previously linked to glaucoma, shows the highest expression in TM3 cells and appears to regulate mitochondrial pathways. In Lmx1bV265D mutant mice, TM3 cells exhibit transcriptional signs of mitochondrial dysfunction associated with elevated IOP. Notably, vitamin B3 treatment significantly mitigates IOP elevation, suggesting a potential therapeutic avenue.*
>
> *This is an excellent and collaborative study involving investigators from two institutions, offering the most detailed single-cell transcriptomic and epigenetic profiling of the mouse limbal tissues-including both TM and Schlemm's canal (SC), from wild-type and Lmx1bV265D mutant mice. The study defines three TM subtypes and characterizes their distinct molecular signatures, associated pathways, and transcriptional regulators. The authors also compare their dataset with previously published murine and human studies, including those by Van Zyl et al., providing valuable crossspecies insights.*
>
> *Strengths:*
>
> *(1) Comprehensive dataset with high single-cell resolution*
>
> *(2) Use of multiple bioinformatic and cross-comparative approaches*
>
> *(3) Integration of 3D imaging of TM and SC for anatomical context*
>
> *(4) Convincing identification and validation of three TM subtypes using molecular markers.*

We thank the reviewer for their comments on the strengths of this study.

> *Weaknesses:*
>
> *(1) Insufficient evidence linking mitochondrial dysfunction to TM3 cells in Lmx1bV265D mice: While the identification of TM3 cells as metabolically specialized and Lmx1b-enriched is compelling, the proposed link between Lmx1b mutation and mitochondrial dysfunction remains underdeveloped. It is unclear whether mitochondrial defects are a primary consequence of Lmx1b-mediated transcriptional dysregulation or a secondary response to elevated IOP. Additional evidence is needed to clarify whether Lmx1b directly regulates mitochondrial genes (e.g., via ChIP-seq, motif analysis, or ATAC-seq), or whether mitochondrial changes are downstream effects.*

We agree and refer the reviewer to our responses to the other referees including Reviewer 1, Comment 1 and Reviewer 2 comments 1 and 17. As noted there, these mechanistic questions are the focus of ongoing and future studies. We have revised the text where appropriate to ensure it accurately reflects the scope of our current data.

> *(2) Furthermore, the protective effects of nicotinamide (NAM) are interpreted as evidence of mitochondrial involvement, but no direct mitochondrial measurements (e.g.,*

> *immunostaining, electron microscopy, OCR assays) are provided. It is essential to validate mitochondrial dysfunction in TM3 cells using in vivo functional assays to support the central conclusion of the paper. Without this, the claim that mitochondrial dysfunction drives IOP elevation in Lmx1bV265D mice remains speculative. Alternatively, authors should consider revising their claims that mitochondrial dysfunction in these mice is a central driver of TM dysfunction.*

We again refer the reviewer to our other response including Reviewer 1, Comment 1 and Reviewer 2 comments 1 and 17.

> *(3) Mechanism of NAM-mediated protection is unclear: The manuscript states that NAM treatment prevents IOP elevation in Lmx1bV265D mice via metabolic support, yet no data are shown to confirm that NAM specifically rescues mitochondrial function. Do NAM-treated TM3 cells show improved mitochondrial integrity? Are reactive oxygen species (ROS) reduced? Does NAM also protect RGCs from glaucomatous damage? Addressing these points would clarify whether the therapeutic effects of NAM are indeed mitochondrial.*

We refer the reviewer to our response to Reviewer 1, Comment 2.

> *(4) Lack of direct evidence that LMX1B regulates mitochondrial genes: While transcriptomic and motif accessibility analyses suggest that LMX1B is enriched in TM3 cells and may influence mitochondrial function, no mechanistic data are provided to demonstrate direct regulation of mitochondrial genes. Including ChIP-seq data, motif enrichment at mitochondrial gene loci, or perturbation studies (e.g., Lmx1b knockout or overexpression in TM3 cells) would greatly strengthen this central claim.*

We refer the reviewer to our response to Reviewer 1, Comment 1.

> *(5) Focus on LMX1B in Fig. 5F lacks broader context: Figure 5F shows that several transcription factors (TFs)-including Tcf21, Foxs1, Arid3b, Myc, Gli2, Patz1, Plag1, Npas2, Nr1h4, and Nfatc2exhibit stronger positive correlations or motif accessibility changes than LMX1B. Yet the manuscript focuses almost exclusively on LMX1B. The rationale for this focus should be clarified, especially given LMX1B's relatively lower ranking in the correlation analysis. Were the functions of these other highly ranked TFs examined or considered in the context of TM biology or glaucoma? Discussing their potential roles would enhance the interpretation of the transcriptional regulatory landscape and demonstrate the broader relevance of the findings.*

Our analysis (Figure 5F) indicates that Lmx1b is the transcription factor most strongly associated with its predicted target gene expression across all TM cells, as reflected by its highest value along the X-axis. While other transcription factors exhibit greater motif accessibility (Y-axis), this likely reflects their broader expression across TM subtypes. In contrast, Lmx1b is minimally expressed in TM1 and TM2 cells, which may account for its lower motif accessibility overall (motifs not accessible in cells where Lmx1b is not / minimally expressed).

Our emphasis on LMX1B is further supported by its direct genetic association with glaucoma. In contrast, the other transcription factors lack clear links to glaucoma and are supported primarily by indirect evidence. Nonetheless, we agree that the transcription factors highlighted in our analysis are promising candidates for future investigation. However, to maintain focus on the central narrative of this study, we have chosen not to include an extended discussion of these additional genes.

> *(6) In abstract, they say a number of 9,394 wild-type TM cell transcriptomes. The number of Lmx1bV265D/+ TM cell transcriptomes analyzed is not provided. This information is essential for evaluating the comparative analysis and should be clearly stated in the Abstract and again in the main text (e.g., lines 121-123). Including both wild-type and mutant cell counts will help readers assess the balance and robustness of the dataset.*

We thank the reviewer for noticing this oversight and have added this value to the abstract and results section.

Lines 41 and 696: 2,491 mutant TM cells.

> *(7) Did the authors monitor mouse weight or other health parameters to assess potential systemic effects of treatment? It is known that the taste of compounds in drinking water can alter fluid or food intake, which may influence general health. Also, does Lmx1bV265D/+ have mice exhibit non-ocular phenotypes, and if so, does nicotinamide confer protection in those tissues as well? Additionally, starting the dose of the nicotinamide at postnatal day 2, how long the mice were treated with water containing nicotinamide, and after how many days or weeks IOP was reduced, and how long the decrease in the IOP was sustained.*

Water intake was monitored in both treatment groups, and dosing was based on the average volume consumed by adult mice (lines 1017–1018, young pups do not drink water and so drug is largely delivered through mothers' milk until weaning and so we do not know an accurate dose for young pups). Mouse health was assessed throughout the experiment through regular monitoring of body weight and general condition.

Depending on genetic context, Lmx1b mutations can cause kidney disease and impact other systems. Non-ocular phenotypes were not the focus of this study and were not characterized.

We added a comment to the method to clarify the NAM treatment timeline. NAM was administered continuously in the drinking water starting at P2 and maintained throughout the experiment. IOP was measured beginning at 2 months and then at monthly time points. NAM lessened IOP at 2 and 3 months. We terminated IOP assessment at 3 months.

Lines 1028-1029: "Treatment was started at postnatal day 2 and continued throughout the experiment."

> *(8) While the IOP reduction observed in NAM-treated Lmx1bV265D/+ mice appears statistically significant, it is unclear whether this reflects meaningful biological protection. Several untreated mice exhibit very high IOP values, which may skew the analysis. The authors should report the mean values for IOP in both untreated and NAM-treated groups to clarify the magnitude and variability of the response.*

We have added supplemental table 7 with the statistical information. Regarding the high IOP values observed in a subset of untreated V265D mutant mice, we consistently detect individual mutant eyes with IOPs exceeding 30 mmHg across independent cohorts and time points [3-5]. It is important to note that IOP is subject to fluctuation and in disease states such as glaucoma, circadian rhythms can be disrupted with stochastic and episodic IOP spikes throughout the day. This may be occurring in those untreated mice. This is also why we strive to use sample sizes of 40 or more. Additionally, we observe that some mutant eyes with IOPs measured within the normal range have anterior chamber deepening (ACD) - a persistent anatomical change associated with sustained or recurrent high IOP that stretches the cornea and may posteriorly displace the lens. This suggests mutant mice experience transient IOP elevations that are not always captured at a single time point due to the stochastic nature of

these fluctuations. To account for this, we include ACD as an additional readout alongside IOP measurements. The reduction in ACD observed in NAM-treated mice provides independent evidence supporting the biological relevance of NAM-mediated IOP reduction.

> *(9) Additionally, since NAM has been shown to protect RGCs in other glaucoma models directly, the authors should assess whether RGCs are preserved in NAM-treated Lmx1b V265D/+ mice. Demonstrating RGC protection would support a synergistic effect of NAM through both IOP reduction and direct neuroprotection, strengthening the translational relevance of the treatment.*

We again thank the referee. We note the possibility of dual IOP protection and neuroprotection in the manuscript (lines 961–963). The goal of the present study, however, was to determine mechanisms underlying IOP elevation in patients with LMX1B variants. Therefore, we limited our focus to IOP elevation (LMX1B is expressed in the TM but not RGCs). Studies of the RGCs and optic nerve in V265D mutant mice treated with NAM take considerable effort but are underway. They will be reported in a subsequent manuscript. Initial data support protection, but that is a work in progress.

Additionally, we recently reported a similar pattern of IOP protection to that reported here using pyruvate - in experiments where we analyzed the optic nerve as the focus of the study was assessment of pyruvate as a resilience factor against high genetic risk of glaucoma [4]. In that case, there was statistically significant protection from glaucomatous optic nerve damage, arguing for translational relevance again with a possible synergistic effect through both IOP reduction and direct neuroprotection.

> *(10) Can the authors add any other functional validation studies to explore to understand the pathways enriched in all the subtypes of TM1, TM2, and TM3 cells, in addition to the ICH/IF/RNAscope validation?*

We agree with the reviewer on the importance of further functional validation of pathways active in TM cell subtypes that influence IOP. However, comprehensive investigation of the pathways active in subtypes need to be in future studies. It is beyond the scope of his already large paper.

> *(11) The authors should include a representative image of the limbal dissection. While Figure S1 provides a schematic, mouse eyes are very small, and dissecting unfixed limbal tissue is technically challenging. It is also difficult to reconcile the claim that the majority of cells in the limbal region are TM and endothelium. As shown in Figure S6, DAPI staining suggests a much higher abundance of scleral cells compared to TM cells within the limbal strip. Additional clarification or visual evidence would help validate the dissection strategy and cellular composition of the captured region.*

We appreciate the reviewer's suggestion and have added additional images to Figure S1 to show our limbal strip dissection. However, we clarify that we do not intend to suggest that TM and endothelial cells are the most abundant populations in these dissected strips. When we say "are enriched for drainage tissues" we mean in comparison to dissecting the anterior segment as a whole. We have clarified this in the text. In fact, epithelial cells (primarily from the cornea) constituted the largest cluster in our dataset (Figure 1A). Additionally, to avoid misinterpretation, we generally refrain from drawing conclusions about the relative abundance of cell types based on sequencing data. Single-cell and single nucleus RNA sequencing results are sensitive to technical factors that alter cell proportions depending on exact methodological details. In our study, TM cells comprised 24.4% of the single-cell dataset and 11.8% of the single-nucleus dataset, illustrating the impact of methodological variability.

Lines 163-164: “Individual eyes were dissected to isolate a strip of limbal tissue, which is enriched for TM cells in comparison to dissecting the anterior segment as a whole.”

> ***Reviewer #1 (Recommendations for the authors):***
>
> *To enhance the reproducibility and transparency of the findings presented in this study, we strongly recommend that the authors make all analysis scripts and computational tools publicly available.*

We agree with the reviewer’s emphasis on transparency and are currently building a GitHub page to share our scripts. However, we did not develop any new tools for this study. All tools that we used are publicly available and provided in our methods section. All data will be available as raw data and through the Broad Institute’s Single Cell Portal.

> ***Reviewer #2 (Recommendations for the authors):***
>
> *The authors are to be commended for a well-written presentation of high-quality data, their comparisons of datasets (other mouse and human scRNAseq data), correlation with clinical glaucoma risk alleles, and curative therapy for the mouse model of Lmx1b glaucoma. There are several minor suggestions that the authors might consider to further improve their manuscript:*
>
> *(1) Lines 42-43: Although their data strongly support the role of mitochondrial dysfunction in Lmx1b glaucoma, they might want to soften their conclusion "supports a primary role of mitochondrial dysfunction within TM3 cells initiating the IOP elevation that causes glaucoma".*

With the inclusion of EM data supporting mitochondrial dysfunction in Lmx1b mutant TM cells, we have revised this sentence to more accurately reflect our findings.

Lines 42-44 (previously lines 42-43): “Mitochondria in TM cells of V265D/+ mice are swollen with a reduced cristae area, further supporting a role for mitochondrial dysfunction in the initiation of IOP elevation in these mice.”

> *(2) Figure 1: Why is the shape of the "TM containing" cluster in 1A so different than the cluster shown in 1B?*

We isolated cells from the 'TM-containing' cluster and performed unbiased reclustering, which alters their positioning in UMAP space. The figure legend has been updated to clarify this point.

Lines 143-144 “A separate UMAP representation of the trabecular meshwork (TM) containing cluster following subclustering.”

> *(3) Line 160: change "data was" to "data were"*

Corrected

> *(4) S4 Fig C: Please comment on why the Columbia and Duke heatmaps for TM3 are not as congruent as the heatmaps for TM1 and TM2.*

We cannot definitively determine the reason for this. However, differences in tissue processing techniques between the Columbia and Duke preparations may contribute. Such variations have been shown to affect cellular transcriptomes in certain contexts. It is possible

that TM3 cells are more susceptible to these effects than others. We have added a statement addressing this point to the figure legend.

Lines 238-240: “Because tissue processing techniques can alter gene expression [52], the heatmap variation between institutes likely reflects differences in processing techniques (Methods) and suggests that TM3 cells are more susceptible to these effects than other cell types.”

> *(5) S9 Fig: It is very difficult to see any staining for TM1 CHIL1 (2nd panel), TM2 End3 (2nd panel), and TM3 Lypd1 (both panels)*

We apologize for the difficulty in visualizing these panels. To improve clarity, we have increased the brightness of all relevant marker signals, within standard bounds, to facilitate easier interpretation.

> *(6) Line 380: "are significantly higher"; since statistical analysis was not reported, please do not use "significantly"*

Done

> *(7) The authors should consider discussing several of their findings that agree with published literature. For example:*
>
> *Figure 3B: "Wnt protein binding" (PMID: 18274669), "TGFb "binding" (numerous references), "integrin binding" (work of Donna Peters), "actin binding"/"actin filament binding"/"actin filament bundle" (CLANs references)*
>
> *S10 Fig c: "ossification" (work of Torretta Borres)*
>
> *S11 Fig A: ID2/ID3 (PMID: 33938911); (B) BMP4 (PMID: 17325163)*
>
> *S12 Fig A: MYOC in TM1 cells (numerous references)*

We appreciate the reviewer’s diligent review and comments regarding these pathways. We have added a comment to the discussion regarding the agreement of these pathways.

Lines 855-858: In addition, the expression of genes that we document generally agrees with the literature. For example, the following genes and signaling molecules have been reported in TM cells, WNT signaling [78], TGF-β signaling [79-85], integrin binding [86-88], actin cytoskeletal networks [89], calcification genes [90, 91], and Myocilin [91-94].

> *(8) Line 541: was confocal microscopy used to measure the "3D shapes" of nuclei or was this done with a single image to determine sphericity?*

This analysis was performed using confocal microscopy and 3D reconstructed models of the TM nuclei. We have added text to clarify this in the figure legend

Lines 553-556: “To rigorously assess whether TM1 nuclei are more spherical, we analyzed their reconstructed 3D shapes from whole mounts images by confocal microscopy, comparing them to TM3 nuclei using the ‘Sphericity’ tool in Imaris.”

> *(9) Line 545: please add a close parentheses after "scoring 1"*

Done

> *(10) S15 Fig: (A) There does not appear to be "good agreement" (line 653) between the datasets for TM1. (C) please provide a better explanation on how to interpret these "Confusion Matrix" results.*

We understand the referee's concern, the patterns likely appear different to the referee due to limited sampling in snRNA-seq data. Based on our results, TM1 seems particularly susceptible, possibly because these cells do not tolerate the isolation process as well. Although we are confident that TM1 shows good agreement between the two techniques based on our experience, we have revised the language in the text to “generally” to reflect this nuance.

Lines 633-635 (previously line 653): The generated clusters and their marker genes generally agreed with our scRNA-seq analyses (Fig 5A-B, S15A Fig).

We have also added additional clarification for how to interpret the Confusion Matrix.

Lines 669-672: “Colors indicate the fraction of cells identified in each ATAC cluster (row) which are also identified in each RNA cell type (columns), where darker colors represent stronger correspondence between RNA and ATAC clusters.”

> *(11) Line 676: The transition from discussing the sc/snRNAseq data to the work in Lmx1b mutant mice is quite abrupt and could use a better transition to introduce this metabolism work.*

We have revised this transition for improved flow but prefer to keep all transitions brief due to the paper's length.

Lines 691-694 (previously line 676): To evaluate the utility of our new TM cell atlas, we used it to examine how Lmx1b mutations affect the TM cell transcriptome and to identify potential mechanisms underlying IOP elevation. We selected LMX1B because it causes IOP elevation and glaucoma in humans and was identified as a highly active transcription factor in our TM cell dataset.

> *(12) Lines 696-697: It appears counter-intuitive that upregulation of ubiquitin pathways would lead to proteostasis (proteosome protein degradation requires ubiquination).*

We have clarified that the protein tagging pathway was significantly upregulated. However, polyubiquitin precursor itself was downregulated. In general, the statistical significance of the protein tagging pathway suggests perturbation of the system tagging proteins for degradation. We have clarified this in the text.

Lines 711-714 (previously lines 696-697): “In addition, mutant TM3 cells showed an upregulation of protein tagging genes. However, there is a downregulation of the polyubiquitin precursor gene (Ubb, P = 4.5E-30), indicating a general dysregulation of pathways that tag proteins for degradation.”

> *(13) Line 715: Please justify why "perturbed metabolism" was chosen to pursue vs the other differentially expressed pathways*

We chose to narrow our focus on TM3 cells because of the enrichment for Lmx1b expression.Most pathways identified in our analysis of TM3 cells implicate mitochondrial metabolism.Therefore, we chose to further explore this avenue. We clarified that perturbed metabolism was the strongest gene expression signature in the text.

Lines 753-754 (previously line 715): “Our findings most strongly implicate perturbed metabolism within TM3 cells as responsible for IOP elevation in an Lmx1b glaucoma model.”

> *(14) Line 759: The authors clearly demonstrate that Lmx1b is most expressed in TM3 cells; however, they did not demonstrate that "Lmx1b was most active"*

ATAC analysis showed that Lmx1b was most active in TM cells overall. We inferred its activity in TM3 because Lmx1b is most enriched in that subtype. This has been clarified in the text.

Lines 799-800 (previously line 759): “More specifically, we demonstrate that Lmx1b is the most active TM cell TF and is enriched in TM3 cells,…”

> *(15) Lines 830-835: Please include references documenting increased TGFβ2 concentrations in POAG aqueous humor and TM, effects of TGFβ2 on TM ECM deposition, and TGFβ2 induced ocular hypertension ex vivo and in vivo.*

Done.

> *(16) Line 875: The authors provide no direct evidence for enhances "oxidative stress" in Lmx1b TM3 cells*

The mitochondrial abnormalities and changed pathways support oxidative stress, but we have not directly tested this. Experiments are currently underway to evaluate its role, but these additional analyses are beyond the scope of this paper. We removed oxidative stress from the sentence.

Lines 920-922 (previously line 875): “Importantly, in heterozygous mutant V265D/+ mice, TM3 cells had pronounced gene expression changes that implicate mitochondrial dysfunction, but that were absent or much lower in other cells including TM1 and TM2.”

> *(17) Line 880: Similarly, the authors have not directly assessed effects on metabolism in TM3 cells; they only have shown changes in the expression of mitochondrial genes that may affect metabolism*

We have no way to specifically isolating TM3 cells to test this. Future work is underway to test this more broadly in isolated TM cells but is beyond the scope of this is already large paper. Considering our gene expression data and the addition of supporting EM data, we have qualified the text.

Lines 930-931 (previously 880): “Our data extend these published findings by showing that inheritance of a single dominant mutation in Lmx1b similarly affects mitochondria in TM cells.”

> *(18) Line 892: What markers were used to detect "cell stress"?*

We have revised the text. Although our RNA data show stress gene changes, characterization of these markers is beyond the scope of the current study and will be included in a subsequent paper.

Lines 945-948 (previously line 892): “However, these processes were not limited to TM3 cells or even to cell types that express detectable Lmx1b, suggesting that they are secondary damaging processes that are subsequent to the initiating, Lmx1b-induced perturbations in TM3 cells.”

Additional author driven change

While revising and reviewing our data, we identified a coding error that resulted in the WT and V265D mutant group labels being switched in Figure 6. Importantly, the significance of

the differentially expressed genes (DEGs), the implicated biological pathways, and the interpretation of pathway directionality in the manuscript remain accurate. The only issue was the incorrect labeling in the figure. We have corrected the labels in Figure 6 to accurately reflect the data. As noted above, all data and code will be made available to ensure full reproducibility of our results.

References

(1) Doucet-Beaupre H, Gilbert C, Profes MS, Chabrat A, Pacelli C, Giguere N, et al. Lmx1a and Lmx1b regulate mitochondrial functions and survival of adult midbrain dopaminergic neurons. Proc Natl Acad Sci U S A. 2016;113(30):E4387-96. Epub 2016/07/14. doi: 10.1073/pnas.1520387113. PubMed PMID: 27407143; PubMed Central PMCID: PMCPMC4968767.

(2) Jimenez-Moreno N, Kollareddy M, Stathakos P, Moss JJ, Anton Z, Shoemark DK, et al. ATG8-dependent LMX1B-autophagy crosstalk shapes human midbrain dopaminergic neuronal resilience. J Cell Biol. 2023;222(5). Epub 2023/04/05. doi: 10.1083/jcb.201910133. PubMed PMID: 37014324; PubMed Central PMCID: PMCPMC10075225.

(3) Cross SH, Macalinao DG, McKie L, Rose L, Kearney AL, Rainger J, et al. A dominantnegative mutation of mouse Lmx1b causes glaucoma and is semi-lethal via LDB1mediated dimerization [corrected]. PLoS Genet. 2014;10(5):e1004359. Epub 2014/05/09. doi: 10.1371/journal.pgen.1004359. PubMed PMID: 24809698; PubMed Central PMCID: PMCPMC4014447.

(4) Li K, Tolman N, Segre AV, Stuart KV, Zeleznik OA, Vallabh NA, et al. Pyruvate and related energetic metabolites modulate resilience against high genetic risk for glaucoma. Elife. 2025;14. Epub 2025/04/24. doi: 10.7554/eLife.105576. PubMed PMID: 40272416; PubMed Central PMCID: PMCPMC12021409.

(5) Tolman NG, Balasubramanian R, Macalinao DG, Kearney AL, MacNicoll KH, Montgomery CL, et al. Genetic background modifies vulnerability to glaucoma-related phenotypes in Lmx1b mutant mice. Dis Model Mech. 2021;14(2). Epub 2021/01/20. doi: 10.1242/dmm.046953. PubMed PMID: 33462143; PubMed Central PMCID: PMCPMC7903917.

https://doi.org/10.7554/eLife.107161.2.sa0